1970

DYNAMIC STUDIES ON THE BEARING CAPACITY OF PILES

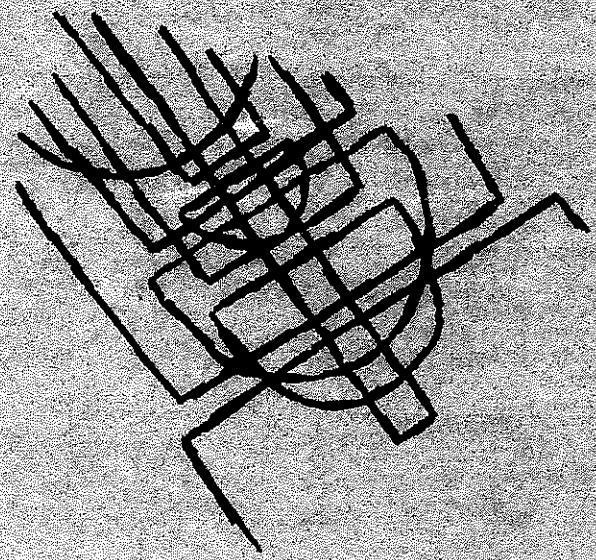

PHASE III VOLUME I

REPORT NO. 48

DIVISION OF
SOLID MECHANICS STRUCTURES AND MECHANICAL DESIGN
SCHOOL OF ENGINEERING CASE WESTERN RESERVE UNIVERSITY

DYNAMIC STUDIES ON THE BEARING CAPACITY OF PILES

Project Report of Phase III

August 1, 1970

by

G. G. Goble

F. Rausche

F. Moses

This research was sponsored by the Ohio Department of Highways and the Federal Highway Administration. The opinions, findings and conclusions expressed in this publication are those of the authors and not necessarily those of the State or the Federal Highway Administration.

Case Western Reserve University
Division of Solid Mechanics,
Structures, and Mechanical Design
University Circle
Cleveland, Ohio 44106

ACKNOWLEDGEMENTS

The cooperation, assistance and advice on technical matters of R. Dowalter, and R. Grover all of the Ohio Department of Highways contributed substantially to the success of this project phase. In administrative matters the assistance of C. R. Hanes, Ohio Department of Highways, was appreciated.

ABSTRACT

An automated prediction scheme is presented which uses both measured top force and acceleration as an input and computes the soil resistance forces acting on the pile during driving. The distribution of these resistance forces acting along the pile is also determined. Shear and dynamic resistance forces are distinguished such that a prediction of total static bearing capacity is possible. Using the shear force prediction a static load versus penetration curve is computed for comparison with the result from a corresponding field static load test.

The method of analysis uses the traveling wave solution of the one-dimensional, linear wave equation. As a means of calculating the dynamic response a lumped mass pile model is used and solved by the Newmark β-method.

Using stress wave theory two simplified methods are developed for predicting static bearing capacity from acceleration and force measurements. These methods can be used during field operations for construction control when incorporated in a special purpose computer. The automated prediction scheme and simplified methods are applied to 24 different sets of data from full scale piles. The piles were all of 12 inches diameter steel pipe with lengths ranging from 33 to 83 feet. Also, 24 sets of data from reduced scale piles are analyzed by the simplified methods. All predictions are compared with

results from static load tests. Correlation is very good for piles driven into non-cohesive soils. For cohesive soils better agreement with static load measurements are obtained than from existing methods.

As a check on the assumed soil response to both pile displacement and velocity results from measurements taken at the pile tip are investigated and discussed. Further, an approach to pile and hammer design is described using the results of stress wave theory.

TABLE OF CONTENTS

Volume I

TABLE OF CONTENTS (Continued)

CHAPTER I

Introduction

Since the beginning of this research activity two progress reports have been issued (Ref. 1 and 2). In the first an extensive literature study, an analytical examination of pile behavior using a lumped mass analysis, and the development of equipment and experimental techniques was reported. Dynamic measurements on both full and reduced scale piles were also reported and a simplified method for predicting capacity was proposed. In the second report an extensive analytical study using a continuous model of the pile was presented. Also, some modifications of the equipment were made and considerable additional data on both full and reduced scale piles were published.

Since the publication of the last report important accomplishments have been achieved and it is the purpose of this paper to present them. The most important of these accomplishments are analytical but they have been made possible and supported by the growing body of experimental data. In this report newly collected data has been integrated within all of the other data. It includes five full scale piles tested on Ohio Department of Highways construction projects and eight special test piles tested at two different sites. New equipment used on the special piles included a new accelerometer with built-in amplifier (to allow recordings of acceleration at the pile tip) and force transducers which were lighter in weight than the one discussed

in Ref. 2.

The methods used in the analytical work generally reverted back to the lumped mass model used in the first phase of the project. The nature of the methods associated with the lumped mass model make possible much more general boundary conditions on the pile. While a lumped mass model is very useful for obtaining numerical results it does not provide a means of understanding pile dynamic behavior. For this reason extensive studies on wave propagation in a continuous pile have been undertaken. The wave studies and the lumped mass model combined make possible a realistic and meaningful analysis of the available dynamic data.

The force and acceleration of the pile top, recorded under a hammer blow, establish redundant information. In the usual dynamic problem only one of these variables is prescribed together with the external forces acting along the sides or at the bottom end of the pile. Pile driving, however, complicates the problem in that information can only be obtained at the pile top while the soil forces acting along the pile are unknown. Thus, the usual analysis process cannot be applied. Generally, the top force and acceleration of the pile are dependent on the external forces so that an inverse process of the usual dynamic analysis will yield information about these unknowns.

Results from these investigations follows: A further modification of the simplified method is proposed having a much

firmer rational basis. A second modification which makes an estimate of the damping resistance also arose from the analytical work. The wave propagation study proposed methods for predicting the resistance distribution along the pile, both static and dynamic (damping). These predictions have been tested on the special test piles where resistance distribution was measured both statically and dynamically, (Fig.1.1 through 1.4) by measuring the force in the pile at a number of locations. Such measurements were taken on full scale piles in cohesive soils (Table 1.1 and 1.2) and on a reduced scale pile in sand (Table 1.3). Correlation is quite good.

In Chapter II of this report -- an introduction to the resistance distribution analysis -- the traveling wave solution is studied. Also reported in this chapter is the development of an external force prediction scheme. It was found that the Phase I and II simplified methods derived from a rigid pile model can be studied on the basis of wave considerations and that an insight in their actual meaning can be obtained. This, together with proposals for improvement (Phase II-A) and the development of a new (Phase III) simplified prediction scheme, is presented at the end of Chapter II. Chapter III summarizes the analytical results from both the external force prediction scheme and from the simplified methods. Special consideration is devoted to the prediction of the load vs. penetration curve and results are compared with those measured during a static load test.

In Chapter IV limitations and shortcomings of the proposed method are critically investigated. Chapter V, finally, summarizes the present work and includes suggestions for possible extensions of the method and further research.

Volume II contains the mathematical derivations along with additional material related to Chapter II of Volume I. Chapter I describes a lumped mass analysis based on Smith (3) and Newmark (4). This lumped mass analysis is a convenient tool for checking the validity of dynamic predictions from wave theory. Chapter II of Volume II presents the static analysis used for computing a theoretical load test by use of the predicted external resistance forces. In Chapter III the traveling wave analysis is developed as discussed in Chapter II of Volume I. Chapter IV is a summary of studies required to properly interpret force and acceleration records. Chapter V discusses the validity and limitations of the soil model used in the present prediction method. Simplified computation schemes which can be used in a special purpose computer are given in Chapter VI. Finally, the computer program used for the prediction of the external forces along the pile is described in Chapter VII by means of a block diagram.

CHAPTER II

Analysis by the Traveling Wave Solution

2.1 Introduction

Already in the nineteenth century a stress solution for a uniform, elastic rod struck by a mass had been derived by Saint-Venant, see Reference (5). The method of analysis used the solution of the one-dimensional, linear and homogeneous wave equation. Superposition of suitable waves yielded results for rods with either prescribed end forces or displacements. Donnell (6) also used this method and extended it by investigating various problems of one-dimensional wave propagation including conical rods, nonlinear material properties and problems where impact forces were applied on locations other than the ends of the rod. The results of these investigations are applicable to problems where the external forces along the bar are known and stresses or velocities of rod particles are to be predicted.

Another approach to the study of wave propagation in rods is particularly convenient for the use of high speed digital computers. This approach, which breaks up the rod into several elements - lumped masses - was introduced for pile driving analysis by Smith (3) and applied by Samson, et al. (7) and LaPay (8) among others. In these studies the attempt was made to determine certain pile, hammer and soil characteristics by using pile set and hammer energy as an input. In the approach presented here both methods - wave and lumped

mass analysis - are used with force and acceleration records measured at the pile top to devise a scheme for finding the external resistance forces acting during the motion of a pile. In this chapter relations which exist between stresses and particle velocities in a stress wave traveling through a rod with various boundary conditions will be discussed. Then conclusions will be drawn on the effects which soil resistance forces have on hammer applied stress waves. For this a spring-damper soil model will be used. A prediction scheme will be described for determining the magnitude of these passive soil forces which are initiated by the motion of the pile under the hammer blow. This method will make use of the two records measured at the pile top: force and acceleration. The acceleration will be applied as an input, i.e. as a sensor wave. Soil reaction forces initiated by this sensor wave also produce stress waves which can be separated from the hammer input by means of the measured force. Knowledge of the mechanics of wave propagation will now give a tool for locating the source of these soil resistance forces and for computing their magnitudes.

Finally, again using wave considerations, existing approximate schemes for predicting static bearing capacity will be critically investigated and a new method will be developed.

2.2 Fundamentals of Wave Propagation in a Uniform, Elastic Rod

A continuous rod under impact having non-zero force or displacement end conditions and external forces acting along its length can best be analyzed by use of a lumped mass system. In such an analysis the rod is divided into connected elements whose elastic and inertial properties are represented by springs and lumped masses, respectively. The method, as developed by Smith (3), uses an Euler integration scheme. The displacements of all rod elements at a certain time are computed by means of a linear extrapolation from values computed for an earlier time. Thus, an approximation error is made and carried through the subsequent computations. The results can only be a good approximation to the behavior of the discrete system if the time increments are chosen small enough. This, however, can introduce numerical errors due to the limited number of digits carried in the computations and will certainly increase the computation time. In order to overcome this difficulty an improved numerical integration was proposed by Newmark (4): At every time step the Newmark method uses the result obtained from Euler method as a prediction and computes a correction by checking on the dynamic balance of the whole system. Prediction and correction are then considered a new prediction and new corrections are computed until the process converges. Only then does the computation proceed to add the next time increment. By use of this method both the accuracy and stability of the solution are improved without increasing, excessively, the computation time.

The mathematical details of the analysis are given in Chapter I, Volume II together with studies on accuracy, stability and computation time of the solution and an examination of the necessary number of pile elements for a good representation of the continuous system.

For deriving qualitative results and for obtaining an insight into the propagation of hammer applied stresses the wave theory treatment of the continuous pile is helpful.

When a pile is struck by a hammer a difference in stress between neighboring cross sections is induced, so that static equilibrium does not exist. This stress gradient causes accelerations of particles. Therefore, a dynamic balance exists between the inertia forces of particles and the stresses. In a uniform, elastic pile where no external forces act, the stress gradient will travel through the rod without being changed in magnitude and the particle velocity or acceleration is predictable for a point along the rod if it is known for some time at another location. This behavior is usually referred to as a stress wave. The speed of propagation of the wave, commonly denoted by c, depends only on the material properties of the rod. It is equal to $\sqrt{E/\rho}$ where E is Young's modulus and ρ is the mass density of the material. In a uniform rod the stress gradient will cause the same particle velocities independent of the location on the rod (of course, the particle velocity is different from the velocity of wave propagation). An important result of this fact is the proportionality which exists between

stress and particle velocity in a stress wave, providing a convenient means of calculating one if the other is known.

When the stress wave arrives at an end, the stress gradient will be changed. For example, at a free end the particles will be subjected to higher accelerations (twice as high in a uniform rod) since no further material is strained in front of the wave. However, due to the higher acceleration a new stress gradient builds up between particles next to the end. The dynamic balance can be maintained only if another wave travels away from the end. This stress wave will be called a reflection wave. At a free end a reflection wave changes the sign of the stresses while the particles continue to move in the same direction. At a fixed end where the stresses build up to twice their original magnitude and no acceleration of particles is possible the particle velocity in the reflection wave will point in a direction opposite to that in the arriving wave but the stresses will have the same sign. A more detailed discussion with quantitative results is given in Chapter III, Volume II.

If a load is applied at some point along the rod, then a tension and a compression wave will be induced on opposite sides of the loaded section causing two stress waves to travel away from the load. In a uniform rod these two waves will have the same stress magnitude equal to one half of the applied stress. This is necessary to satisfy the condition of equilibrium at the loaded point. In order that the continuity condition be satisfied, the particle

velocities in both waves also have to be the same.

If no internal damping or external forces are present, stress waves will continue to travel along the rod always generating reflection waves at the ends. After the impact forces cease, the stresses at a particular cross section will oscillate about the static value. Under the same conditions velocities will oscillate about zero if the rod is fixed at one end or about the value obtained from Newton's Second Law for a rigid body in the case of the unsupported rod.

For this analysis two records, continuous over time, are available. The first question is which one is more convenient to use as an input. Because of the proportionality connecting stress and velocity in a wave in an infinitely long rod either the force or the velocity (acceleration integrated over time) seem to be equally well-suited. Comparing the measured force with velocity obtained from the measured acceleration shows that this proportionality exists only in the beginning of the record. This can be observed in Figure 2.1. Deviations from this proportionality can be due either to the finite pile length and reflection waves or the action of the soil, resisting the motion of the pile particles. If the pile is of finite length and no forces are assumed to act along the pile then by accounting for reflection waves generated at either end of the pile the velocity can be calculated from the force or vice-versa. The output from the calculation can then be compared with the other measured quantity.

Suppose that the velocity were derived from the measured force for a free pile of actual length L. If this solution agreed with the measured velocity, then this would indicate that the actual pile had indeed no resistance forces acting. In general, this will not be true. A difference between the actual and the derived velocity could be interpreted as a top velocity effect due to the soil resistance forces.

The other alternative is to compute the force on top of the free pile of length L using the velocity as an input. The difference between measured and computed force at the top is the force effect due to the soil action. Since it is intended to predict the forces along the pile it seems natural to select the second method of analysis. This yields a top force effect versus time relation due to the resistance forces. The advantage of this choice will become apparent when such curves are analyzed.

To understand the meaning of the above described top force effect, the boundary conditions must be examined. The free pile solution is defined to have the prescribed measured velocity at the top and zero forces along its length and bottom end. The actual pile has the same velocity at the top and the real resistance forces acting along its length and bottom end. Thus, the difference between the measured top force of the actual pile and that of the free pile will be the top force for a pile whose top is fixed and to which the actual resistance forces are applied. This difference will be referred to as the Measured Delta Curve.

It is advantageous to deal with the Measured Delta curve rather than either measured force or acceleration, since the effect of the actual resistance forces on the force at the pile top has been separated from the forces due to the applied velocity. The measured velocity or force show very different characteristics depending on the hammer properties. Properties of the Measured Delta curves are independent of these hammer characteristics and, therefore, can be compared even if obtained from different driving systems.

It is assumed that the resistance forces acting on the actual pile can be represented by concentrated equivalent forces. The Measured Delta curve can then be treated as being the result of a superposition of top force effects from each of these concentrated forces. Each of these top force effects is due to the action of only one particular force acting on the pile with a fixed top. Such a top force effect will be called a Resistance Delta curve. In the case of a pile having a resistance force acting at only one station, the Measured Delta curve would be equal to the Resistance Delta curve for this station.

The Resistance Delta curve is a theoretical force versus time relation. It can be obtained as a function of time, for each force acting on the pile. Since resistance forces acting on the pile depend on displacement and velocity at the point of action, the Resistance Delta curve is computed by first computing the top force for a pile with the actual top velocity and the considered resistance force acting. Then the free pile solution has to be subtracted as

in the case of the Measured Delta curve. It must be kept in mind, however, that the actual resistance forces obtained this way influence the pile displacements and velocities so that the Resistance Delta curve curve computed in the above described way can only yield an approximation of the real top force effect. Examples for both Measured and Resistance Delta curves will be given below after a discussion of the relationship between resistance forces and displacements and velocities.

2.3 Relations Between Delta Curves and Soil Resistance

In the previous section a way of determining soil reaction forces was described. Soil behavior will be treated as being dependent on the pile displacement and velocity, assuming that the soil motion is negligible during the short time considered. The knowledge of pile top velocity and force makes it possible to predict the velocity of any other point along the pile, allowing conclusions on the soil resistance. The Measured Delta curve will be used to determine the magnitudes of the soil model parameters.

(i) Shear Resistance at a Point Along the Pile

Shear resistance will be designated herein as all of those resistance forces which are independent of the rate of loading. Thus, shear resistance parameters of soils or of the pile soil interface can be determined in a static test. Although the type of soil failure at the pile bottom is very different from that at the pile skin no differentiation will be attempted. Furthermore, the term

shear resistance will be used independently of the nature of these static forces. They might be due to either cohesion or internal friction.

Triaxial tests on sands and clays show basically the same tendency of shear versus displacement behavior. The shear strength can be represented in the first approximation by a linear elastic-pure plastic force deformation relationship. While in clays it is usually not possible to reach higher values of shear stress even for large deflections after the break in the force deformation curve, sandy soils commonly show a continuing very gradual strength increase. Since this strength increase is much smaller than in the first part of the curve it might not be essential for considerations dealing with relatively small dynamic displacements. However, some special considerations must be used to interpret the results obtained from an analysis based on such an assumption. This will be discussed further in Chapter III.

The ultimate shear resistance is reached at a pile deflection value which is usually called "quake" in the pile dynamics literature. Thus, the stiffness of the soil, for deflections smaller than the quake, is the ultimate shear strength divided by the quake. It can be assumed that the soil has the same stiffness during unloading. See Figure 2.2 for an example.

The value for the quake was found not to be critical for pile driving analysis. Smith (3) for example, recommends a value of 0.1 inches. It was found in analyzing actual records that the

displacement reached at the time of maximum velocity is usually in the neighborhood of this value. Choosing that displacement as the value for the quake has the advantage that the quake will always be exceeded by the pile displacements. This is a necessary condition for obtaining a final set under the hammer blow and for reaching the ultimate capacity. Also, the number of unknowns will be reduced since the knowledge of ultimate shear strength is now sufficient to describe the shear versus displacement behavior completely. Table 2.1 lists the quake values used for some of the piles analyzed. As an upper bound .12 inches has been used. Because of the action of resistance forces the displacements at maximum velocity are usually smaller at the lower parts of the pile than at the top. Thus, the quake will not be constant throughout the depth of the pile.

The force versus time relation of a shear resistance force is easily described when the displacement of the pile is known at the point where the resistance acts. The displacement at the point where the force acts will be zero as long as the stress wave due to the impact does not arrive at this section. At a time, given by the distance from the top divided by the wave speed, the displacement will start to increase and a reaction force will be exerted on the pile. This force will send out reaction waves in both directions along the pile according to the previously discussed conditions of equilibrium and continuity. The reaction force will be directed upwards and consequently the stress in the upward traveling wave

will be compressive and that in the downward moving wave will be tensile. Because of the choice of quake discussed above the quake will be reached at the time when the particle velocity at the considered section becomes a maximum. After this time no further increase in reaction force can be observed, i.e. the reaction force stays constant until the displacement starts to decrease. Then unloading will begin.

In order to describe the Resistance Delta curve for a shear resistance at some point, say at a distance x_i below the top, a hypothetical case is considered: The pile is fixed at the top, the bottom is a free end (except if the shear is acting at the bottom end itself) and the shear force is assumed to be known as a function of time, as developed above. For the discussion here this relation can be simplified by assuming that the shear resistance force is zero until a time x_i/c and equal to the ultimate shear resistance thereafter (Figure 2.3a). This assumed resistance force versus time relation is realistic as long as no unloading occurs.

The stresses in the two generated waves are equivalent to one half the ultimate resistance force. First the upward moving wave is considered. Its stress is compressive. At a time $2x_i/c$ it will reach the fixed top causing there a reaction force of twice the force in the wave - i.e. a force equal to the ultimate shear resistance. The reflection wave, now traveling downwards, will also have a compressive stress equivalent to one half of the

ultimate shear resistance. This reflection wave will be reflected a second time at the pile bottom. Here a free end condition is encountered causing a new reflection wave with tension stresses. At a time $(2x_i + 2l)/c$ this new reflection wave will again reach the top but this time with opposite stresses. The top force effect, therefore, becomes zero at this time. Figure 2.3b illustrates the action of this initially upward moving stress wave.

Consider now the initially downward moving stress wave which has a tensile stress, again equivalent to one half of the ultimate shear resistance, it is observed that at a time L/c this wave reaches the free bottom end causing a reflection wave of compressive stress. This wave reaches the top at time 2L/c. The effect at the fixed top will be a reaction force of twice the force in the wave, i.e. a force equal to the ultimate shear resistance. A reflection wave caused at this instant will not return before time 4L/c. No consideration will be given to effects after this time. Figure 2.3c shows the way the initially downward moving wave travels along the pile and finally Figure 2.3d is a plot of the Resistance Delta curve for the shear resistance obtained from superimposing the top force effects of both waves. Summarizing, this Resistance Delta curve reaches a value equal to the ultimate shear resistance at time $2x_i/c$, twice that value at time 2L/c and decreases again to one times the ultimate shear resistance at time $2(x_i + L)/c$. If the shear resistance force acts at the bottom end of the pile, then the two waves act as one wave moving together

upward with a stress equivalent to the ultimate shear resistance. Examples of these Resistance Delta curves will be demonstrated in the next section of this chapter.

(ii) Dynamic Resistance Forces

Dynamic resistance forces are usually assumed to be proportional to the pile velocity at the location of the resistance force. This can be modeled by a linear viscous damper and, therefore, dynamic resistance forces are also called damping forces. The linear force velocity relation is the feature which distinguishes dynamic from shear resistance forces. Thus, dynamic resistance forces change magnitude while shear resistance forces stay constant after the quake is reached.

In order to construct a Resistance Delta curve for a damper at a distance x_i below the top, the force versus time relation must be found. In the case of a linear damper this means that the velocity of the pile section where the damper acts must be known. Waves due to the damping forces, however, will influence this velocity and the computation amounts to a rather difficult bookkeeping of reflection waves. Examples are discussed in Chapter III, Volume II. For obtaining an understanding of the main features of a Resistance Delta curve for a damper, the assumption will be made that the damping forces are small compared to the forces applied at the top of the pile. If this is the case then the velocity at the location of the damper can be approximated by the pile top velocity at a time x_i/c earlier. This is valid until the wave applied by the hammer has been

reflected and reaches the damper a second time. Since the reflection was at a free end the velocity in the reflection wave will have the same sign as the applied wave thus increasing the velocity at the damper. Without giving more detail about further changes of the velocity at the damper the Resistance Delta curve for this damper will now be investigated. Again the top force effect due to the damper will be the result of a superposition of the effects of the two waves generated by the damping force. One wave will move upwards to the top so that the damping force can be observed at the top in equal magnitude at a time x_i/c later. The second wave will arrive at the top - after reflection at the bottom end - with a time delay of $(2L - x_i)/c$. The maximum force effect at the pile top due to the damper will be observed at or after this time because both contributions, from upward and downward traveling waves, add up. Since in most of the cases of pile driving the impact applied velocity will decrease immediately after its maximum, also the effect at the top will decrease after its maximum which is different from the Resistance Delta curve for a shear resistance.

2.4 Discussion of Computing Delta Curves and Their Meaning

In the preceding sections two different kinds of Delta curves were introduced; the Measured and the Resistance Delta curve. Both have in common that they represent resistance forces acting along the pile, providing a means of separating resistance force effects on the pile top from the effect of the hammer applied force.

If Resistance Delta curves are selected so that their total sum is equal to the Measured Delta curve, then the resistance forces are known which were actually acting on the pile when acceleration and force were recorded.

In order to obtain either a Measured or a Resistance Delta curve two other curves must be found. First, the "free pile solution", i.e. the force on top of a pile having no other external forces acting whose top input velocity is the measured record. The second curve is the force on top of a pile which has again the measured velocity but has resistance forces acting along the pile. In the case of the Measured Delta curve this second curve is the force curve measured in the field. In the case of the Resistance Delta curve this second curve is determined analytically as explained in the next paragraph.

The first curve, which is the free pile solution, is obtained either by performing a lumped mass analysis or by using Equation 3.18, of Volume II. This equation gives the exact solution by accounting for the effects of the applied forces as well as those from reflection waves. Equation 3.18 can be applied without the use of a digital computer. For obtaining the second curve - a pile top force due to a resistance force acting on the pile having the measured velocity at the top - a lumped mass analysis must be employed because the force versus time relation depends on the pile motion. In the case of the Measured Delta curve this second solution, where the resistance forces act along the pile and the measured velocity is prescribed

on top, is the recorded force itself.

Figure 2.4 shows the "free pile solution" as obtained from Equation 3.18. The velocity from which this solution was derived is also plotted after having been multiplied by the proportionality factor EA/c. (A is the cross sectional area of the pile, EA/c relates particle velocity to force in a stress wave).

Three Measured Delta curves are presented in Figures 2.5, 2.6, and 2.7. The records were obtained on a special test pile. Figure 2.5 shows the measured force and velocity and the Measured Delta curve from records taken when only half of a 50 foot pile had been driven into the ground. The soil offered little resistance to driving. The curves in Figure 2.6 are results obtained after the pile had been driven to a depth of 48 feet. A load test performed after this record showed an ultimate strength of only 47 kips. Later, the pile was extended and driven to a depth of 58 feet. At this depth the pile tip reached a hard layer. Figure 2.7 shows results obtained from records taken under these conditions. A load test was again performed which carried a load of 180 kips. Higher loads could not be applied because of instability in the test set-up.

All three Measured Delta curves in Figures 2.5, 2.6, and 2.7 show a steep increase at a time 2L/c after impact due to the returning impact wave which has been changed under the action of resistance forces. For the pile which was only partially driven into the ground it was not possible to obtain higher impact velocities than shown

in Figure 2.5 because of the relation between resistance and applied energy for Diesel hammers, one of which was used to drive this pile. The fact that the top velocity increases again at a time 2L/c after impact indicates that the resistance forces were reflecting forces of smaller magnitude than the applied force. The Delta curve itself stays zero (small values both positive and negative, due to measurement inaccuracies, were set to zero until the point where the Delta curve starts definitely to increase) until a short time before the steep increase. After the maximum it decreases again with a steep slope. The late onset of positive Delta values indicates no resistances along the upper portion of the pile skin and the rapidly decreasing nature of the curve shows that the dominant resistance forces were dynamic.

The Delta curve in Figure 2.6 shows somewhat different features. A short time after impact positive Delta values are observed corresponding to the fact that resistance forces are acting along the upper portion of the pile. The curve again displays a sharp decline after the maximum but holds some constant value until time 4L/c. Thus, large dynamic forces and small shear resistance forces are present.

A very different Delta curve is obtained from those records shown in Figure 2.7, taken after the pile has penetrated the hard layer. The resistance encountered by the shorter pile along the skin can again be observed before the steep increase. This time, however, the maximum of the Delta curve is much larger as compared

to these skin forces. Also the amount of decrease of Delta after the maximum is relatively small. Another interesting observation can be made on the measured force record in Figure 2.7. This force shows a definite increase after a time 2L/c after impact. Clearly, this increase must be due to the reaction waves sent out by the high resistance forces acting at the tip of the pile.

The negative values in the Measured Delta curves occuring after 4L/c and before 6L/c are due to the fact that the resistance forces do not stay constant but decrease in magnitude. Simplified examples in Chapter III, Volume II will clarify this fact.

For obtaining an insight into the meaning of the Resistance Delta curves, five different combinations of resistance forces were analyzed. According to the definition of a Resistance Delta curve a lumped mass analysis was performed with the resistance force (or forces) acting on the pile and the measured velocity (in this example the velocity of Figure 2.7 was used) imposed on the pile. The free pile solution was then subtracted from the pile top force.

First a shear resistance force having an ultimate of 75 kips was placed at the pile tip. Figure 2.8 shows that the resistance Delta curve for this case obtains a value of 150 kips after a time 2L/c after impact. Subsequent oscillations are due to the finite number of elements in the lumped mass analysis.

Next, a shear resistance of 50 kips was placed at a distance

of 0.6L below the top of the pile. Figure 2.9 shows that in this case the Resistance Delta curve first reaches a value equal to this shear force at a time 0.6(2L/c) after impact and a value of twice that much at 2L/c (always after maximum velocity). It would be expected that the Delta curve would decrease again to 50 kips at (1 + 0.6)2L/c. However, because of unloading (the applied velocity has decreased considerably) the Delta curve actually decreases to even smaller values.

Two shear resistance forces of 25 kips ultimate each were placed at the pile at a distance 0.4L and 0.8L below the top. The result is plotted in Figure 2.10. Corresponding to the distances from the top at which these forces act the Delta curve shows a value of 25 kips at 0.4(2L/c) and 50 kips at 0.8(2L/c) after impact. Finally, at 2L/c after impact the Delta curve increases to two times the acting ultimate resistance forces (100 kips) due to the return of the bottom reflected waves. The decrease, thereafter, is again due to both returning tension waves and unloading.

Similar investigations were performed with dynamic resistance forces. Figure 2.11 shows the Resistance Delta curve for a damper at the pile tip. The damping coefficient is 0.2(EA/c). The Delta curve is in this case an image of the applied velocity shifted over a time 2L/c and multiplied by a factor 0.2(EA/c)2. This behavior can be predicted by wave considerations (see Equation 3.41 of Volume II).

A damper located at 0.6L below the top having the same coeffi-

cient exhibits a Delta curve value greater than zero already at a time 0.6(2L/c). This is shown in Figure 2.12. However, the proportionality between Delta curve and velocity cannot be observed after time 2L/c after impact since the Delta curve becomes the result of a superposition of two waves: The wave reaching directly to the top and the wave initially moving towards the bottom of the pile where it is reflected. When the latter wave reaches the damper on the way upward, it itself will influence the damping force. Together with this wave reaching the damper after having been reflected at the pile tip. This velocity will superimpose on the velocity applied by the hammer reaching the damper directly. The damping force at this instant, therefore, will increase. Its effect will be carried to the top by the directly upward moving wave and, in addition, the previously generated damping force will increase the Delta curve a second time due to the arrival and reflection of the initially downward moving wave. The absolute maximum of the Resistance Delta curve in Figure 2.12 is the result of this superposition.

2.5 Proposed Prediction Scheme for Computing Soil Resistance

The behavior of stress waves due to resistance forces indicated that, from the early portion of the Measured Delta curve, conclusions could be drawn on the location and magnitude of the shear resistance forces and that, from the variation of the curve, a criterion could be derived for separating dynamic from shear resistance forces.

The first step to be undertaken in devising an automated routine for prediction of resistance forces is to compute the Measured Delta curve. This is possible in closed form using Equation 3.18 of Volume II. The Phase III simplified method is then used, with the Measured Delta curve to make a first estimate of total maximum dynamic and shear resistance forces. This prediction scheme will be discussed both in Section 2.6 and in Chapter VI of Volume II.

Next, an assumption must be made about the distribution of the dynamic resistance forces. Since criteria are not available which would indicate locations of dynamic forces several distributions are attempted and then a final selection made. In a first trial the total dynamic resistance is assumed to act only at the bottom end of the pile. Its influence on the top force is proportional to the top velocity with a time delay of 2L/c, as demonstrated in Figure 2.11. This gives a means of reducing the Measured Delta curve by the dynamic effect so that a Reduced Delta curve is generated which reflects the effects of shear resistance forces only. For ease in predicting the shear resistance forces, this Reduced Delta curve is reduced further to cancel out the effects of the reflection waves arriving from the bottom. In this case a Resistance Delta curve for one half of the total shear resistance force placed at the pile bottom is subtracted. The reason for this is that such a Resistance Delta curve approximates the top force effects of all bottom end reflected waves due to shear

resistance forces, including the immediate reflection effect of the bottom shear resistance. It is now assumed that the Resistance Delta curves for the various resistance forces to be determined are zero until $2x_i/c$ after impact and equal to the ultimate shear resistances, thereafter, where they are acting at a distance x_i below the top. Then, by requiring that the sum of the individual Resistance Delta curves is equal to the Reduced Delta curve, the magnitudes of the ultimate shear resistances at all locations, x_i, are found by successively solving starting with the uppermost resistance forces. Thus, the bottom shear resistance will be determined from the Reduced Delta curve at 2L/c after impact.

In order to complete the prediction, the damping coefficient for the bottom damper must be computed. Since the maximum pile tip velocity can be approximately predicted using both Measured Delta curve and measured top velocity, as shown in Equation 3.58, Chapter III of Volume II, the damping coefficient can be calculated by dividing the maximum total dynamic resistance by the maximum pile tip velocity. Only wave considerations have been used for predicting the complete set of soil resistance parameters. Simplifying assumptions, however, were used since the effects of resistance forces on pile displacments and velocities can, initially, only be estimated. Thus, a check and refinement on the predicted forces must be made. Now the predicted shear resistance forces and the bottom damper forces (for the first trial of damping distribution) as determined above are placed at corresponding elements of a lumped

mass pile model, and an analysis is performed that yields a new predicted top force and the velocities and displacements along the pile. Subtracting the new predicted top force from the measured one gives a new difference curve which can again be thought of as a Delta curve.

Errors in the prediction of soil resistance forces causing this new Delta curve - which will be referred to as an Error Delta curve - can arise in part from inaccurately estimating the pile tip velocity so that the damping coefficient times maximum velocity will not amount to the maximum damping force necessary. Other errors may be introduced due to the neglected portions of the shear resistance Delta curves before the ultimate shear resistance is reached. This error will be larger for longer rise times at impact, i.e. the longer it takes for the displacements to reach the quake. If this time is longer than twice the time in which two consecutive elements reach the quake, then the effect of the increasing resistance force on the next lower element will add to the predicted top force. These errors will cause a deviation of the predicted from the measured force over the first 2L/c after impact. Deviations in the later portion of the record will be corrected after the first 2L/c match sufficiently well.

Improvements on the new prediction can be obtained by first computing a new damping coefficient using the pile tip velocity determined by the last lumped mass analysis and then by computing corrections on the previously predicted shear resistance forces by

using the Error Delta curve as a Measured Delta curve. By repeating this process it is usually possible to finally obtain an Error Delta curve which is small over the first 2L/c of the record after impact. (See also Chapter III of Volume II for a sample computation). A criterion on the quality of the match can be established by integrating the Error Delta curve over certain intervals, say from 0 to 2L/c and from 2L/c to 4L/c, and dividing the integrals by the time intervals used. It was found that the requirement of making the average value small is sufficient for obtaining a good match of the predicted and measured force records. The only time that rapid changes in the predicted top force occurs is at 2L/c after impact. At this time reflection waves from hammer applied velocity and resistance forces reach the top. Otherwise Resistance Delta curves show a smooth behavior. Special consideration is given to their match at 2L/c (see Chapter II of Volume II). Once the absolute value of the average error of the first 2L/c cannot be improved or once it is sufficiently small, attention is directed to the later portion of the record (2L/c to 4L/c). In this portion a difference between measured and predicted force can arise due to an incorrect prediction of total dynamic resistance forces. Comparing the Resistance Delta curve obtained for a damper at the pile tip as in Figure 2.11 with that for a shear resistance force, Figure 2.8, it is found that the shear resistance produces a higher top force effect after 2L/c than the damper. Thus, if the Error Delta curve is matched over the first

2L/c but becomes positive after 2L/c, i.e. the predicted top force is smaller than the measured, then the shear resistance force at the tip has to be increased and the dynamic resistance has to be decreased. Of course, for a negative Error Delta curve after 2L/c the opposite is necessary, namely some shear resistance has to be replaced by damping. The match over the later portion, therefore, is dependent on the distinguishing features between dynamic and shear resistance behavior.

Once a best match is obtained for a model with one damper at the pile tip two other approaches are used for distributing the dynamic resistance forces. First, the damping is distributed along the pike skin so that the first portion of the record (2L/c after impact) is matched by the effects of the dynamic forces only, or if the damping forces are too small, a uniform damping distribution is used together with shear resistance. In a third trial one damper is placed at the location where the maximum skin shear resistance force was determined in the first distribution method. Another damper - if the total dynamic resistance force is larger than the replaced skin shear resistance force - is again placed at the pile tip. In both cases of damping distribution the damping coefficients are first determined from the requirement that the sum of the Resistance Delta curves for all dampers equals, at 2L/c after impact, twice the value of total damping computed from the Phase III method at this time. Of course, these damping coefficients are modified in later iterations for an improved match.

Since the maxima of the velocities along the pile during the

first L/c after impact, i.e. before the impact wave is reflected at the bottom, are dependent on the magnitude of resistance forces and not on the kind of resistance forces acting (as long as no reflection waves are superimposed it is possible to obtain an estimate on the maximum velocities from Measured Delta curve and measured velocity). The velocities obtained from the best match in the first method can be used for computing the damping coefficients for the dampers distributed according to the two trial distributions.

Obtaining a match for these distributions must be done under consideration of the variation of the Resistance Delta curves for dampers along the skin. Thus, it is best, for ease in computation, to set up an influence matrix which contains numbers reflecting the top force effects at a time j of a damper at some location i. A similar matrix can be set up for the influence of shear resistance forces. These two matrices, which actually contain the information given by the Resistance Delta curves, provide only for a distinct numbers of points as discussed in Chapter III of Volume II.

Once a final Error Delta curve has been obtained for all three damping distributions a final result for estimating shear resistances and damping can be obtained by using a linear combination of all three results. A minimum of the final Error Delta curve can be obtained by performing a least square analysis on the previously obtained smallest Error Delta curves for the three types of damping distribution.

Again, as in all previous predictions, negative results for

the soil resistance parameters cannot be allowed as an outcome of the least square analysis. Thus, the minimum Error Delta curve might not be permissible and a recalculation must be performed in order to make negative values at least zero. Details of the computations are given in Chapter III of Volume II in an example problem.

2.6 Derivation of Simplified Models for Predicting Static Bearing Capacity

In this section a short discussion will be given about existing and newly developed simplified methods for predicting total static bearing capacity from the available dynamic measurements. In Chapter VI of Volume II more detail is presented. The need for a reliable prediction of static bearing capacity was the reason for taking measurements of force and acceleration on top of the pile as outlined in Chapter I. It was hoped that a simple force balance at the time when the top velocity reaches zero would give a good correlation with the static load test result obtained immediately before or after striking the pile. Such a prediction method has advantages if a special purpose computer is to be employed for displaying the result during the driving operation. Experience with this Phase I prediction (the predicted static capacity was calculated from force plus total pile mass times deceleration at the time of zero velocity) showed that more consistent results were obtained by using a deceleration value which was averaged over some time. It was found that this new prediction scheme, which is

referred to as the Phase II model, gave good results for full scale piles driven into well drained soils. The predictions were not reliable, however, for short piles and piles driven into highly cohesive soils. One major motivation for the analytical studies of pile phenomena was to find the justifications and limitations of these simple prediction schemes.

The velocity of the pile top can be expressed as a function of both static resistance forces and measured top force. Then computing a velocity difference yields an equation from which the total shear resistance along the pile can be calculated. This equation proves that the Phase II model was a sound approach for computing static bearing capacity. Since only few changes in the Phase II model are necessary the new computation scheme, which can replace Phase II also with respect to simplicity, is called Phase II-A. The Phase II-A model also works for short piles since it now accounts for the effects of pile elasticity. Generally high predictions can still be obtained from cohesive soils since some of the dynamic forces are still acting at and after the time of zero top velocity.

In order to obtain an estimate of dynamic resistance forces encountered during the hammer blow, the idea of a Delta function was used. The disadvantage of this Phase III method - which separates damping from shear resistance by considering the part of the Delta curve when the impact wave returns - is the complexity of the computations involved. Therefore, a special purpose computer needs

to have some storage capacity. In cohesive soils the results from this method might still be high as in the other methods but the magnitude of the predicted damping forces usually indicates the reliability of the static capacity computed. Thus, more information is obtained than from the other models. Chapter VI, Volume II, gives derivations and formulations for all of these methods.

CHAPTER III

Results and Correlation

3.1 Introduction

Experimental data were obtained from both full scale and reduced scale piles. For each of these two pile types 24 complete sets of data were available for analysis. A description of the piles tested is given in Tables 3.1 and 3.2.

Several results can be obtained from a single data set when applying the methods discussed in Chapter II. These results can be summarized as follows:

(i) Match of measure and computed pile top forces during driving.

(ii) Static bearing capacity.

(iii) Shear resistance distribution along the pile.

(iv) Pile force and velocity at the bottom during driving.

In addition, the predicted shear resistance forces can be used for a static load-displacement analysis as discussed in Chapter II of Volume II. Such an analysis produces a pile top force versus displacement relation which can be compared with the same curve from the actual field load test. Thus, a further result is

(v) Predicted static load-deflection curves.

Load versus deflection curves obtained in a static load test often show strength increases with large pile top deflections. Deflections of these magnitudes are not reached under typical hammer blows. Thus, the prediction of static bearing capacity must be associated with the

dynamic displacements of the pile under the blow. A question arises, therefore, as to what the "expected" bearing capacity will be as predicted from a hammer blow. Using an example, this question is discussed in Section 3.2.

In Section 3.3 the results (i), (ii), (iii) and (v) all as obtained from wave analysis are presented and illustrated with Figures.

Section 3.4 is devoted to the discussion of predictions of static bearing capacity from simplified models. The correlation scheme developed in Section 3.2 using pile elastic considerations is applied. Finally, in Section 3.5 measured and analytically predicted pile forces and velocities are compared.

3.2 Proposed Method for Correlating Predicted with Measured Pile Bearing Capacity

The proposed correlation method will be presented using data set No. 3 as an example. The description of the corresponding pile is given in Table 3.1. This data set was subjected to wave analysis and both damping and shear resistance forces were predicted. The predicted shear resistance forces were then used for a static analysis as described in Chapter II of Volume II. The load versus penetration (L.P.) curve resulting from this analysis and the corresponding curve measured in the static load test are both plotted on the left hand side of Figure 3.3. Both L.P. curves show similar behavior up to the point where the predicted curve suddenly levels off. This is the

point where the theoretical load curve reaches the predicted ultimate bearing capacity at all pile elements. The measured L.P. curve, however, shows further increase without an indication that an ultimate bearing capacity can be reached. This measured L.P. curve is quite typical for piles driven into sands. It exhibits no single point which can reasonably be defined as an ultimate load. If it is assumed that the soil resistance forces are only dependent on the pile displacements, i.e. increases of resistance forces with time are neglected, then the question arises as to what measured bearing capacity must be compared with the predicted value.

In a static load test a load is applied on top of the pile. This load compresses first the pile and then the soil. The elastic deformations of the pile are considerable for all of the piles considered in this study. (The pile of data set No. 3, for example, compresses 0.57 inch under a uniform load of 100 kip.) Because of this pile elastic deformation the pile tip moves at a much smaller rate than the pile top. In general, the pile tip will be the last point along the pile to reach the quake penetration. If the static soil resistance law of Figure 2.2 were completely correct then the ultimate capacity would be reached at that pile top penetration which produces a pile tip penetration equal to its quake. But this is the case only in theory. In reality, the soil resistance forces increase even after the quake penetration is exceeded but at a smaller rate. Since the pile penetrations during driving are usually

small, the assumed elasto-plastic relationship establishes a good approximation for the dynamic case. It can be expected, however, that with a higher dynamic penetration a higher shear resistance would be reached. Consequently, the dynamic displacements of the pile have to be considered in more detail. In Figure 3.4 the displacements, as obtained from the wave analysis, at the top, the middle and the tip of the pile have been plotted. The pile top reaches a maximum deflection of 0.77 inches while the pile tip only penetrates to a maximum of 0.29 inches into the soil. The expected bearing capacity, resisting the motion of the pile, corresponds to pile deflections of 0.77 inches at the top and 0.29 inches at the tip. In general, the static load test will not reach these two penetration values simultaneously. Thus, an exact correlation between dynamic prediction and static load test in not possible. For this reason a sensible way of comparing the static load test result with the dynamic prediction is the following correlation scheme:

> Find the maximum dynamic deflection of the pile top under the hammber blow and obtain the corresponding load value from the L.P. curve of the field static load test. Call this load the bearing capacity at maximum dynamic deflection, R_d.

3.3 Results from Wave Analysis

In this section the results of applying wave analysis to all data sets listed in Table 3.1 are discussed and static predictions are compared with results of the static load test. Exceptions were

data sets No. 1, 2 and 4. The wave analysis could not be applied to these data since the rise time of force and velocity was longer than 2L/c so that reflection waves returned from the pile bottom before the maximum velocity was reached at the pile top. An example record is shown in Figure 3.1. The reason for such records is an early combustion in the hammer which cushioned the blow excessively.

For pile 531-76 (data set No. 3) the same hammer was used. However, a single record was obtained having the usual impact properties. Figure 3.2 is a plot of the top forces both predicted by wave analysis and measured. Also the velocity measured at the pile top (used as input for the analysis) is plotted after being multiplied by EA/c. All three curves differ by a small amount in the beginning of the record where the proportionality between force and velocity should hold. This difference is due to a relatively slow response of the strain signal conditioning equipment which explains the lag between the two measured curves. Then also a phase shift between input velocity and output force arises from approximating the continuous pile by ten finite elements. These differences, however, do not present a serious problem since only the portion of the record after maximum velocity is studied where phase shifts have small effects (the slope of the curve is smaller than at impact). Phase shifts of this kind can be observed also in the records discussed below. In some cases where the force transducer was mounted at a considerable distance above the accelerometers the force record might show an earlier rise than the velocity. The effects will be neglected.

Another remark concerning pile 531-76 seems appropriate. This pile was tapered; its cross sectional area was decreasing over one third of its length. The present analysis does not have the capability of handling the effects of a variable cross section. Pile No. 3 was the only pile analyzed with this property. It was assumed that the effects of variable stiffness are small in this case since only a short portion of the pile was affected. In Figure 3.3 results from wave analysis and static load test are graphically summarized. As discussed in Section 1 the graph at the left hand side shows the measured and predicted L.P. curves. The dotted line indicates the maximum dynamic deflection and R_d is found where it intersects the measured L.P. curve.

On the right hand side of Figure 3.3 the distribution of predicted shear and predicted maximum damping forces is represented in the form of a plot of the forces, the predicted forces in the pile are shown for R_o applied at the pile top. (R_o is the ultimate bearing capacity predicted). The meaning of the dynamic force distribution is related to the static curve. For plotting this curve, the maximum of the damping forces from each element is used. It is assumed that these forces occur at the same time and act statically along the pile, balanced by a pile top force which is equal to their sum. Thus, a pile force curve similar to that for shear resistance forces is obtained. The sum of all maxima of dynamic resistance forces is called max D. This value is listed in Table 3.3 together with other important analysis results to give an indication of the

relative magnitude of damping forces as compared to shear resistance.

The shear resistance forces, predicted for pile No. 531-76, are acting at the lower pile half, distributed rather uniformly. Since this pile was an actual construction pile no force measurements were obtained from locations below grade. However, the blow count (number of blows per unit pile length penetration) gradually increased with depth. Dynamic resistance forces predicted were small and acted at the pile tip only. Agreement between predicted bearing capacity, R_o, and measured capacity, R_d, was good. This correlation is discussed in more detail in Section 3.4.

Figure 3.5 presents the measured and predicted pile top force and the measured velocity of data set No. 5. This data set was obtained on a special test pile (10). The pile was only 33 feet long and equipped with strain gages at both pile top and bottom. The hammer force was larger at impact than the pile resistance, thus, it is not surprising that zero velocity was not reached within 4L/c. Because of the short length of the pile (one millisecond corresponds to approximately L/2c) the rise time is relatively long and the accuracy of predicting the resistance force locations is, therefore, affected. The match between the predicted and measured pile top force is poor at time 2L/c after maximum velocity and later. Because of the relatively constant value of the top velocity it cannot be expected that dynamic resistance forces decrease immediately after their maximum. Both shear and dynamic resistance forces, therefore, show a similar behavior and do not provide the necessary force time relation

to separate them and improve the match.

In Figure 3.6 the predictions from wave analysis are compared with the static load test. Agreement is good between R_o and R_d (see dotted line in L.P. curve). A deficiency of the predictions can be found in the distribution of shear resistance forces. Apparently, the wave method failed to predict the proper pile tip resistance force. However, a shift of the predictions over one analysis element is equivalent to a time shift of only 0.2 milliseconds (the time necessary for the wave to travel a tenth of the pile length). The accuracy of both the measurements and the method is not sufficient to distinguish forces acting at such small distances.

A rather arbitrary criterion for choosing the quake was adopted. It is described in Chapter II and in Chapter III of Volume II. The quake of a point along the pile was assumed to be equal to the displacement at maximum velocity. This assumption made possible the computation of the shear resistances from the Measured Delta curve at time $t_m + 2x_i/c$. Suppose, another quake, say a larger one would be assumed. Then the shear resistances would have to be obtained from the Measured Delta curve at another time. Since the total amount of shear resistance acting on the pile is independent of the quake magnitude another quake would merely shift the force predictions to some other point of the pile. It is likely that such a shift in the force prediction occurred for the pile under discussion. This pile had a relatively slow rise time, thus, the shear resistance, for some elements, was already large before the quake was reached. The force actually

acting at the pile tip could, therefore, not be distinguished from the force acting at the element above.

In Figure 3.7 and 3.8 results are presented from data set No. 6. Both data set No. 6 and No. 5 were obtained on the same pile but at different times. Although a strength gain was observed after the waiting period, the hammer applied forces were still larger than the resistance force, so that in both cases essentially the same match was found.

Results from data set No. 7 are presented in Figures 3.9 and 3.10. The pile, F-50, was the above discussed 33 foot long pile extended by a pile section of 18.5 feet. Strain records were taken at three locations along the pile during the static load tests. The match of the measured with analytically predicted pile top force shows differences a short time after maximum velocity. These differences must be due to measuring inaccuracies (the velocity multiplied by EA/c is greater than the force which, if true, means that negative resistance forces act near the top of the pile). Also, in the later part of the record differences in the match can be observed which are probably due to an inadequate soil model.

The shear resistance distribution shows more pile tip resistance in the prediction than in the measurements. However, the fact that the pile had basically point bearing properties is seen in both measurement and prediction.

The results shown in Figures 3.11 and 3.12 for data set No. 8 are again similar to those for set No. 7. The test pile was the

same but the time of testing was different allowing some soil setup. This time the prediction R_o = 230 kips was too high as compared to R_d = 200 kips. Probably, damping forces were predicted too small.

The same test pile, F-50, was extended by a nine foot pile section to give a total pile length of 60.5 feet (F-60). Records were taken again before and after a waiting period. The analysis results for one blow of each data set are shown in Figures 3.13 to 3.16. The match for data set No. 9 is poor for a short time after the maximum velocity. Again, as in the case of Figure 3.9 this must be due to measuring inaccuracies since the proportional velocity is greater than the force.

Data set No. 11 was obtained on an actual construction pile. Measurements were taken only at the pile top. The match shown in Figure 3.17 is good until time 2.5L/c after maximum velocity. After this time the analytically predicted pile top force decreases. It was found that the match could not be improved by replacing damping forces with shear resistance since unloading occurred. In studying Resistance Delta curves (Chapter II) it was found that the force effects at the pile top form both damping and shear forces decrease after the velocity has become zero. Therefore, the match cannot be improved after this time (see also Section 3.6 of Volume II).

The prediction of static bearing capacity, R_o, is higher than R_d (Figure 3.18). Comparing both L.P. curves, the predicted and the measured, throughout the examples given, it is observed that the predicted curve usually shows a steeper slope. Two reasons

can be responsible for this difference. First the static quake is larger than the assumed value and second the soil creeps under the applied load during the relatively slow load test. Certainly, the second reason will always yield an effect. Thus, max d_A is smaller than necessary for an accurate correlation and, consequently, R_d is smaller than the ultimate strength to be predicted.

Special problems were encountered in matching the measured pile top force for data set No. 12. The pile was an actual construction pile driven into stiff silt and clay and tested after a waiting period. The special feature of the record shown in Figure 3.19 is a continuous increase of the pile top force. Also unusual is the behavior of the pile top velocity. After the first local maximum this velocity decreases only slightly and reaches, thereafter, a second maximum which is higher than the first. This phenomenon was observed for all blows in this data set but for no other pile. Reasons for such a record can be soft cushion properties or hammer self-cushioning by early ignition. In addition, a very high precompression force of 66 kips had to be subtracted. Even after subtracting this force from the record, the rise time was relatively long. The late occurance of the first local maximum velocity produces slowly increasing resistance forces which, therefore, have relatively large effects before the quake is reached. The automated prediction routine, however, requires a short impact and, therefore, fails to produce a good match. (See also the discussion of data set No. 5). Figure 3.20 shows the predicted pile top force

from the automated routine. A large difference (35 kips) can be observed between measured and predicted top force at time t_8, $(t_m + 2\frac{8}{10}L/c)$, although no resistance force was assigned to the eighth element. However, shear resistance forces of 65 and 73 (kips) were predicted for the ninth and tenth element respectively. Clearly, the resistance forces produce a top force effect at earlier times than expected due to the slow rise time at impact. To correct the match 35 kips resistance were subtracted from the predicted force for the ninth element and a lumped mass analysis performed. The pile top force obtained from this analysis was now smaller than measured at t_8. This is reasonable since bottom reflected waves affect the pile top force already at time t_8. Adding now 10 kips to the resistance of the eighth element (now 40 kips) produces the match shown in Figure 3.19. Thus, the prediction of bearing capacity was 25 kips lower when obtained "by inspection" rather than from the automated routine. A shortcoming of the match in Figure 3.19 is the very low predicted pile top force for $t > t_m + 2L/c$. The solution obtained by the computer program shows differences of equal magnitude before and after $t_m + 2L/c$. Both predictions, however, show a similar steep decrease in the later part of the record because of an inadequate soil modeling for unloading. The results corresponding to both matches are given in Table 3.3 and are plotted in Figure 3.21 for the match of Figure 3.19.

Results from data set No. 13 are shown in Figures 3.22 and 3.23. The pile was one of the special test piles described in Chapter I.

The soil was a silty clay. A low static capacity of 69 kips was measured in the load test immediately after driving. The velocity was increasing at time 2L/c after impact, indicating the very low driving resistance. The precompression force subtracted from the force record was 26 kips, a large force compared to the ultimate capacity. The measured and predicted pile top force are both shown in Figure 3.22. This match was obtained by applying more damping forces than resistance forces. Better agreement between the analytical and the measured force could not be obtained because of the relatively constant velocity. Thus, the soil model is, again, not able to describe the soil behavior correctly. The predictions, however, are good as shown in Figure 3.23 and summarized in Table 3.3. Of course, the conditions met here, very low capacity, would not be encountered in a service pile.

A much better match, of predicted and measured force, was obtained for the same pile tested after a waiting period. The results for this data set, No. 14, are shown in Figures 3.24 and 3.25. Here, however, the static capacity prediction was too high. From force measurements, along the pile, taken during the load test, it was found that relatively large resistance forces were acting along the skin of the pile. This fact was clearly recognized by measurements and analysis. An interchange of skin damping forces with skin shear resistance forces would improve the prediction.

Data sets No. 15 and 16 were obtained from the second special test pile at the same site as the pile just discussed. Although,

the pile was longer, its ultimate bearing capacity was smaller than for the shorter pile. Very similar observations as in No. 13 and 14 can be made on the results of both data sets. The preditions and measurements are plotted in Figures 3.26 to 3.29.

Data set No. 17 was from an actual construction pile without special instrumentation. The soil was gravelly sand. Predictions and measurements were in good agreement as shown in Figures 3.30 and 3.31.

Another construction pile was tested but this time driven into clayey silt (Data Set No. 18). The static resistance of the pile was small although the blow count indicated sufficiently high soil resistance forces. The match between predicted and measured pile top force during driving was almost perfect, but the prediction of bearing capacity was too high. Thus, the damping forces determined for obtaining the match were actually too low. Figures 3.32 and 3.33 present the results. It should be mentioned that this pile gave the poorest prediction for static bearing capacity among all piles tested.

Data set No. 19 was obtained at the same pile after it was extended and driven to a depth of 74 feet. This time the maximum bearing capacity determined in a load test after a waiting period was 160 kips. Both Figures 3.34 and 3.35 show matches for the pile top force during driving. Both matches are of the same quality but different at time 2L/c after impact and later. The match in Figure 3.34, which was obtained from the computer routine,

shows fair agreement throughout the record. The pile top force shown in Figure 3.35, predicted by subtracting 10 kips from the predicted toe shear force agrees very well with the measured top force up to time 2L/c but deviates substantially thereafter. These results indicate the difficulties in obtaining a match which satisfies the criteria introduced in Chapter III of Volume II. Here, as well as in all other cases where the match was only fair, these criteria were not satisfied and the iteration was stopped after the eighth cycle in each damping distribution trial. The prediction from the second match agrees better with the load test result (see Table 3.3). Figure 3.36 shows the static results both predicted automatically and measured. A great portion of shear resistance forces were predicted to act along the skin of the pile. This result is not surprising for a pile driven into cohesive soil.

Data set No. 20 gives another construction test pile in coarse grained soil. Figures 3.37 and 3.38 summarize the analysis results. The match of the dynamic forces is good and the prediction of static bearing capacity agrees well with the load test result. The blow count was low until the pile was driven to a depth of 40 feet when driving suddenly became hard. This observation agrees well with the prediction that most of the resistance forces act at the pile tip.

Figures No. 3.39 to 3.46 present the analysis results for the second test pile described in Chapter I. As outlined, the pile was driven and tested in two steps. First the pile was driven to a

depth of 50 feet (Ri-50). This pile was embedded in silty and clayey soil. Later the pile was driven until a stiff soil layer was reached and driving became very hard (Ri-60). The two data sets (No. 21 and 22) for the shorter pile gave results similar to the test piles To-50 and To-60 (Data sets No. 13 through 16). The difference was that the waiting period did not influence the soil properties as much as in the case of the To - piles. Figure 3.39 through 3.42 show the correlation between measurements and predictions. Again as in other cases of piles in cohesive soils, relatively high dynamic and skin resistance forces were observed. A remark on the measured force curve in Figure 3.39 is appropriate. This force record did not show negative (tensile) forces before the precompression force was subtracted. Due to the small resistance forces, however, the top force decreased to very small values at time 2L/c after impact. Thus, after subtracting the precompression force of 26 kips, negative values appear in the force curve.

The top force matches for Ri-60 are not very good. A reason for this can be found in the inadequate soil model. Velocity and force measurements were taken at the tip of this pile and examples of them will be presented in Chapter V of Volume II. Predictions of shear force distribution and bearing capacity are good in this case even though the predicted top force correlation is not good. A discussion of this is given in Chapter IV. The analysis correctly reflected the strength gain of shear forces along the pile skin during the waiting period. This can be seen by comparing the force

distributions along the pile in Figures 3.44 and 3.46.

Attempts to analyze the reduced scale pile data of Table 3.2 were also made. However, similar to the data sets No. 1, 2 and 4 of Table 3.1 most of the reduced scale pile data had force rise times longer than 2L/c. Figure 3.47 shows both the measured force and velocity (multiplied by EA/c) and also a predicted top force obtained by assuming soil parameters and checking on the result by performing a lumped mass analysis. Then corrections were made and the process repeated. Data set No. 12 was used here as an example. The maximum velocity occurs only at a time 3L/c. Thus, the wave prediction method is not applicable.

The attempt was made to obtain data from reduced scale piles such that the maximum velocity occurs at an earlier time. This was done by reducing the cushion between hammer and pile head and resulted in the measured force record shown in Figure 3.48. Due to the very short rise time and the relatively slow repose of the strain signal conditioner such large deviations were produced in the necessary proportionality between pile top force and velocity that a meaningful analysis could not be performed. In Figure 3.48 a predicted force curve is shown which was obtained by using the static resistance of the pile as a pile tip resistance force. No effort was made to improve the match.

3.4 Prediction of Static Bearing Capacity

In the previous section results from wave analysis have been presented by using a single blow as an example. Important results from each of these blows are listed in Table 3.3. However, more than one blow was usually analyzed. In addition, the simplified methods presented in Chapter II and in Chapter VI of Volume II were applied to all data sets for predicting static bearing capacity. The predictions are listed in Table 3.4 for full scale piles and in Table 3.5 for the reduced scale piles. Only simplified methods were used for the analysis of reduced scale pile data.

In most cases a number of blows have been analyzed. Since the correlation scheme, developed in Section 1, requires comparing the measured bearing capacity at the maximum dynamic displacement of the blow, each individual prediction should be compared with a particular load test value, R_d. However, it was observed that the predictions for different blows are usually quite uniform (except for the results from Phase I). Furthermore, the maximum dynamic displacement changes only slightly from blow to blow. It seems, therefore, justified, to compare the averages of the predictions, R_o, with the R_d values used to correlate the analysis results in Section 3.3.

The predictions listed in Table 3.4 and 3.5 indicate the improvement of the results by applying any of the methods derived from wave considerations as compared to the rigid pile models (Phase I and II). Best results were obtained using the wave

analysis. For application in a field special purpose computer, the Phase IIA method seems as well sutied as any of the earlier methods. Also, the Phase III method can be applied if some storage capacity is provided in such a computer. Thus, the two early methods are discarded in further considerations.

A brief statistical investigation of the Phase IIA and the Phase III simplified methods together with the results from wave analysis was made on the full scale pile results. In studying the predictions obtained from the wave analysis, it was found that the differences between measured and predicted static bearing capacity depend mainly on the magnitude of the dynamic resistance forces. Dynamic resistance forces, however, depend on the soil properties and not on static bearing capacity. For piles with high damping errors in dynamic predictions can result in relatively large differences between measured and predicted static bearing capacity. A reasonable safety factor can be developed from such a study taking into account the uncertainties in the predictions.

Consider Figure 3.49. In this diagram the differences $R_o - R_d$ were plotted for the three methods under investigation. The differences were arranged in the same order as in Table 3.4, omitting the results obtained from modifying the solution from the automated routine. Also, the results from data set No. 12 were omitted because of the unusual records which needed special consideration. Thus, 20 sets of predictions remain for analysis. Figure 3.49 displays an interesting trend, namely, with a few exceptions the differences are

either all high or all low. Thus, these differences must be either due to assumptions inherent in all three methods or due to a lack of information in the records. The largest differences were found in the predictions for pile W-56 (Data set No. 18). This pile was driven into a clayey silt. The match between predicted and measured pile top force during driving was very good (Figure 3.32). Thus, the soil model adopted seems not to be sufficient to describe the behavior of this soil. However, this soil model was the basis in deriving all three methods.

The variety of soil conditions represented by the sample of 20 full scale piles chosen in Figure 3.49 is a fairly representative sample. The statistical computation is done in the same way as suggested by Olson and Flaate (9) for the treatment of results from energy formulae. Accordingly, the measured capacity, R_d, is stated as a function of the predicted capacity, R_o. A best fit straight line

$$R_d = mR_o + b \tag{3.1}$$

is then determined for each set of predictions by the least square method. The results are shown in Figures 3.50, 3.51, and 3.52 for Phase IIA, Phase III and the wave analysis, respectively. As a measure of the precision in the predictions the variances, σ_m^2 and σ_b^2 of m and b are calculated. For illustration, the lines

$$R_d = (m \pm \sigma_m)R_o + (b \pm \sigma_b) \qquad (3.2)$$

are plotted together with the best fit lines. Table 3.6 lists all parameters calculated together with the correlation coefficient for the three methods under investigation. Also the outcome of statistical invesitgations on energy formulae results from 93 piles in sandy soils, given in (9), are shown for comparison.

The best predictions can be expected from the wave analysis method. But even the simplified methods, Phase IIA and Phase III, yield a better correlation coefficient than any of the energy formulae. It should be observed that from the 20 sets of data under investigation 9 were taken on piles in cohesive soils while the data in (9) were all from piles in sandy soils.

Compared to the two earlier methods the predictions for reduced scale piles listed in Table 3.5 were considerably improved only by the application of the Phase IIA method. The Phase III method did not yield improvements because - with a few exceptions - a short time impact was not achieved under the blow. Exceptions were data sets No. 21 through 24 in Table 3.2 where the agreement between R_o and R_u was much better. It is not necessary for correlating the reduced scale pile predictions to find the value of R_d since the pile elasticity of these piles is small and the slope of the measured L.P. curve was always small at ultimate.

3.5 Forces and Velocities along the Pile during Driving

For the two special test piles described in Chapter I dynamic force records were obtained on various locations along the pile. Pile tip velocities were also obtained on piles Ri-50 and Ri-60. In this section examples will be given as to how such measurements compare with the results from analysis.

On the right hand side of Figure 3.53 the discretized pile is shown as applied in the lumped mass analysis. Also, the locations where forces were recorded are indicated. On the left hand side of the same figure the recorded forces for three different locations below the top are shown. For comparison the forces are shown in the spring between elements 5 and 6 and in the lowest spring. Since the pile (Ri-50) was 50 feet long, one element length is 5 feet. However, the force in the pile was measured at one foot above the pile bottom. Thus, the force predicted by the analysis cannot be equal to the measured pile tip force. It can be seen that the predicted curve (10) stays between the measured curves (III) and (IV).

The force measurement taken at a distance of 29 feet above the toe plate (II) agrees well with the spring force between element 5 and 6. The effects of the precompression force and a time lag due to measuring inaccuracies give some deviations.

A similar comparison for measured and predicted forces at the middle and the bottom end of the pile are shown for Ri-60 in Figure 3.54. This time the difficulties arising from different locations in analysis and measurement are avoided by plotting the pile toe

resistance force as given by the soil model. The agreement of these forces is as good as for the forces at the middle of the pile.

In Figures 3.55 and 3.56, finally, measured and predicted pile tip velocities are plotted. Good agreement is found for both piles Ri-50 and Ri-60.

CHAPTER IV

Discussion of Methods and Results

The studies presented in this report lead to results of two types. First, an analysis method for impact driven piles is presented which provides information about both soil response and pile behavior. Second, a contribution is made to the development of a dynamic testing method for piles. Both the analysis and the dynamic testing method are based on force and acceleration records taken during a hammer blow.

While the dynamic testing method can be utilized in construction control as a replacement for the static load test, the wave analysis method is also useful for determining the soil resistance distribution for use in more detailed pile behavior analyses. It is also possible to use the basic approach of wave considerations for other problems associated with pile driving. Such applications will be discussed in Section 4.1.

Several assumptions were made in developing both analysis and dynamic testing method. Implications and resulting limitations of these approaches are discussed in Sections 4.2 and 4.3.

Section 4.4 is devoted to a summary of observations regarding measurement techniques and related questions of accuracy.

4.1 Possible Applications of Wave Analysis Method

(i) Summary of Analysis Process

The approach used in this paper for analyzing pile behavor and soil response under a hammer blow can be summarized as follows:

Force and acceleration are measured at the pile top during driving. These two records are used to separate the free pile impact stress waves from the waves due to soil action. The stress waves are then interpreted regarding the magnitude and location along the pile of the soil resistance. From the soil force versus time behavior, thus determined, conclusions are drawn about the type of resistance force, whether static or viscous.

In separating impact from soil action waves, the concept of Delta curves proved helpful. An important fact is that a Measured Delta curve can be obtained in closed form from a force and velocity record even without a high speed computer. Measured Delta curves are shown in Figures 2.5, 2.6, and 2.7. After some experience it is possible to estimate soil response properties from such Measured Delta curves even without the use of a complex analysis. Resistance Delta curves were developed to assist in interpreting the Measured Delta curve. As an example consider Figure 2.6. At time 2L/c after impact the Measured Delta curve has a maximum of approximately 300 kips. Within a short time after the maximum the curve decreases to about one half of the maximum. Thus, approximately half of the total resistance seems to be damping. Also the fact that skin forces act along the pile is seen in the record.

(ii) Pile and Hammer Selection

In developing an automated routine for the prediction of soil resistance forces a number of equations were derived which can be utilized in other applications. As an example the selection of a satisfactory pile is illustrated.

Example 1:

Suppose a pile of known material such as steel or concrete has to be driven by a hammer whose maximum impact velocity, max v_A, is known. Then Equation 3.43 of Volume II can be modified to yield

$$\max v_n = 2 \max v_A - c/EA \, S_{n,o} \tag{4.1}$$

where it is assumed that no dynamic resistance forces act on the pile. In the presence of skin shear forces Equation 4.1 is still valid by replacing $S_{n,o}$ by S_o, i.e. the sum of all shear forces acting. Therefore, if it is desired to drive a pile such that it has an ultimate bearing capacity of S_o^* then for the pile tip to exceed the quake and have a permanent set the following condition must be satisfied

$$2 \max v_A > (c/EA)S_o^* \tag{4.2}$$

which requires that

$$A > (c/2E)S_o^*/\max v_A \tag{4.3}$$

In these considerations damping was not considered. However, for the condition of just reaching a positive velocity this is not necessary since dynamic resistance forces are small for small velocities. If it is intended to require the pile tip to reach a certain velocity, max v_n, then Equation 3.43 has to be used in its original form together with an estimate of the maximum damping force, d_n max v_n, (which can be assumed depending on the soil properties). Thus,

$$A = \frac{c\, S_o^* + d_n \text{ max } v_n}{E\ 2\text{max } v_A - \text{max } v_n} \qquad (4.4)$$

The reverse approach can be used to find the necessary hammer impact velocity by prescribing the pile cross sectional area and solving for max v_A. Estimates on pile set can be obtained by integrating Equation 3.43 over time until $v_n(t)$ reaches zero.

(iii) Interpretation of Pile Force Records

In addition to producing a useful set of analysis equations, wave considerations also lead to a more complete understanding of pile behavior. Another example will be used to explain why pile driving records (force or velocity) seldom give a clear indication of the time when the impact wave returns from the bottom, as discussed by Tomko (10).

Example 2:

It was observed in Chapter III that damping forces exerted by

the soil usually act primarily at the pile bottom. For the case of only a damper at the pile bottom Equation 3.41 of Volume II gives the damping force $D_n(t)$ from the applied velocity $v_{n,a}(t)$. The reflection of the impact wave plus the effect of the damper causes a wave to travel upwards with a particle velocity at time t and at a distance x below the top.

$$v_{up}(t - \frac{L - x}{c}) = v_{n,a}(t) - \frac{cd_n}{EA} \frac{2v_{n,a}(t)}{1 + (cd_n)/EA} \tag{4.5}$$

or using again the definition 3.50 of Volume II, Equation 4.5 can be written as

$$v_{up}(t - \frac{L - x}{c}) = v_{n,a}(t)[1 - 2\alpha_n \frac{c}{EA}] \tag{4.6}$$

Suppose, a pulse is applied at the free pile top at a time zero for a pile with a free bottom end condition. If the pulse has duration Δt and a particle velocity v_A^* then for no damper at the bottom the pile top velocity is given by

$$v_{top}(t) = \begin{cases} v_A^* & \text{for } 0 \leq t \leq \Delta t \\ \\ 2v_A^* & \text{for } r\frac{2L}{c} \leq t \leq r\frac{2L}{c} + \Delta t \end{cases} \tag{4.7}$$

and zero otherwise, where $r = 1,2,\ldots,$ indicates the time interval considered. Equation 4.7 is plotted in Figure 4.1a.

If a damper is acting at the pile bottom, then, due to the reflection of the upward traveling wave whose particle velocity is given by Equation 4.6

$$v_{top}(t) = \begin{cases} v_A^* & \text{for } 0 \leq t \leq t \\ 2v_A^*(1 - 2\alpha_n \frac{c}{EA}) & \text{for } 2L/c \leq t \leq 2L/c + \Delta t \\ 2v_A^*(1 - 2\alpha_n \frac{c}{EA})^2 & \text{for } 4L/c \leq t \leq 4L/c + \Delta t \\ 2v_A^*(1 - 2\alpha_n \frac{c}{EA})^r & \text{for } r2L/c \leq t \leq r2L/c + \Delta t. \end{cases} \tag{4.8}$$

and zero otherwise. In Figure 4.1b,c,d this pile top velocity is plotted for values of $\frac{c}{EA}\alpha_n = 0.1, 0.5, 0.9$, respectively. It can be observed that $\alpha_n = EA/2c$, i.e. $d_n = EA/c$, gives the solution for an infinitely long pile. No waves are reflected from the bottom. This damping coefficient, $d_n = EA/c$, can be thought of as a critical value. If the soil acts like a damper having this critical damping coefficient then in absence of all other resistance forces

$$\max D_n = \max v_A(EA/c) \tag{4.9}$$

But, because of the proportionality between pile top force and velocity, which holds at t_m, the time of maximum velocity

$$\max D_n = F_A(t_m) \tag{4.10}$$

In this context, it is interesting to examine the damping coefficients obtained from the analyses for different soil types. A list of these parameters is given in Table 4.1. The damping coefficients listed in this table are non-dimensionalized by dividing d_n by EA/c. "Critical damping", therefore, corresponds to a value 1.0 in Table 4.1. It can be observed that only two data sets (No. 18 and 19), which were obtained on the same pile, are greater than unity. Relatively often, however, values in the neighborhood of 1/2 can be observed.

Of course, damping values, non-dimensionalized with respect to pile elastic properties, cannot be used for comparing the behavior of different types of soils. Table 4.2 lists the natural coefficients, d_n. These parameters must be considered with respect to their dimensions. Thus, element surface or the total cross sectional area of the pile toe must be considered when comparing the damping coefficients determined for different piles. A commonly employed method of referring to damping coefficients (7) is in relation with ultimate shear resistance. This procedure was not adopted in developing the predictor method since it was intended to obtain damping and shear parameters independently. However, for further studies of predicted soil parameters this method could lead to comparable values for different pile and soil types. Further investigations are needed, however, to distinguish more accurately between skin and toe damping at the bottom element.

A shear resistance force, acting at the pile tip and having a magnitude equal to $F_A(t_m)$, will also produce a wave such that at

time t_m + 2L/c no effect of the impact wave reflected at the pile bottom can be observed. In fact, any combination of resistance forces produce this effect if they sum to $F_A(t_m)$. These observations can be applied to the interpretation of the three-dimensional force plots shown in Figures 1.2 and 1.3. (Three or four force measurements were available. The graph was completed by interpolation).

In Figure 1.2 a plot is shown where $F_A(t_m)$ = 165 kips and S_o + max D = 107 kips from wave analysis. Thus, there is less force than necessary to cancel out the effects of the reflected impact wave at t_m + 2L/c at the top. Accordingly, a decrease in the pile top force can be observed when the reflection wave arrives at the top. The plot also gives an impression as to how the waves travel through the pile.

Figure 1.3 shows the plot of force measurements taken on a pile with high toe resistance. $F_A(t_m)$ = 290 kips and S_o + max D = 280 kips. This means that not much change should be observed in the pile top force at time t_m + 2L/c. Indeed, the force record at this time proves this statement. The steep top force increase in the record at a later time is due to the rapid decrease of impact force immediately after the maximum. Since S_o remains on until zero velocity, its effect on the top is to cause an increased force.

Figure 1.1 is based on measurements on a pile with relatively high skin resistance forces (To-60, data set No. 16). $F_A(t_m)$ =

155 and S_o + max D = 200 kips were obtained from measurement and analysis, respectively. This case shows a top force increase already at a short time after time t_m. At time t_m + 2L/c a drop of pile top force can be observed. In this case relatively high resistance forces were found by wave analysis along the pile skin whose effects at the pile top are spread over same time before the bottom reflection wave returns. For this reason no distinct indication of wave returns can be observed in the force record.

(iv) Prediction of Pile Stresses

Since the force and acceleration records taken at the pile top predict the soil resistance force distribution, it must also be possible to compute the stresses in the pile during driving. This problem is simplified by the fact that a distinction between dynamic and shear resistance forces is not necessary. Hence, estimates can be obtained from the Measured Delta curve without performing a complete prediction analysis.

In general, compression stresses reach extreme values only at the pile top or pile bottom. Along the pile skin only distributed forces act which cause a compression wave above and a tension wave below their respective locations. The effect of a superposition of such compression waves can be observed at the pile top.

A bound on the maximum toe compression stress, $\sigma_n(t)$, can be given by assuming all resistance forces to act at the pile bottom. But since the maximum total resistance force is given by the Measured Delta curve, it is possible to estimate the pile tip stress:

$$\sigma_n(t) \leq \frac{1}{2A} \Delta(t_m + 2L/c) \tag{4.11}$$

Tensile stresses, which can be critical in driving concrete piles, occur only in the case of small resistance forces and are due to the decrease of the impact velocity. In the absence of resistance forces the stresses, $\sigma_i(t)$, at point $x = x_i$ is, for $0 \leq t \leq (2L + x_i)/c$,

$$\sigma_i(t) = E/c[v_A(t - \frac{x_i}{c}) - v_A(t - \frac{2L - x_i}{c})] \tag{4.12}$$

This follows from a superposition of the applied wave, having particle velocity, $v_A(t)$, at the pile top at time t, with its own reflection wave. Thus, tension stresses can occur when the particle velocity of the bottom reflection wave is larger than that of the downward traveling impact wave. The largest tension stress to occur in the pile is, therefore, given by the maximum difference in pile top velocity during the first 2L/c time interval (after maximum velocity). Compression stresses due to resistance forces below $x = x_i$ reduce this tension stress such that, from the Measured Delta curve, an estimate on this stress can be given. Thus, for $x_i \neq L$

$$\sigma_i(t) = E/c[v_A(t - \frac{x_i}{c}) - v_A(t - (\frac{2L - x_i}{c})] - \frac{1}{A}[\Delta(t_m + \frac{2L}{c})/2 - \Delta(t_m + \frac{2x_i}{c})] \tag{4.13}$$

Such invesitgations on the stresses in piles suggest that the hammer and cushion properties have to be selected with respect to the pile strength. In order to prevent tensile stresses in concrete piles, cushioning has to be added to obtain a uniform pile top velocity.

Excessive compression stresses in the pile can be prevented by keeping the hammer impact velocity so low that the corresponding stress is one half of the yield stress.

Implications of this kind are known to hammer manufacturers but records and wave considerations as outlined can give valuable information for certain combinations of hammers, piles and soils.

4.2 Discussion of Soil Force Prediction Analysis

The wave considerations in Chapter II and Chapter III of Volume II were limited up t a time 4L/c after impact. This time interval may not always be sufficient when L is small (as for the reduced scale piles) in order for the soil response to be fully developed. Since a resistance force distribution along the pile is usually of minor interest for short piles, no serious limitation seems to restrict the applicability of the method. Clearly, a rigid body, i.e. a pile of zero length, cannot be analyzed regarding resistance force distribution.

A related problem is encountered when the pile is sufficiently long but the impact is too "slow". In such a situation only approximate solutions are found. A match of pile top forces might be obtained by using the lumped mass analysis and assigning soil resistance parameters in a trial and error fashion as indicated above.

However, the results thus obtained depend mainly on the assumptions regarding soil stiffness and to a smaller degree on the actual soil properties, since these factors can be found from the record due to the numerous reflections occurring during buildup. Two extreme situations may clarify what is meant. A "very slow" impact is the static load test which allows a match between measured and predicted pile top force from the assumption that all resistance forces are concentrated at any one point. A corresponding soil stiffness, necessary for the match, can be computed, but the resistance distribution along the pile cannot be determined from the top record. The "fastest possible" impact exhibits a step shaped displacement function (the velocity is applied as pulses) in which case the force distribution can be predicted independent of any knowledge regarding the quake. The latter case is ideal for the present method.

In this context the choice of the quake should be discussed. Frequently, in the analysis, quake values are used which are relatively small compared to values commonly recommended. Forehand and Reese (11) give quake values up to 0.30 inches for certain soil types. Also, the investigations in Chapter V of Volume II showed that the quake might be larger for soft, cohesive soils than the displacement at maximum dynamic deflection. There are several reasons, however, why the adopted method still gives good results.

A first reason is that, in all records analyzed, a precompression

force was acting upon the pile and was imposing displacements such that the soil structure was already compressed before the impact wave arrived and caused the soil to yield.

Second, the sum of the ultimate resistance forces, $S_{i,o}$, is determined directly from the Measured Delta curve, independent of the choice of quake. Incorrect assumptions for the quake will, therefore, mainly result in errors in the shear resistance force distribution. This, of course, is true only for small errors in the quake and does not apply to cases where the quake was not reached in the considered time interval. In such cases, the ratio of shear to damping forces will be affected at 2L/c after impact in the Measured Delta curve.

In the analysis, quakes were used with only small differences between neighboring elements. It can be assumed that actually the quakes do not vary substantially with depth. Erroneous assumptions in these quakes will, therefore, produce a shift of all resistance forces along the pile length. The results shown in Figures 3.6 and 3.8 exhibit such a force shift over one element length.

Other errors in resistance force distribution can arise where large damping and skin resistance forces are present. In such cases, an incorrect damping distribution will necessarily result in shear resistance forces at locations other than measured in the static load test. An example of such erroneous results is given in Figure 3.25. Here a large damping force was assigned to a point where actually a relatively large shear force was acting.

Note, however, that the character of the shear resistance distribution was still preserved. Errors of this kind occur since no indications as to the damping distribution were found in the records. Because of this lack of information a damping distribution was used which yields the best match. This approach solved the problem only approximately since even a perfect match does not necessarily give a correct solution.

A remark on the uniqueness of a solution obtained by matching the measured force is appropriate. Certainly, a match with zero differences between predicted and measured forces is not possible, however, within the accuracy of the method it is possible to obtain several solutions with an equivalent match quality. For example it was observed that different damping distributions can lead to almost identical pile top forces. To obtain a solution for the 2n parameters, p_i, which describe either the damping or the shear force behavior at least 2n simultaneous equations have to be satisfied

$$\Delta(t_j) = \sum_{i=1}^{2n} \Delta_i(t_j) \qquad (4.14)$$

$$j = 1, 2, \ldots, 2n$$

where $\Delta(t_j)$ is the Measured Delta curve and $\Delta_i(t_j)$ is the Resistance Delta curve for the i-th location, both values taken at a suitably chosen time t_j. For example

$$t_j = t_{j-1} + 2\frac{L}{nc} \qquad (4.15)$$

$\Delta(t)$ is the Measured Delta and $\Delta_i(t)$ is the Resistance Delta curve associated with p_i.

Of course, the t_j can be chosen arbitrarily over the domain such that actually an infinite number of equations are available. However the smaller the difference $t_j - t_{j-1}$ becomes in Equation 4.15 the smaller the differences between consecutive equations. Thus, if n is too large an ill conditioned set of equations can result which allows several possible solutions. It can be concluded that the information contained in $\Delta(t)$ is not sufficient for obtaining a unique solution.

In cases where a good match was obtained with relatively poor predictions of static bearing capacity the use of another, more realistic, soil model would add the information necessary for obtaining a good match together with good predictions. Sandy soils do not present problems of this kind, since the chosen soil model is appropriate.

Several results were obtained with a relatively poor top force match. (See Figures 3.22, 3.26, 3.39 and 3.41 for data sets No. 13, 15, 21 and 22, respectively). A better match cannot be obtained when employing the present soil model. Even a quake value different from the one assumed would not improve the situation as can be seen from Figures 5.2 and 5.3 of Volume II. (The theoretical damping forces do not decrease at a sufficiently high rate). By

choosing somewhat smaller shear resistance forces, the error in the match of dynamic pile top forces is spread over some time before and after time 2L/c after impact. As a result the prediction of total static bearing capacity is relatively good but errors in the match of dynamic pile top forces are made before the time when the reflected impact wave returns.

Piles with relatively small resistance forces (the impact force is larger than the sum of all resistance forces) usually show little variation in the pile top velocity. Therefore, Resistance Delta curves do not exhibit the characteristic differences between shear and dynamic resistance which makes it possible to distinguish between these forces. For predicting the maximum dynamic resistance forces the analysis uses the assumption, stated in Chapter V of Volume II on cohesive soils, of a damping force drop independent of the pile velocity. The Phase III simplified method of predicting static bearing capacity uses the same idea for piles with small resistance. Since the Phase III prediction scheme is used as a first guess of the amount of damping forces in the wave analysis, a reasonable final result is obtained. In such cases, the criteria for a good match cannot be satisfied since the predicted force is always too large after t_m + 2L/c. The analysis routine is programmed in such a way that first attempts are made to improve the latter region of the match by adding more damping and reducing shear resistance forces. If no improvement can be obtained, then the matching criteria are relaxed such that the iteration terminates within a few more

cycles. In this way, more damping is predicted than computed by the Phase III scheme, which means a more conservative result for the static bearing capacity prediction. Certainly, predictions obtained in this manner, can only be considered an estimate on the static bearing capacity and further studies on soil models, particularly with regard to the damping, are necessary to devise a better basis for wave analysis of soils driven into soft cohesive soils.

Entirely different problems were encountered on piles driven into cohesive soils but tested after a waiting period long enough to allow the pore water pressure in the soil to dissipate. (Only the first few blows after the waiting period can be expected to reflect a situation different from that encountered immediately after driving). In such cases, the wave analysis produced a very good match between predicted and measured dynamic pile top force. Figures 3.24, 3.28 and 3.32 show such good matches. However, the predictions of ultimate shear resistance were much higher than determined in the static load test. This surprising result can be explained if static and dynamic measurements are obtained and analyzed in a manner similar to those shown in Chapter V of Volume II. Apparently, the present soil model does not distinguish sufficiently well between static and dynamic resistance forces, in cohesive soils. In other words, the linear relationship between pile velocity and damping forces does not hold for all soil types.

While dynamic analysis of piles driven into cohesive soils presents problems regarding proper soil modeling, predictions of

static capacity and the static force distribution are reliable for piles in well drained soils. Frequently, it was found that the match was not good in the latter portion of the record. However, as discussed in Chapter V of Volume II the soil model is very sensitive to small differences in either the quake value or the pile displacement after zero velocity (during unloading). Figure 5.4 of Volume II shows a case where the measured pile resistance force behaved much smoother than the force determined from using the soil model. Thus, oscillations in the pile top force, not present in the measured record, can be explained from this soil model sensitivity. Since the unloading portion of the record is not considered for predictions of resistance forces and their distribution, no error is introduced into the result.

4.3 Simplified Prediction Schemes for Dynamic Testing Method

As outlined in Chapter I a dynamic testing method was proposed (12) for predicting pile bearing capacity. In the application of this method, the time of testing is delayed for a few days so that soil relaxation after driving cannot affect the results. A detailed discussion of the problem of soil relaxation after driving is given by Yang (13). That dynamic records, in fact, reflect the change of soil properties during a waiting period is shown in Chapter V of Volume II. Records obtained this way are then used to predict static bearing capacity from any of the simplified

computation schemes discussed in Chapter VI of Volume II. A special purpose computer can be used to perform the computation and display the result immediately after the blow.

Differences between predicted and actual static bearing capacity can arise from incorrect assumptions about both pile and soil behavior. The investigations in Chapter VI of Volume II clearly show the errors made by assuming the pile to behave like a rigid body in the Phase I and II method. The Phase IIA prediction scheme is a modification of the Phase II method where the pile elasticity has been taken into account. This computation scheme is easily programmed in a special purpose computer. Results seem more reliable than from the best of the energy formulae. Differences between measured and predicted static bearing capacity arise from an uncertainty about the magnitude of damping forces. Since the Phase IIA method uses an average slope approach similar to the Phase II scheme, average damping forces are included in the static prediction. The choice of the time at which this average is taken insures, however, that the influence of dynamic resistance forces will be small.

A Phase III method was developed using the idea of the Delta curves. This method has the advantage of predicting both maximum damping forces and static bearing capacity. Figure 4.2 shows a plot of differences between the measured and predicted static bearing capacity versus maximum damping forces predicted from the Phase III method. The data set used is the same as for the statistical investigations in Chapter III. In this figure, relative

differences and relative damping forces were used for showing the trend more clearly. The conclusion can be drawn that a high percentage of predicted damping force induces more uncertainty about the accuracy of the static result. As can be expected cohesive soils are responsible for the largest errors in the method. Thus, the predictions of static capacity of piles in sandy soils can be considered very reliable. The only exception was F-30 which is a relatively short pile.

A disadvantage of the Phase III method is the complexity of the computations involved. However, it is hoped that simplifying assumptions (e.g. as to the time of toe zero velocity) can possibly lead to a computation scheme more suitable for a special purpose computer application. More studies are necessary in this direction.

4.4 Measurements

Comparisons between predicted and measured pile top force in Chapter III frequently showed differences because of measurement inaccuracies. Most commonly differences in the response of signal conditioning equipment for strain and acceleration lead to time lags. Such differences are serious when short piles are analyzed. (The time lag is Figure (3.48) corresponds to 0.3 L/c). Another error source is the difference in the locations of force and acceleration transducers. Of course, the time lags arising from signal conditioning and recording location can cancel out.

Acceleration measurements were performed with piezoelectric

accelerometers. For measurements at the pile bottom an accelerometer was used having a built-in amplifier. This reduces the effects of cable noise. A disadvantage of this accelerometer is the small recordable minimum acceleration (negative accelerations act away from the base of the transducer). Thus, mounting the instrument upright onto the pile toe plate results in an acceleration cut off at a 250 to 350 g-level. A cutoff of a recorded peak value of 100 g's with a duration of 1 millisecond amounts to a velocity error of 1.6 ft/s. Toe accelerations can become very large, positive or negative, depending on the soil resistance forces. Thus, in records where the above mentioned level was reached, uncertainty exists as to the actual pile toe acceleration and velocity. Figures 3.55 and 3.56, presented in Chapter III, compare measured with predicted pile tip velocity. Good agreement was obtained in these cases because the accelerations did not exceed the recordable limit.

Another difficulty with comparing acceleration measurements at the pile bottom with analysis results from a lumped mass system is the difference in location between recorded and computed results. For short rise times with respect to the pile element length only an average value can be expected from the analysis while the measurement records the extreme toe bottom behavior.

Force records present another problem. Usually it is assumed that no residual forces act on the pile. While this assumption might hold for the first blow, after a waiting period errors might be made for all subsequent blows. Neglecting such residual soil

forces will affect the soil force distribution only, since at the onset of each new blow a state of equilibrium exists for the pile soil system.

CHAPTER V

Conclusions and Recommendations

The methods for pile analysis presented above use measurements, an exact wave theory and a lumped mass analysis in conjunction with assumptions regarding the functional relation between soil forces and pile motion. The analysis makes possible the computation of the magnitude of dynamic and static soil resistance forces acting on the pile under a hammer blow. The static soil resistance forces correspond to those forces acting on the pile during a static load test. Another facet of the presented work is the development of a simple prediction scheme for static bearing capacity based on pile elastic theory.

The field measurements of force and acceleration proved to be accurate enough for commonly encountered full scale piles. The information contained in the records was sufficient to predict the magnitude and distribution of the soil resistance forces as long as the soil model was adequate. Distinction of soil force types regarding their velocity or displacement dependency was very successful for piles in sandy soils and yielded relatively good approximations in cohesive soils.

The present method bypasses a major shortcoming of other pile dynamic analyses found in the literature, namely the uncertainty of hammer input and soil parameters. In fact, the results obtained from the automated prediction scheme can be used to give information

on soil behavior which is in contrast to the usual procedures of first obtaining the soil properties by laboratory testing and then performing the pile analysis.

The predictions of static bearing capacity show a correlation substantially better than those obtained from existing methods (References 9, 10). Improvements can be expected when further soil investigations are performed in a manner as discussed in Chapter V of Volume II. Thus, different from the usual soil mechanics approach of obtaining soil properties in the laboratory, knowledge about the gross soil response to a certain pile type is obtained. The cylindrical piles, which were used throughout the experimental work reported herein, are very common, however, other pile types might possibly show different behavior due to a pile shape influence. It is possible that an H-pile, for example, would behave very differently than a pipe pile. It is hoped that such an effort would lead to an improved soil rheological model which equally well, describes both non-cohesive and cohesive soils. A more realistic model than presently used is discussed in Reference 14. Then, from such an improved soil model, a classification of the soil type surrounding the pile could complete the prediction of pile static behavior by indicating the soil creep and strength gain behavior.

The computer program was devised for the case of a uniform pile. In order to minimize the input data, ten elements were always used with a time increment of one half of the critical time

(see Chapter I of Volume II). These assumptions might not hold for long or nonuniform piles. For generalizing the present routine, a study on Measured Delta curves for piles with variable stiffnesses and the revision of the lumped mass analysis is recommended.

It was found that damping forces usually act in a large amount at the pile tip while smaller magnitudes of dynamic resistance forces act at the pile skin. In order to simplify the program and save computing time it is recommended that the damping distribution be selected a priori and only one solution be obtained.

Another important facet of pile driving is the selection of hammers, piles, and cushions. In Chapter IV suggestions were given on how such problems may be approached by means of wave considerations. The objective of such investigations would be a closed form method for estimating the necessary properties of piles and pile driving equipment.

Regarding the measurements of pile top force and acceleration the following recommendations can be made:

(i) The transducer cushion (i.e. the cushioning between hammer and force transducer, initially added for obtaining smoother records) has to be reduced, if not completely eliminated, to obtain a faster impact.

(ii) Another type of signal conditioning equipment for strain has to be used for smaller time lags between the force and velocity record.

As discussed in Chapter IV, care has to be taken in recording

pile toe accelerations for piles with low resistance since it is possible that up to twice the top accelerations occur, exceeding the accelerometer capacity.

The results obtained from the present method were very encouraging. This method seems well-suited to be employed in subsurface soil explorations. A related study is reported by Tsai, Schmid (14) where an instrumented penetrometer is used for data collection. However, the present method has the advantage of providing knowledge about resistance forces acting along the pile skin.

Another important result of the studies presented in this report was the improvement of an existing simplified prediction scheme for static bearing capacity. A further step to a realistic dynamic pile testing procedure will be to incorporate the Phase IIA scheme in a special purpose computer and to test the method on a sufficient number of piles in the field where common pile materials like timber and concrete are also included. Also, tests on piles of greater length and of variable cross section should be performed. The Phase III method should be modified such that a relatively simple computer can perform the necessary computations. This new computer should yield as an output the predictions of both maximum damping force and the static bearing capacity. With more results from piles tested under different conditions a statistical analysis should then be performed so that an answer about the reliability and precision of the method can be obtained. It would then be possible to recommend with confidence a design load for a certain dynamic prediction of static bearing capacity.

References

1. Goble, G. G., Scanlan, R. H., Tomko, J. J., "Dynamic Studies on the Bearing Capacity of Piles", Project Report of Phase I, Case Institute of Technology, July, 1967.

2. Goble, G. G., Tomko, J. J., Rausche, F., Green, P. M., "Dynamic Studies on the Bearing Capacity of Piles", Project Report of Phase II, Case Western Reserve University, July, 1968.

3. Smith, E. A. L., "Pile Driving Analysis by the Wave Equation", Journal of Soil Mechanics and Foundations, American Society of Civil Engineers, 86, August, 1960, pp. 35-61.

4. Newmark, N. M., "A Method of Computation for Structural Dynamics", Proceedings, ASCE, 85, EM3, 1959, p. 67.

5. Timoshenko, S. and Goodier, J. M., "Theory of Elasticity", McGraw-Hill, Second Edition, 1951, p. 438.

6. Donnell, L. H., "Longitudinal Wave Transmission and Impact" Transactions, ASME, Applied Mechanics Division, APM-52-14, 1930.

7. Samson, C. H., Hirsch, T. L. and Lowery, L. L., "Computer Study of the Dynamic Behavior of Piling", Journal of the Structural Division, Proceedings, ASCE, Paper No. 3608, ST4, August, 1963.

8. LaPay, W. S., "Dynamic Pile Behavior - Literature Survey and Response Studies", Master's Thesis, Case Institute of Technology, 1965.

9. Olson, R. E. and Flaate, R. S., "Pile Driving Formulas for Friction Piles in Sand," Journal of the Soil Mechanics and Foundation Division, ASCE, Vol. 93, No. SM6, November, 1967, pp. 279-296.

10. Tomko, J. J., "Dynamic Studies on Predicting the Static Bearing Capacity of Piles", Ph.D. Disseration, Case Western Reserve University, 1968.

11. Forehand, P. W. and Reese, J. L., "Prediction of Pile Capacity by the Wave Equation", Journal of the Soil Mechanics and Foundation Division, ASCE, 90, (March 1964), pp. 1-25.

12. Goble, G. G., Scanlan, R. H., Tomko, J. J., "Dynamic Studies on the Bearing Capacity of Piles", paper presented to the Highway Research Board Annual Meeting, Jan. 1967, Washington, D. C.

13. Yang, N. C., "Relaxation of Piles in Sand and Inorganic Silt", Journal of the Soil Mechanics and Foundation Division, Proc. ASCE, SM2, March 1970.

14. Tsai, K. W. and Schmid, W. E., "Penetrometer Method for Determining Soil Parameters", Proceedings of the Seventh International Conference on Soil Mechanics and Foundation Engineering, Mexico, 1969, Vol. 1, pp. 443-448.

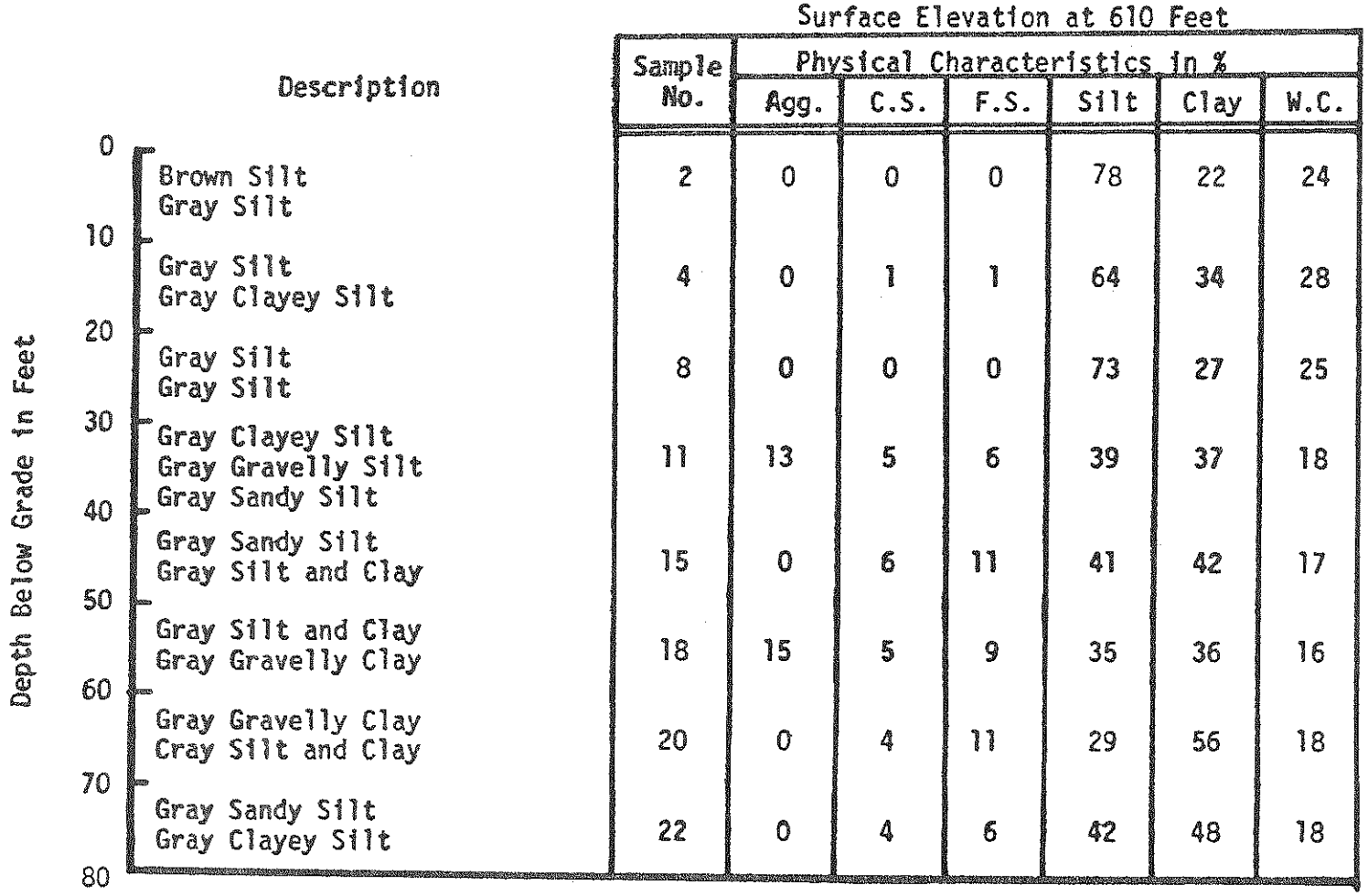

Sample No.	Physical Characteristics in %					
	Agg.	C.S.	F.S.	Silt	Clay	W.C.
2	0	0	0	78	22	24
4	0	1	1	64	34	28
8	0	0	0	73	27	25
11	13	5	6	39	37	18
15	0	6	11	41	42	17
18	15	5	9	35	36	16
20	0	4	11	29	56	18
22	0	4	6	42	48	18

TABLE 1.1: SOIL CHARACTERISTICS AT TEST SITE IN TOLEDO

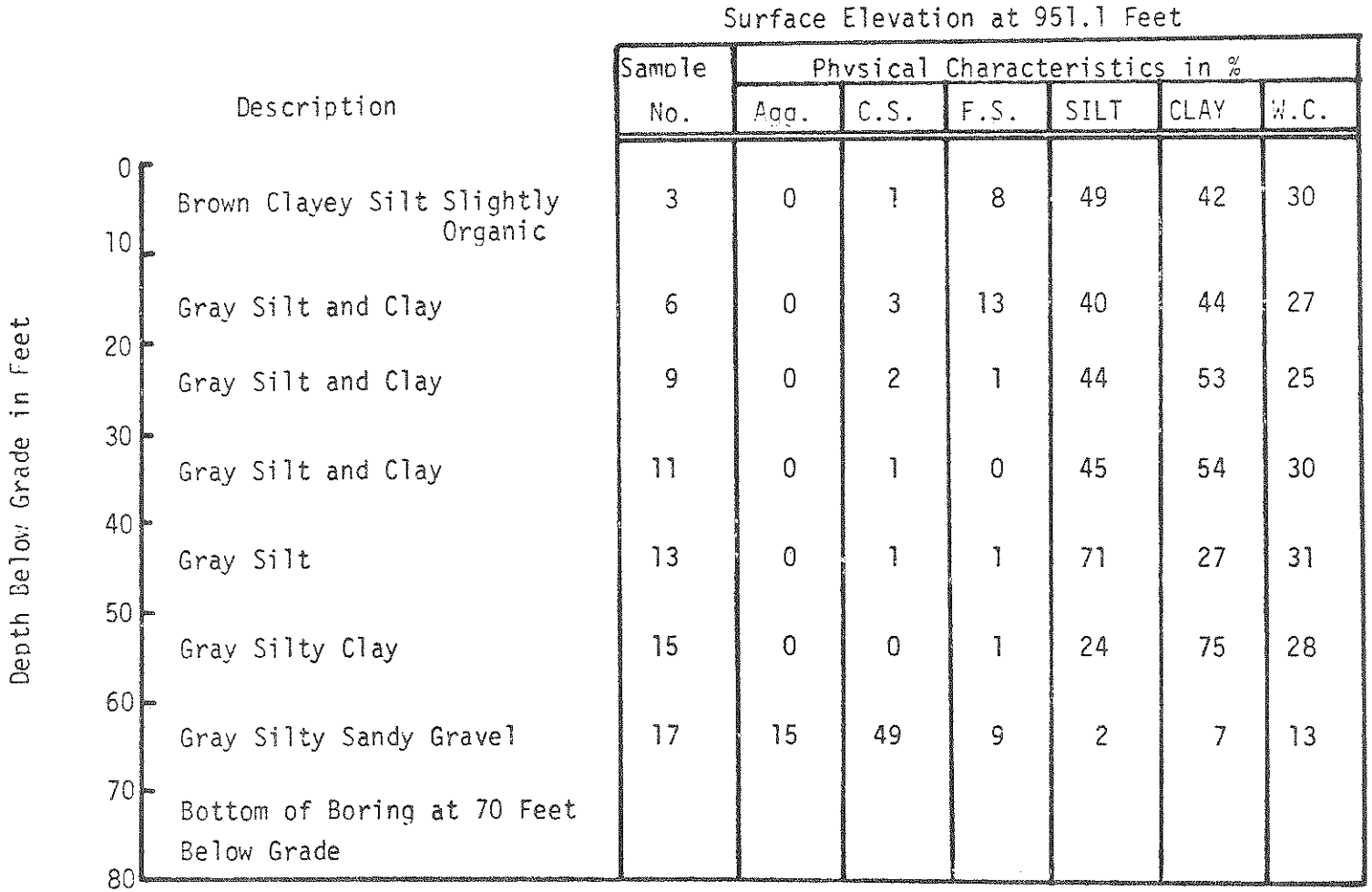

Description	Sample No.	Physical Characteristics in %					
		Agg.	C.S.	F.S.	SILT	CLAY	W.C.
Brown Clayey Silt Slightly Organic	3	0	1	8	49	42	30
Gray Silt and Clay	6	0	3	13	40	44	27
Gray Silt and Clay	9	0	2	1	44	53	25
Gray Silt and Clay	11	0	1	0	45	54	30
Gray Silt	13	0	1	1	71	27	31
Gray Silty Clay	15	0	0	1	24	75	28
Gray Silty Sandy Gravel	17	15	49	9	2	7	13
Bottom of Boring at 70 Feet Below Grade							

TABLE 1.2: SOIL CHARACTERISTICS AT TEST SITE IN RITTMAN OHIO

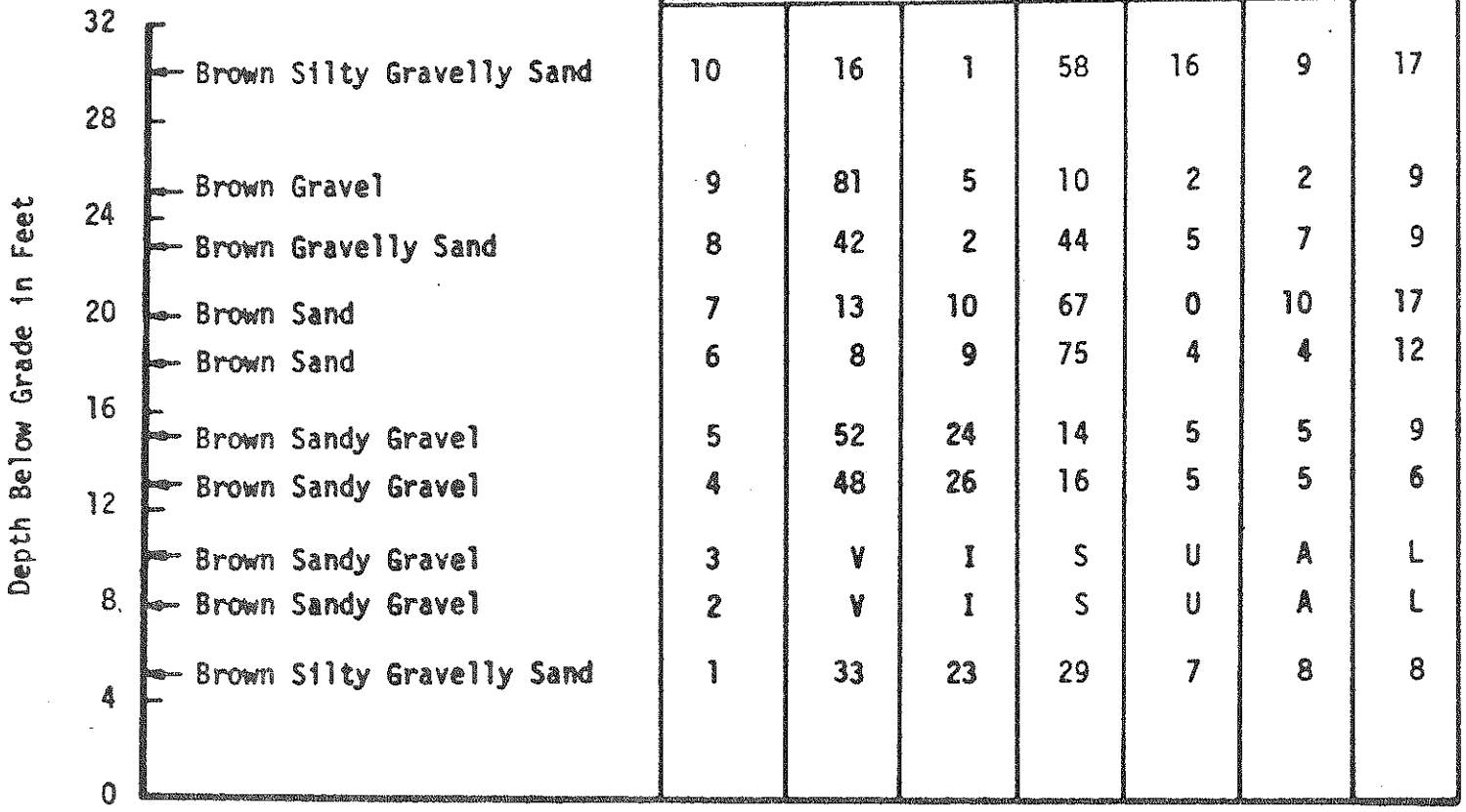

Sample No.	Physical Characteristics in %					
	Agg.	C.S.	F.S.	Silt	Clay	W.C.
10	16	1	58	16	9	17
9	81	5	10	2	2	9
8	42	2	44	5	7	9
7	13	10	67	0	10	17
6	8	9	75	4	4	12
5	52	24	14	5	5	9
4	48	26	16	5	5	6
3	V	I	S	U	A	L
2	V	I	S	U	A	L
1	33	23	29	7	8	8

TABLE 1.3: SOIL CHARACTERISTICS AT TEST SITE FOR REDUCED SCALE PILES

Pile No.	Pile Name	q_1	q_5	q_{10}
3	531-76	.12	.12	.09
5	F-30	.07	.06	.05
6	F-30A	.09	.07	.05
7	F-50	.10	.08	.07
8	F-50A	.10	.07	.05
9	F-60	.12	.09	.07
10	F-60A	.11	.09	.07
11	Cincinnati	.11	.09	.06
12	272 Toledo	.12	.09	.07
13	To-50	.08	.07	.06
14	To-50A	.11	.09	.07
15	To-60	.07	.06	.05
16	To-60A	.10	.08	.06
17	Logan	.12	.12	.10
18	W-56	.12	.10	.07
19	W-76	.12	.10	.07
20	Chillicothe	.10	.08	.06
21	Ri-50	.06	.06	.05
22	Ri-50A	.12	.12	.10
23	Ri-60	.11	.10	.09
24	Ri-60A	.11	.10	.08

Not listed values can be obtained by interpolation

TABLE 2.1: TABULATION OF QUAKES USED IN PREDICTION ANALYSES

DATA SET NO.	PILE NAME	DATE DRIVEN	DATE LOAD TESTED	DATE OF DYN. MEAS.	SOIL	LENGTH L	AREA A IN^2	HAMMER	REMARKS
1	C-1	12-28-66	12-30-66	1-3-67	G.Sa.	58	5.81	D-12	Fluted and Tapered
2	531-70	4-12-67	5-12-67	4-13-67		70	5.81		
3	531-76	4-13-67	4-17-67	4-18-67		82	5.81		
4	531-83	4-18-67	4-18-67	4-18-67		82	5.81		
5	F-30	6-21-67	6-21-67	6-21-67	Si & Sa	32.5	9.82	L.B.	Special Test
6	F-30A	6-21-67	6-28-67	6-28-67		32.5	9.82		
7	F-50	6-28-67	6-28-67	6-28-67		50.5	9.82		
8	F-50A	6-28-67	7-5-67	7-6-67		50.5	9.82		
9	F-60	7-7-67	7-7-67	7-7-67		59.5	9.82		
10	F-60A	7-7-67	7-20-67	7-20-67		59.5	9.82		
11	Cincinnati	12-22-67	1-4-68	1-4-68	G.Sa.	69	6.66	D-12	
12	272 Toledo	4-10-68	4-17-68	5-18-68	Si.&C	54	6.66	L.B.	
13	To-50	9-6-68	9-6-68	9-6-68	see Table 1.1	49	9.82	D-12	Special Test
14	To-50A	9-6-68	9-9-68	9-10-68		49	9.82		
15	To-60	9-11-68	9-11-68	9-11-68		59	9.82		
16	To-60A	9-11-68	9-18-68	9-18-68		59	9.82		
17	Logan	11-25-68	11-5-68	11-5-68	G.Sa	57	6.66		
18	W-56	6-11-69	6-18-69	6-18-69	Si.&C	55	6.66		
19	W-76	6-19-69	6-24-69	6-24-69		75	6.66		
20	Chillicothe	9-18-69	9-25-69	9-25-69	G.&S	40.5	6.66		
21	Ri-50	1-6-70	1-6-70	1-6-70	see Table 1.2	49	9.31		Special Test
22	Ri-50	1-6-70	1-6-70	1-6-70		49	9.31		
23	Ri-60	1-9-70	1-9-70	1-9-70		61.5	9.31		
24	Ri-60A	1-9-70	1-20-70	1-20-70		57	9.31		

All piles were of 12-inch diameter pipe.

G.Sa. Gravelly Sand
Si & Sa Silt and Sand
Si & C Silt and Clay
G & S Gravel and Sand

D-12 Delmag
L.B. Linkbelt 440

TABLE 3.1: DESCRIPTION OF FULL SCALE TEST PILES

DATA SET NO.	PILE NAME	DATE DRIVEN	DATE LOAD TESTED	DATE OF DYN. MEAS.	SOIL	LENGTH L FT	REMARKS
1	2-R-10	7-27-67	7-27-67	7-27-67	Silt and Clay	10.8	
2	2-R-10A	7-27-67	8-1-67	8-1-67		15.8	
3	2-R-15	8-1-67	8-1-67	8-1-67		15.8	
4	2-R-15A	8-1-67	8-4-67	8-4-67		20.8	
5	2-R-20	8-4-67	8-4-67	8-4-67		20.8	
6	2-R-20A	8-4-67	8-9-67	8-9-67		23.8	
7	3-R-10	8-18-67	8-18-67	8-18-67		10.8	
8	3-R-10A	8-18-67	8-22-67	8-22-67		15.8	
9	3-R-15	8-22-67	8-22-67	8-22-67		15.8	
10	3-R-15A	8-22-67	8-28-67	8-28-67		20.8	
11	3-R-20	8-30-67	8-30-67	8-30-67		20.8	
12	3-R-20A	8-30-67	9-5-67	9-5-67		23.8	
13	1-T-15/20	11-25-67	11-25-67	11-25-67	see Table 1.3	22.4	3 additional force records
14	1-T-15/20	11-25-67	12-2-67	12-2-67		22.4	
15	2-T-15/20	12-28-67	12-28-67	12-28-67		22.4	
16	2-T-15/20A	12-28-67	1-13-68	1-13-68		22.4	
17	3-T-15	6-11-68	6-11-68	6-11-68		22.4	
18	3-T-15/20A	6-11-68	6-17-68	6-17-68		22.4	
19	4-T-15/20	6-29-68	6-29-68	6-29-68		22.4	
20	4-T-15/20A	6-29068	7-3-68	7-3-68		22.4	
21	6-T-15	7-31-69	7-31-69	7-31-69		20.1	Record of Toe Acceleration
22	6-T-15A	7-31-69	8-7-69	8-7-69		20.1	
23	6-T-20	8-7-69	8-7-69	8-7-69		20.1	
24	6-T-20A	8-7-69	8-15-69	8-15-69		20.1	

Cross Sectional Area = 1.7 in^2 for all listed piles

TABLE 3.2: DESCRIPTION OF REDUCED SCALE TEST PILES

DATA SET NO.	PILE NAME	LOAD TEST RESULT AT max d_A R_d	LOAD TEST RESULT AT ULTIMATE[1] R_u	PRECOMPRESSION FORCE S_p	PREDICTED SHEAR FORCES S_o	PREDICTED STATIC RESISTANCE R_o	TOTAL MAX. DAMPING FORCES max D
3	531-76	154	198	18	141	159	15
5	F-30	86	107	33	55	88	39
6	F-30	107	112	30	106	136	24
7	F-50	172	224	29	138	167	41
8	F-50	200	238	52	178	230	52
9	F-60	176	204	29	171	200	25
10	F-60	174	242	40	158	198	52
11	Cincinnati	137	190	39	122	161	17
12	272 Toledo	183	221	66	138	229	22
12[2]	272 Toledo	183	221	66	138	204	22
13	To-50	60	69	26	36	62	57
14	To-50	93	94	33	86	119	88
15	To-60	32	43	29	26	55	69
16	To-60	75	86	25	94	119	106
17	Logan	165	220	13	167	180	54
18	W-56	90	92	20	123	143	125
19	W-76	125	160	22	139	161	141
19[2]	W-76	125	160	22	129	151	127
20	Chillicothe	152	207	18	133	151	18
21	Ri-50	40	46	23	22	45	88
22	Ri-50	64	64	15	70	85	105
23	Ri-60	176	-[3]	22	167	189	92
24	Ri-60	174	-[3]	9	185	194	48

[1]Ultimate may be defined here as the maximum value obtained in the load test
[2]Obtained by inspection
[3]Load test incomplete

ALL RESULTS IN KIPS

TABLE 3.3: SUMMARY OF RESULTS FROM WAVE ANALYSIS

DATA SET NO.	PILE NAME	R_d	R_u	PHASE I	PHASE II	PHASE IIA	PHASE III	WAVE ANALYSIS
1	C-1	180	193	174^{1}	138^{1}	173^{3}	170^{3}	*
2	531-70	122	190	201^{3}	197^{3}	141^{3}	173^{3}	*
3	531-76	154	198	170^{4}	157^{4}	115^{4}	137^{4}	159^{1}
4	531-83	110	200	211^{3}	187^{3}	143^{3}	154^{3}	*
5	F-30	86	107	125^{5}	113^{5}	110^{5}	98^{5}	91^{2}
6	F-30A	107	112	162^{4}	152^{4}	164^{5}	172^{5}	136^{1}
7	F-50	172	224	281^{3}	197^{3}	177^{3}	175^{3}	163^{3}
8	F-50A	200	238	294^{4}	258^{4}	205^{4}	236^{4}	233^{2}
9	F-60	176	204	288^{4}	251^{4}	207^{4}	233^{4}	210^{2}
10	F-60A	174	242	255^{3}	226^{3}	188^{3}	195^{3}	180^{2}
11	Cincinnati	137	190	250^{3}	185^{3}	138^{3}	175^{3}	166^{3}
12	272	183	221	315^{7}	275^{7}	267^{7}	231^{7}	204^{1}
13	To-50	60	69	69^{3}	63^{3}	77^{5}	60^{5}	69^{2}
14	To-50A	93	94	121^{6}	129^{6}	105^{6}	115^{2}	119^{1}
15	To-60	32	43	89^{4}	81^{4}	77^{4}	62^{4}	56^{2}
16	To-60A	75	86	141^{3}	137^{3}	113^{3}	121^{3}	122^{2}
17	Logan	165	220	275^{4}	223^{4}	180^{4}	177^{4}	173^{2}
18	W-56	90	92	207^{4}	227^{4}	161^{4}	184^{4}	151^{4}
19	W-76	125	160	276^{5}	264^{5}	167^{5}	143^{1}	151^{1}
20	Chillicothe	152	207	316^{3}	200^{3}	180^{3}	173^{3}	163^{2}
21	Ri-50	40	46	-	-	64^{3}	70^{3}	45^{1}
22	Ri-50A	64	64	-	-	120^{3}	110^{3}	84^{3}
23	Ri-60	176	-	264^{3}	251^{3}	140^{3}	172^{3}	184^{2}
24	Ri-60A	174	-	179^{2}	184^{2}	162^{3}	187^{3}	187^{2}

Numerals on predictions indicate the number of blows analyzed.
*Force rise time too slow for application of the wave analysis.

TABLE 3.4: SUMMARY OF RESULTS FOR PREDICTING STATIC BEARING CAPACITY ON FULL SCALE PILES

PILE NO.	PILE NAME	R_u	PHASE I	PHASE II	PHASE IIA	PHASE III
1	2-R-10	12.1	19.6^{2}	19.2^{2}	12.9^{3}	19.3^{3}
2	2-R-10A	12.1	23.5^{2}	17.4^{2}	15.5^{3}	23.4^{3}
3	2-R-15	13.0	26.2^{3}	17.1^{3}	20.7^{3}	30.2^{3}
4	2-R-15A	16.3	31.8^{3}	26.4^{3}	21.0^{3}	34.2^{3}
5	2-R-20	18.1	33.5^{4}	37.1^{4}	22.2^{4}	38.4^{4}
6	2-R-20A	20.2	39.4^{4}	44.8^{4}	32.6^{4}	41.7^{4}
7	3-R-10	10.8	15.0^{3}	16.3^{3}	13.0^{3}	22.2^{3}
8	3-R-10A	11.5	26.9^{3}	16.5^{3}	12.7^{3}	21.8^{3}
9	3-R-15	11.0	20.2^{3}	14.8^{3}	8.5^{3}	27.8^{3}
10	3-R-15A	15.3	31.8^{3}	23.4^{3}	13.8^{3}	32.5^{3}
11	3-R-20	16.0	24.0^{3}	20.4^{3}	9.5^{3}	35.1^{3}
12	3-R-20A	17.7	34.8^{6}	34.9^{6}	20.5^{6}	35.2^{6}
13	1-T-15/20	15.8	23.0^{1}	16.1^{1}	12.1^{1}	9.6^{1}
14	1-T-15/20A	17.4	26.4^{3}	23.5^{3}	16.1^{3}	22.5^{3}
15	2-T-15/20	15.0	17.9^{1}	14.3^{1}	8.7^{1}	15.5^{1}
16	2-T-15/20A	22.0	20.6^{1}	20.5^{1}	13.1^{1}	24.7^{1}
17	3-T-15/20	14.0	16.7^{2}	12.8^{3}	13.1^{3}	14.6^{3}
18	3-T-15/20A	15.1	22.2^{2}	16.4^{3}	15.4^{3}	18.1^{3}
19	4-T-15/20	12.4	13.1^{5}	10.3^{5}	12.3^{5}	13.6^{5}
20	4-T-15/20A	13.8	15.4^{4}	11.9^{4}	13.0^{4}	18.0^{4}
21	6-T-15	12.6	25.2^{2}	14.3^{2}	9.8^{2}	12.7^{2}
22	6-T-15A	14.5	18.3^{3}	15.4^{3}	10.8^{3}	15.5^{3}
23	6-T-20	12.8	24.5^{3}	11.7^{3}	12.7^{3}	16.6^{3}
24	6-T-20A	15.2	14.3^{2}	13.2^{2}	8.0^{2}	17.3^{2}

Numerals on predictions indicate the number of blows analyzed.

TABLE 3.5: SUMMARY OF RESULTS FOR PREDICTING STATIC BEARING CAPACITY ON REDUCED SCALE PILES

METHOD	SLOPE $m \pm \sigma_m$	INTERCEPT (kips) $b \pm \sigma_b$	CORRELATION COEFFICIENT r
Phase IIA	0.99 $\pm$0.15	-19 $\pm$22	.83
Phase III	0.86 $\pm$0.11	-7 $\pm$17	.87
Analysis	0.94 $\pm$0.07	-11 $\pm$10	.94
Enging. News	.33	+74	.29
Gow	.32	+74	.36
Hiley	.92	+14	.72
Pacific Coast	1.04	+14	.76
Jambu	.87	+20	.81
Danish	.77	-4	.81
Gates	1.81	-96	.81

TABLE 3.6: STATISTICAL PARAMETERS FOR SIMPLIFIED METHODS AND ENERGY FORMULAS (16)

	ELEMENT NUMBER										
DATA SET NO.	1	2	3	4	5	6	7	8	9	10	EA/c
3	0	0	0	0	.017	0	0	0	.173	.148	10.5
5	0	0	0	0	.025	0	0	0	.160	.158	17.8
6	0	0	0	0	.104	0	0	0	.129	.317	17.8
7	0	0	0	0	0	0	0	0	.158	.150	17.8
8	0	0	0	.009	.081	.046	.049	.055	.055	.090	17.8
9	0	0	0	0	.003	0	.001	.024	.028	.140	17.8
10	0	0	0	0	.001	.005	.003	0	.560	.394	17.8
11	0	0	0	0	.134	0	0	0	0	.041	12.1
12	0	0	0	0	0	0	0	0	0	.254	12.1
13	0	0	0	.032	0	0	0	.114	.234	.122	17.8
14	0	0	0	.435	0	0	0	0	.112	.412	17.8
15	0	0	.157	.012	0	0	.001	.008	0	.554	17.8
16	0	0	.312	0	0	0	0	0	.431	.424	17.8
17	0	0	.009	0	0	.012	0	.020	.025	.455	12.1
18	0	0	0	.021	.445	.032	.040	.047	.042	1.312	12.1
19	0	.072	.053	0	.308	0	.042	0	0	2.370	12.1
20	0	0	.110	0	0	0	0	0	0	.260	12.1
21	0	0	0	.100	0	0	0	0	.263	.292	16.9
22	0	0	.039	0	0	0	0	0	.246	.309	16.9
23	0	0	0	.087	0	.013	0	0	.017	.338	16.9
24	0	0	0	.110	.016	.017	.018	.019	.020	.117	16.9

TABLE 4.1: DIMENSIONLESS DAMPING COEFFICIENT $d_n/(EA/c)$ AS DETERMINED BY WAVE ANALYSIS

DATA SET NO.	ELEMENT NUMBER 1	2	3	4	5	6	7	8	9	10	Element length ft	Enclosed cross sectional area in^2
3	0	0	0	0	.18	0	0	0	1.82	1.55	8.20	28 (at tip)
5	0	0	0	0	.45	0	0	0	2.86	2.80	3.25	128
6	0	0	0	0	1.85	0	0	0	2.29	5.65	3.25	128
7	0	0	0	0	0	0	0	0	2.80	2.68	5.05	128
8	0	0	0	.16	1.44	.82	.88	.98	.99	1.60	5.05	128
9	0	0	0	0	.06	0	.02	.43	.49	2.50	5.95	128
10	0	0	0	0	.03	.09	.05	0	.10	6.97	5.95	128
11	0	0	0	0	1.62	0	0	0	0	.50	6.90	113
12	0	0	0	0	0	0	0	0	3.17	3.17	5.40	113
13	0	0	0	.56	0	0	0	2.03	4.17	2.17	4.90	128
14	0	0	0	7.75	0	0	0	0	2.00	7.35	4.90	128
15	0	0	2.81	.20	0	0	.02	.14	0	9.89	5.90	128
16	0	0	5.55	0	0	0	0	0	7.67	7.54	5.90	128
17	0	0	.06	0	0	.14	0	.24	.30	5.50	5.70	113
18	0	0	0	.25	5.37	.39	.48	.57	.51	15.84	5.50	113
19	0	.87	.64	0	3.70	0	.50	0	0	28.6	7.50	113
20	0	0	1.33	0	0	0	0	0	0	3.15	4.05	113
21	0	0	0	1.67	0	0	0	0	4.44	4.93	4.90	113
22	0	0	.65	0	0	0	0	0	3.90	5.22	4.90	113
23	0	0	0	1.47	0	.23	0	0	.29	5.70	6.15	113
24	0	0	0	1.85	.28	.29	.30	.32	.34	1.97	5.70	113

TABLE 4.2: NATURAL DAMPING COEFFICIENTS d_n[kips/ft/sec] AS DETERMINED BY WAVE ANALYSIS

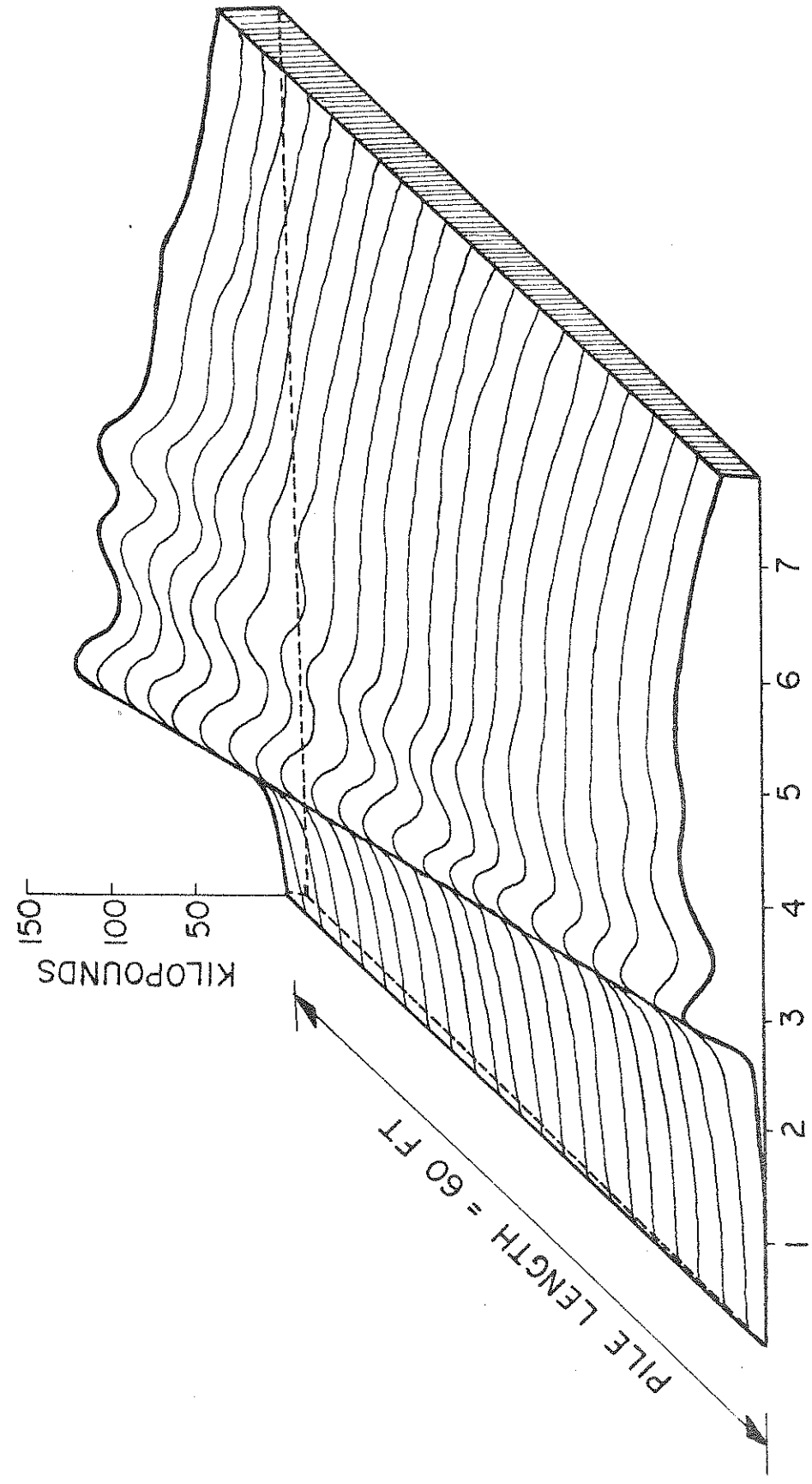

FIGURE 1.1: FORCES IN PILE UNDER A HAMMER BLOW (To-60 BLOW No. 4-A)

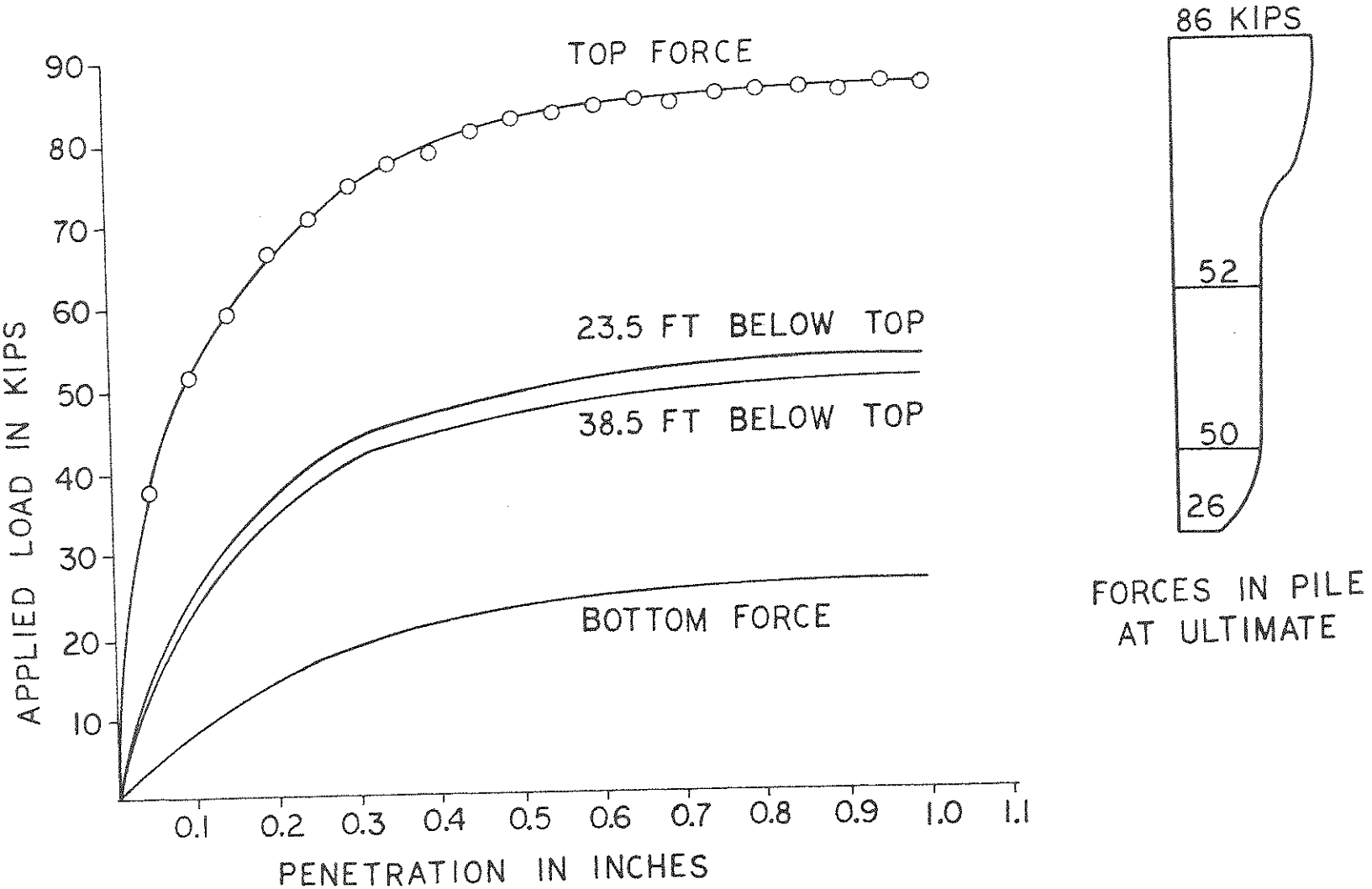

FIGURE 1.2: STATIC LOAD TEST RESULTS FOR FULL SCALE PILE To-60

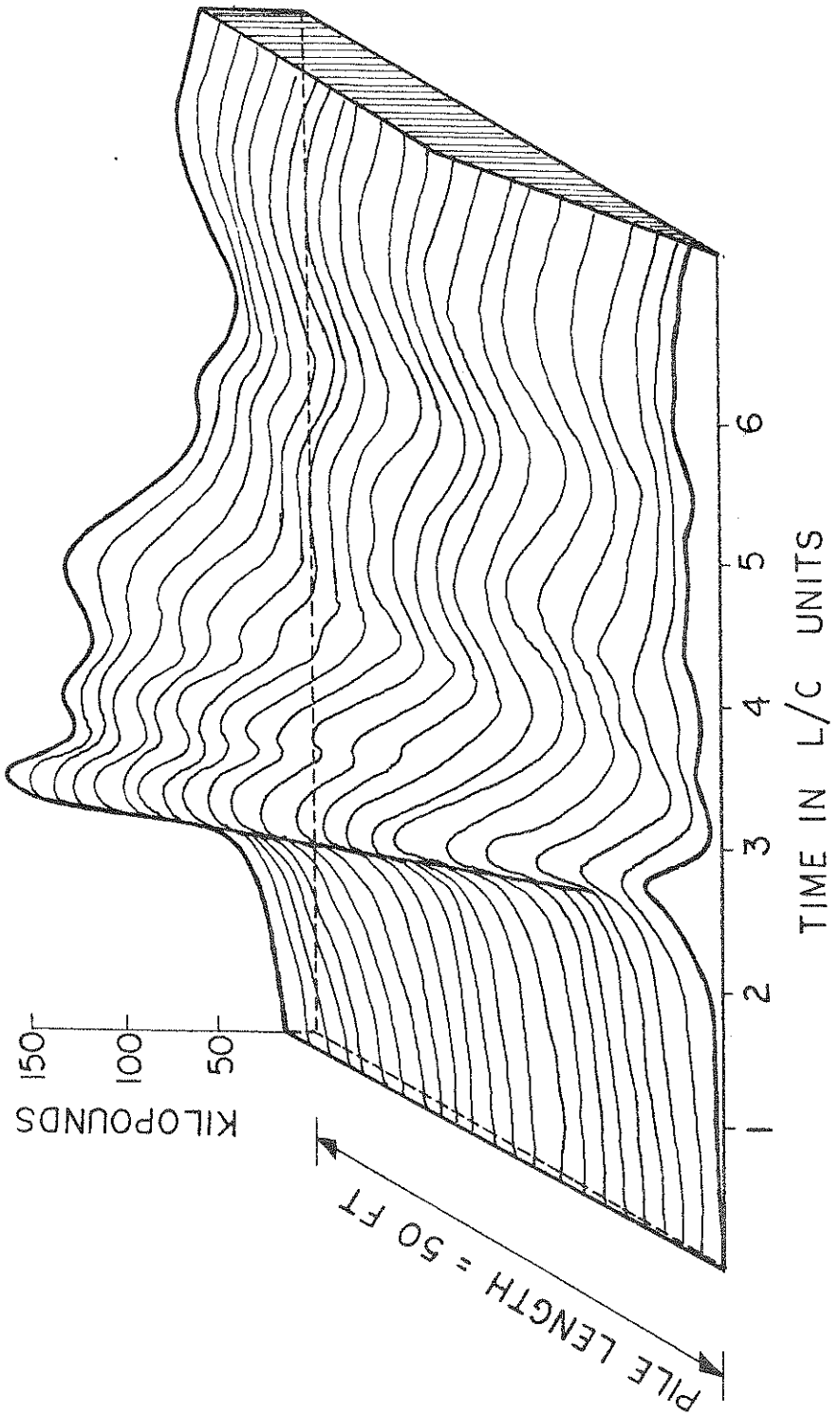

FIGURE 1.3: FORCES IN PILE UNDER A HAMMER BLOW (Ri-50 BLOW No. 8-A)

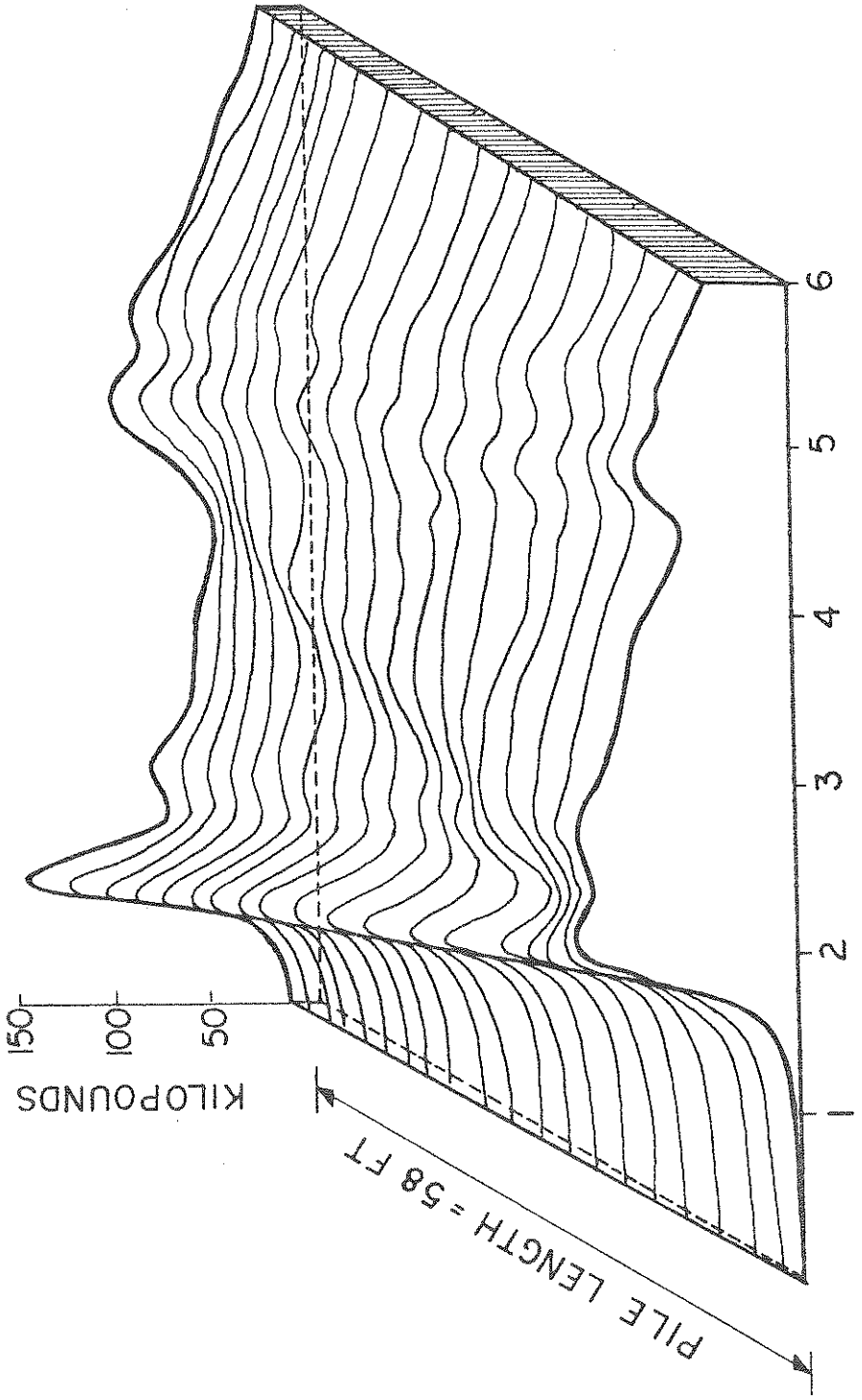

FIGURE 1.4: FORCES IN PILE UNDER A HAMMER BLOW (Ri-60 BLOW No. 22)

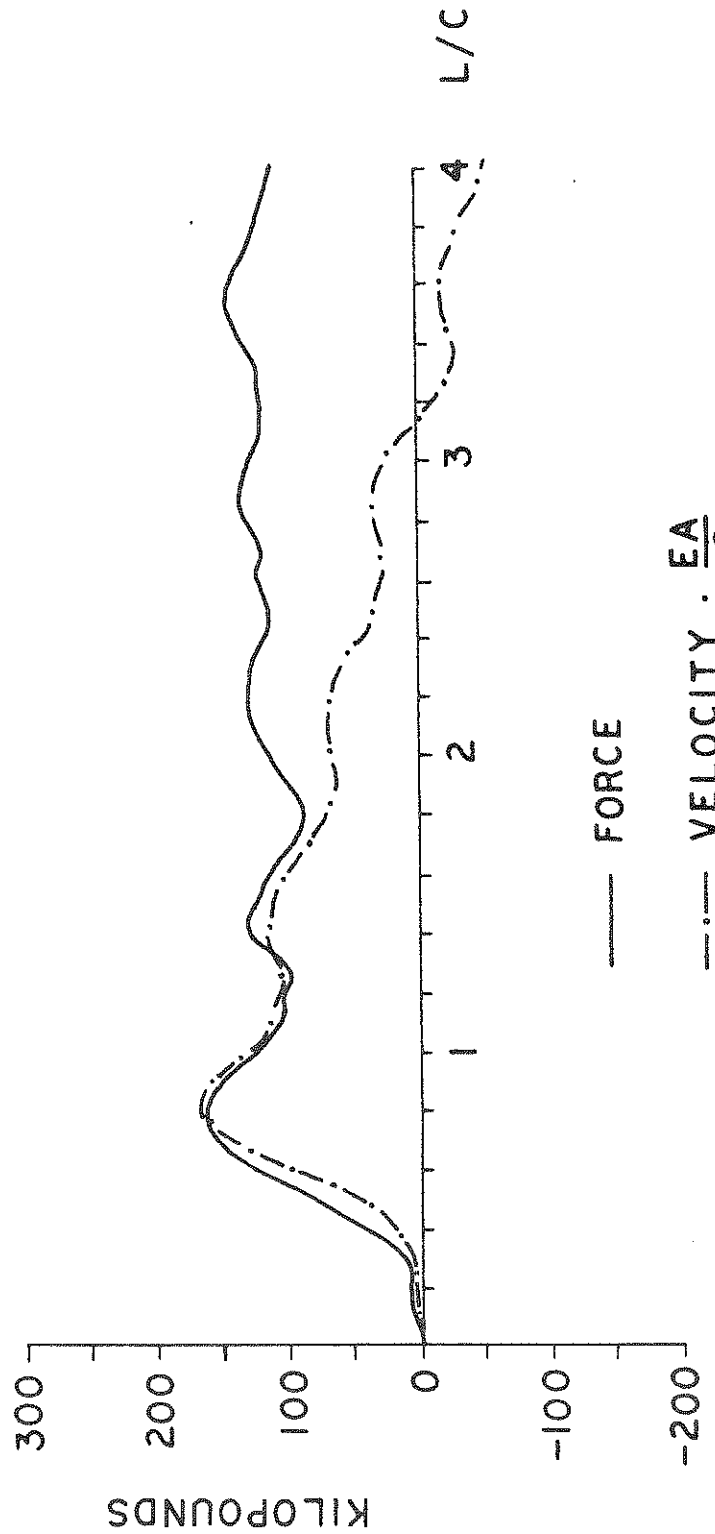

FIGURE 2.1: TYPICAL FORCE AND VELOCITY RECORD (FULL SCALE PILE F-60A, BLOW NO. 26-A)

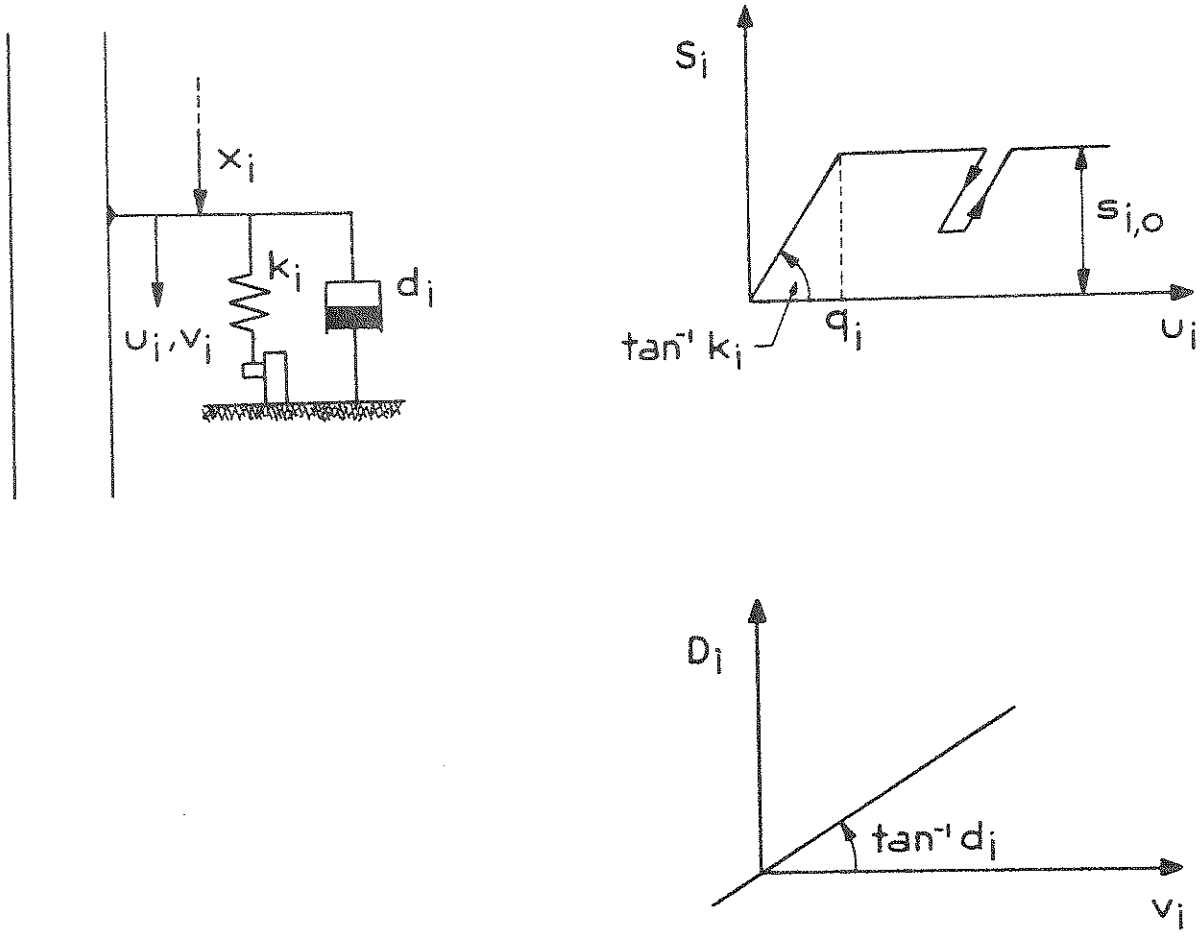

FIGURE 2.2: SOIL RESISTANCE LAW

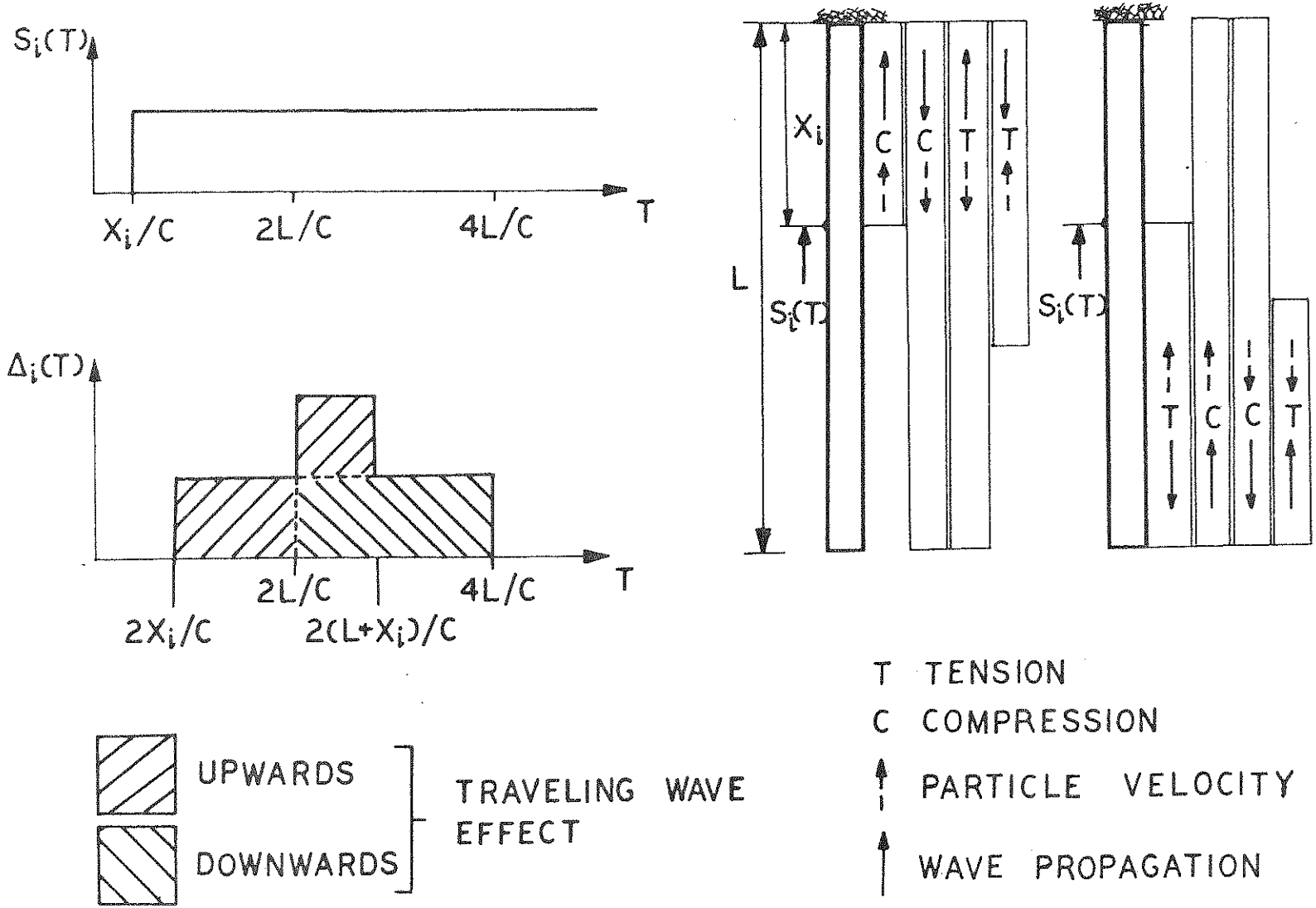

FIGURE 2.3: DEVELOPMENT OF RESISTANCE DELTA CURVE FOR CONSTANT SHEAR FORCE

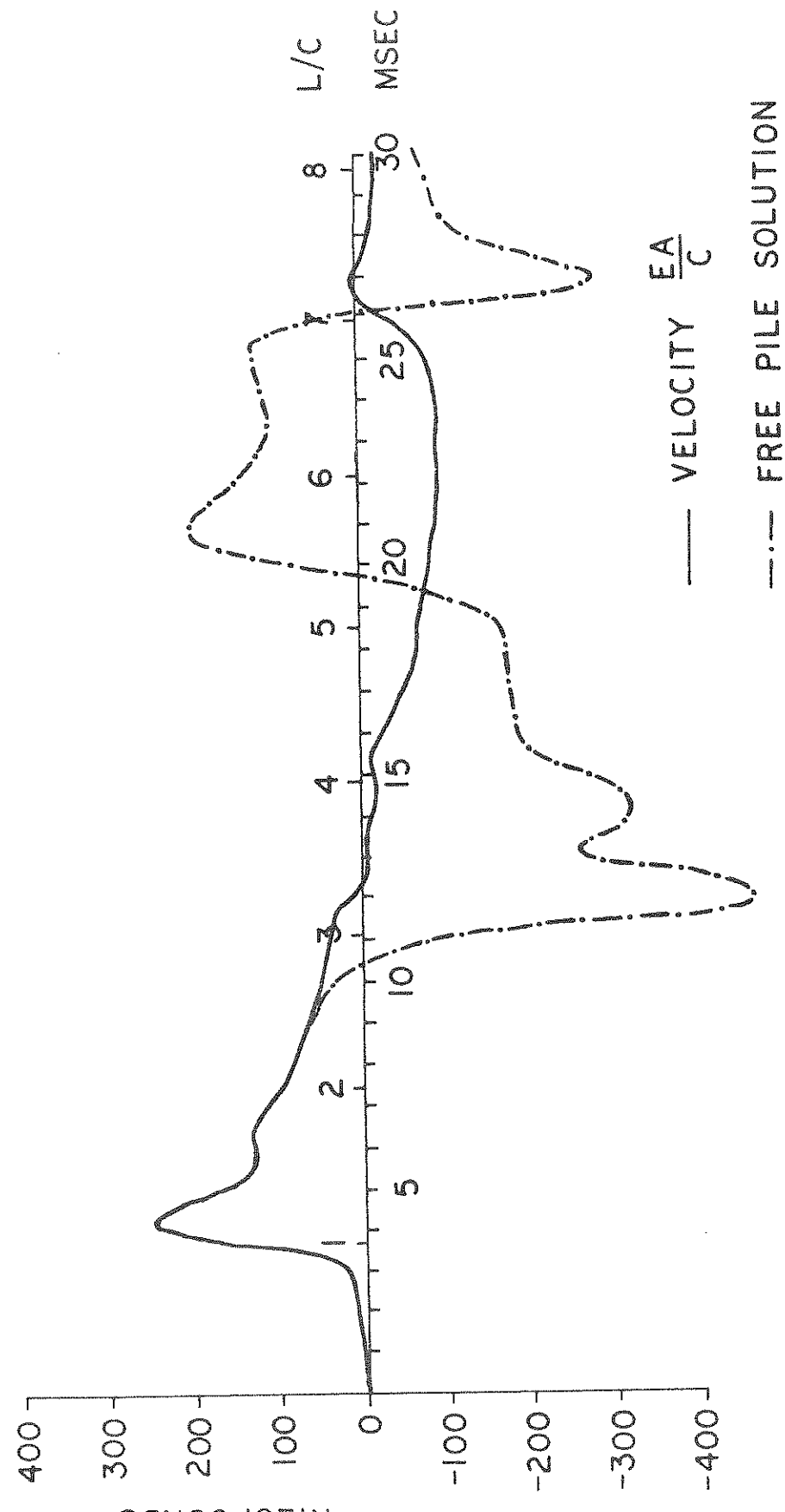

FIGURE 2.4: VELOCITY MULTIPLIED BY EA/c AND FREE PILE SOLUTION (RI-60 BLOW No. 18)

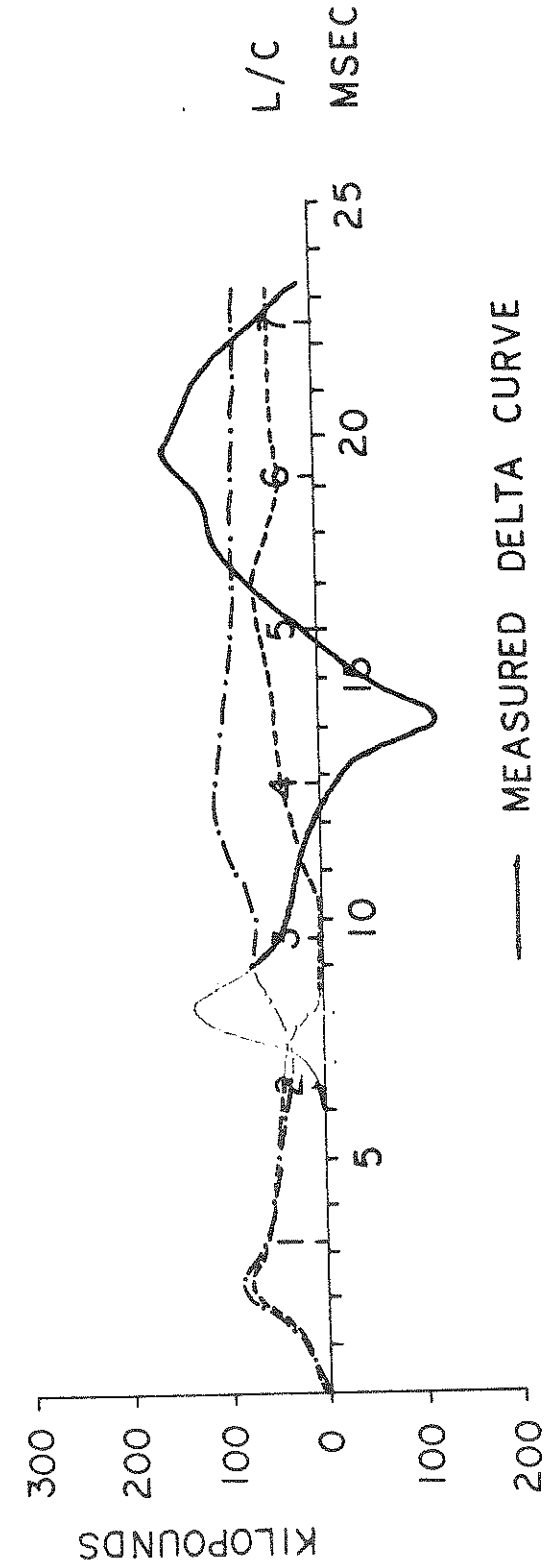

FIGURE 2.5: MEASURED FORCE AND VELOCITY AND DERIVED MEASURED DELTA CURVE (RI-50, HALF DRIVEN)

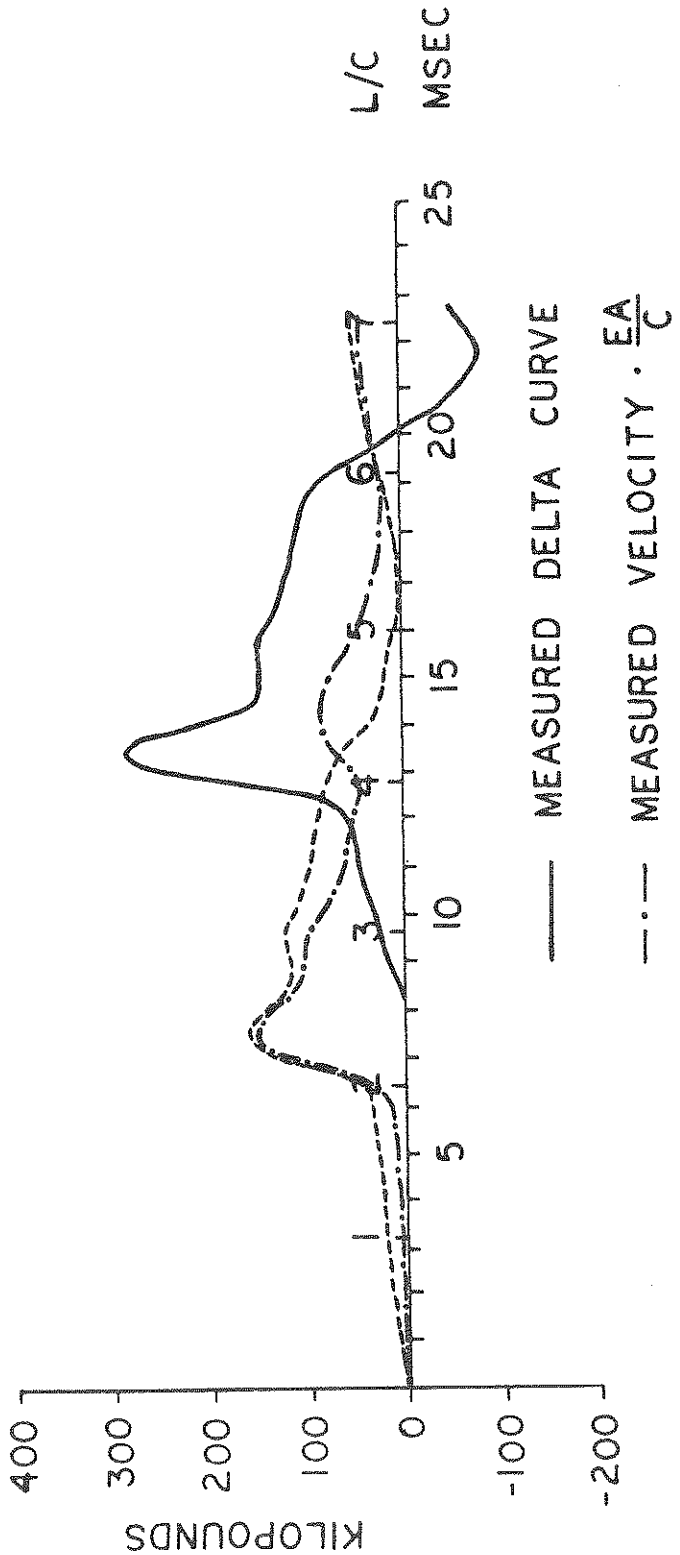

FIGURE 2.6: MEASURED FORCE AND VELOCITY AND DERIVED MEASURED DELTA CURVE (RI-50, BLOW NO. 20)

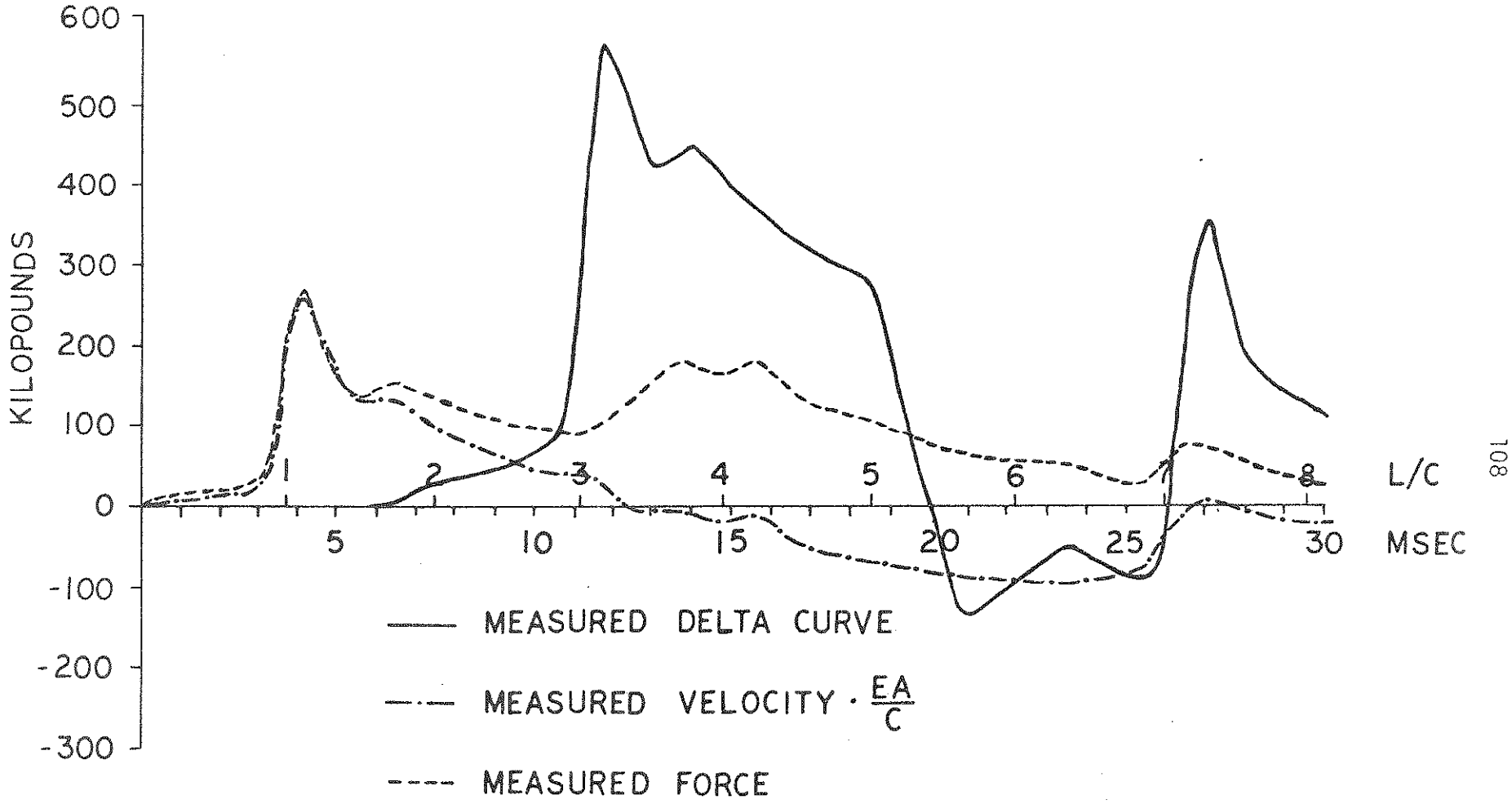

FIGURE 2.7: MEASURED FORCE AND VELOCITY AND MEASURED DELTA CURVE (Ri-60, #18)

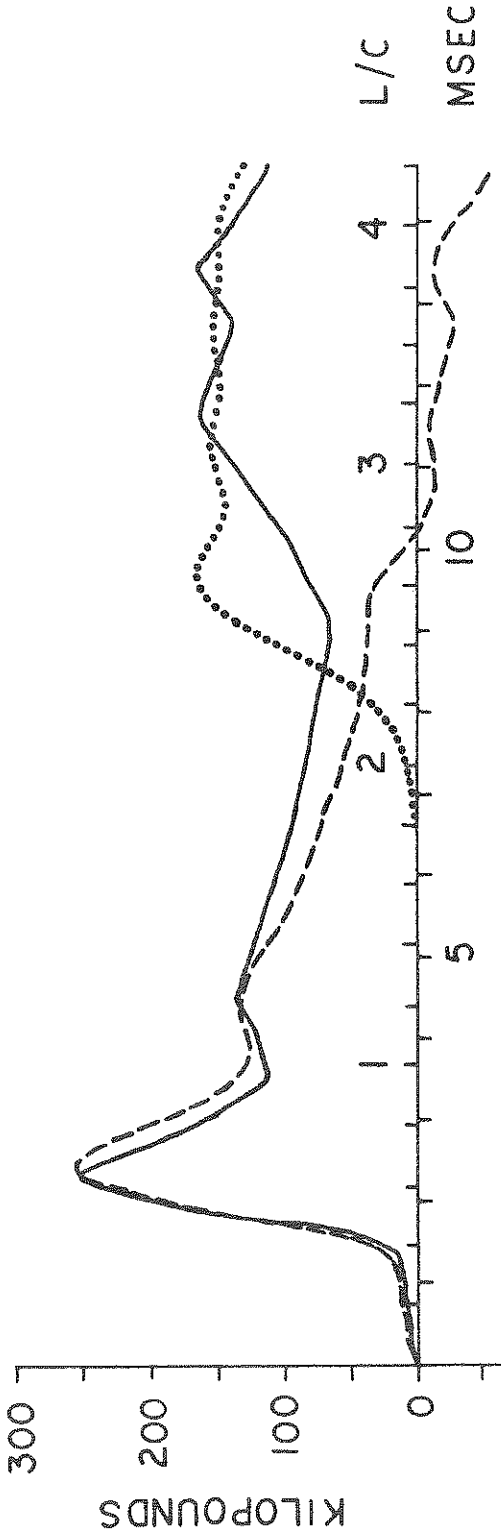

FIGURE 2.8: MEASURED FORCE AND VELOCITY AND RESISTANCE DELTA CURVE FOR SHEAR RESISTANCE FORCE OF 75 KIPS AT PILE BOTTOM END

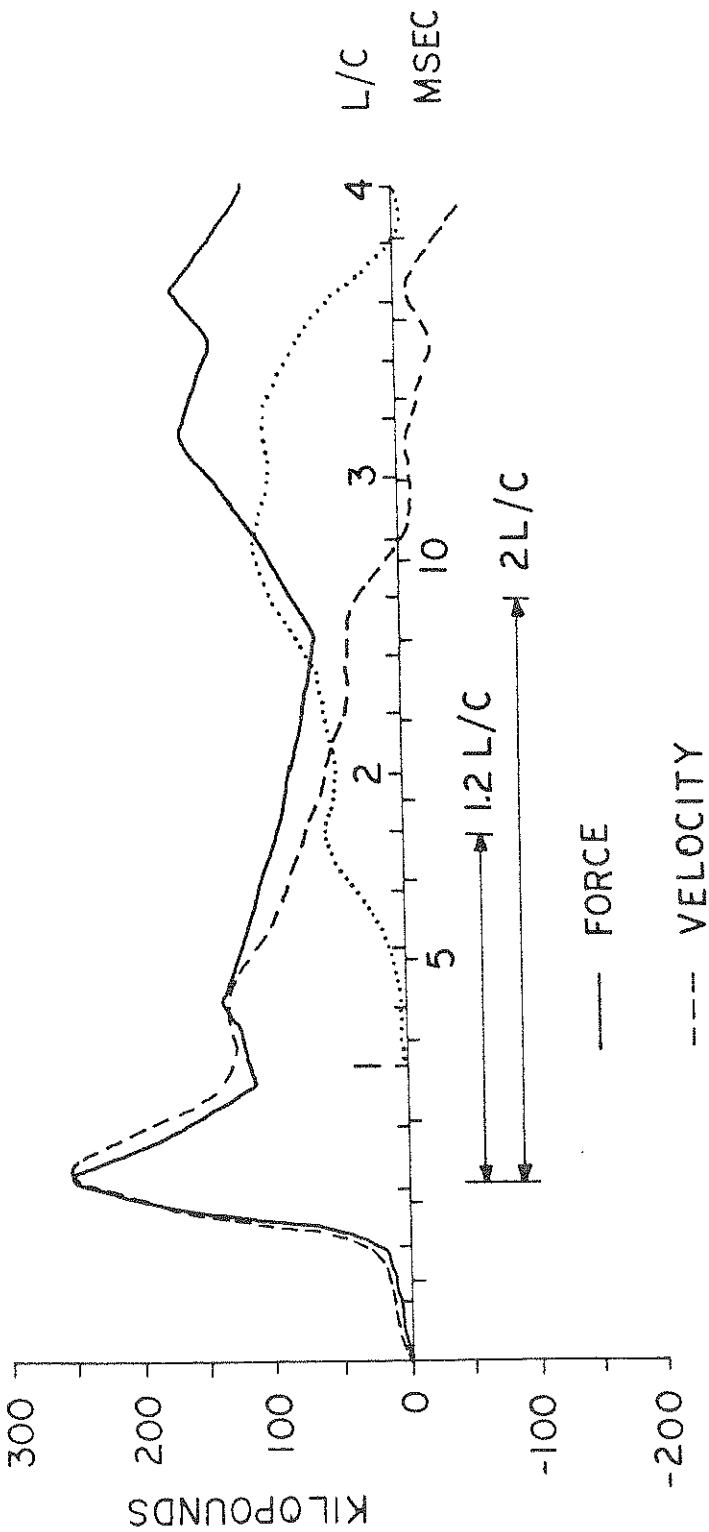

FIGURE 2.9: MEASURED FORCE AND VELOCITY AND RESISTANCE DELTA CURVE FOR SHEAR RESISTANCE FORCE OF 50 KIPS AT 0.6 L

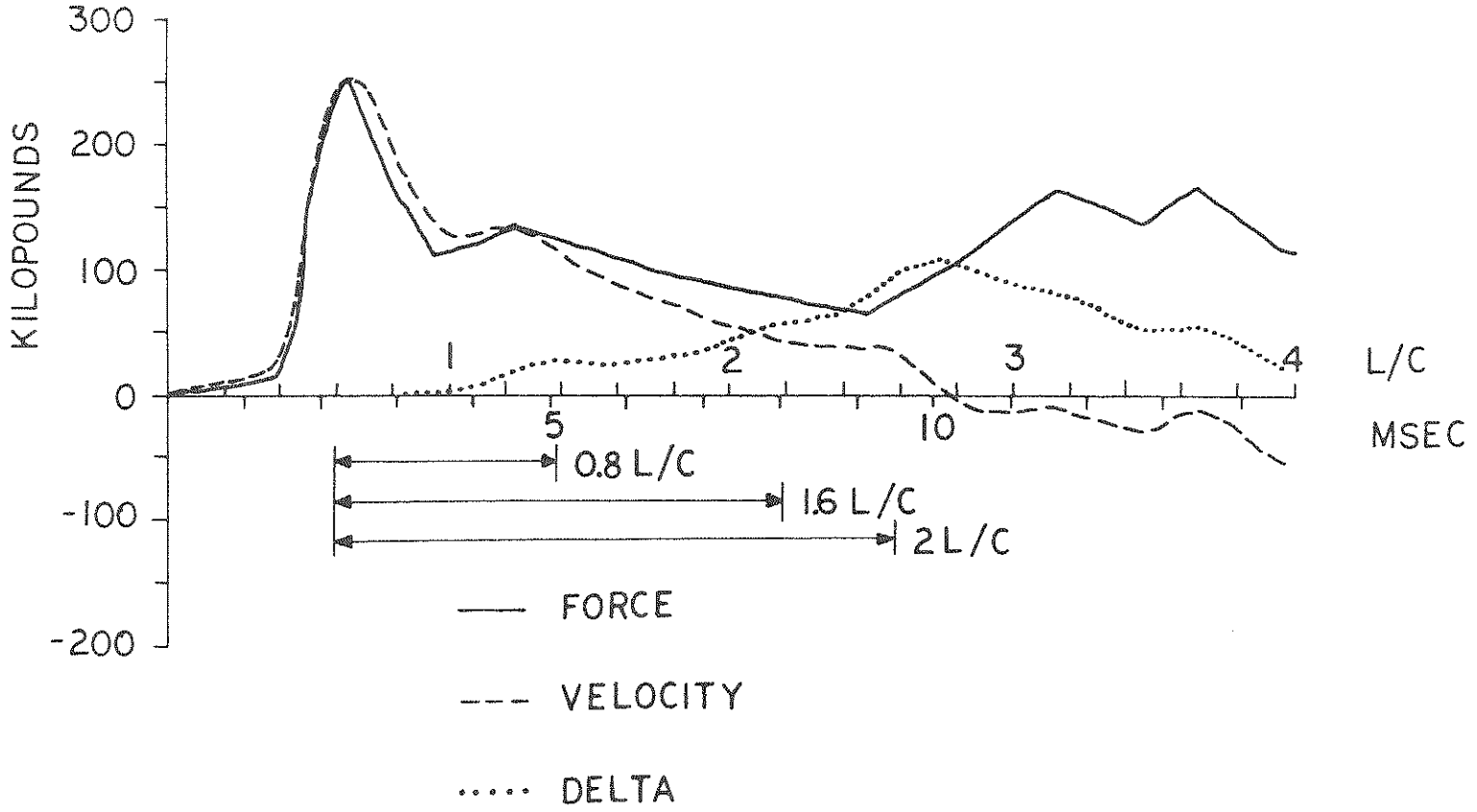

FIGURE 2.10: MEASURED FORCE AND VELOCITY AND RESISTANCE DELTA CURVE FOR A SHEAR RESISTANCE FORCE OF 25 KIPS AT BOTH 0.4 L and 0.8 L

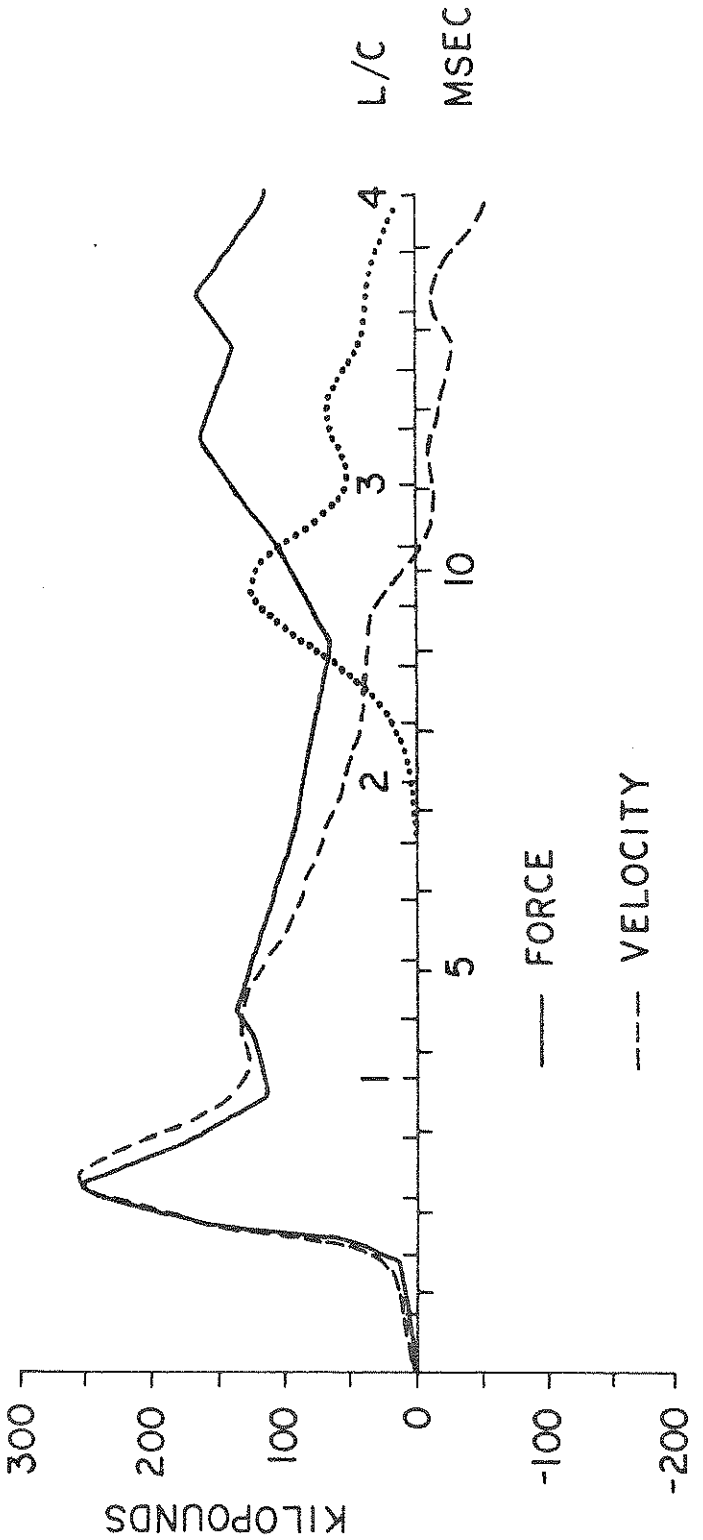

FIGURE 2.11: MEASURED FORCE AND VELOCITY AND RESISTANCE DELTA CURVE FOR A DAMPER AT THE PILE TIP (d_n = EA/c)

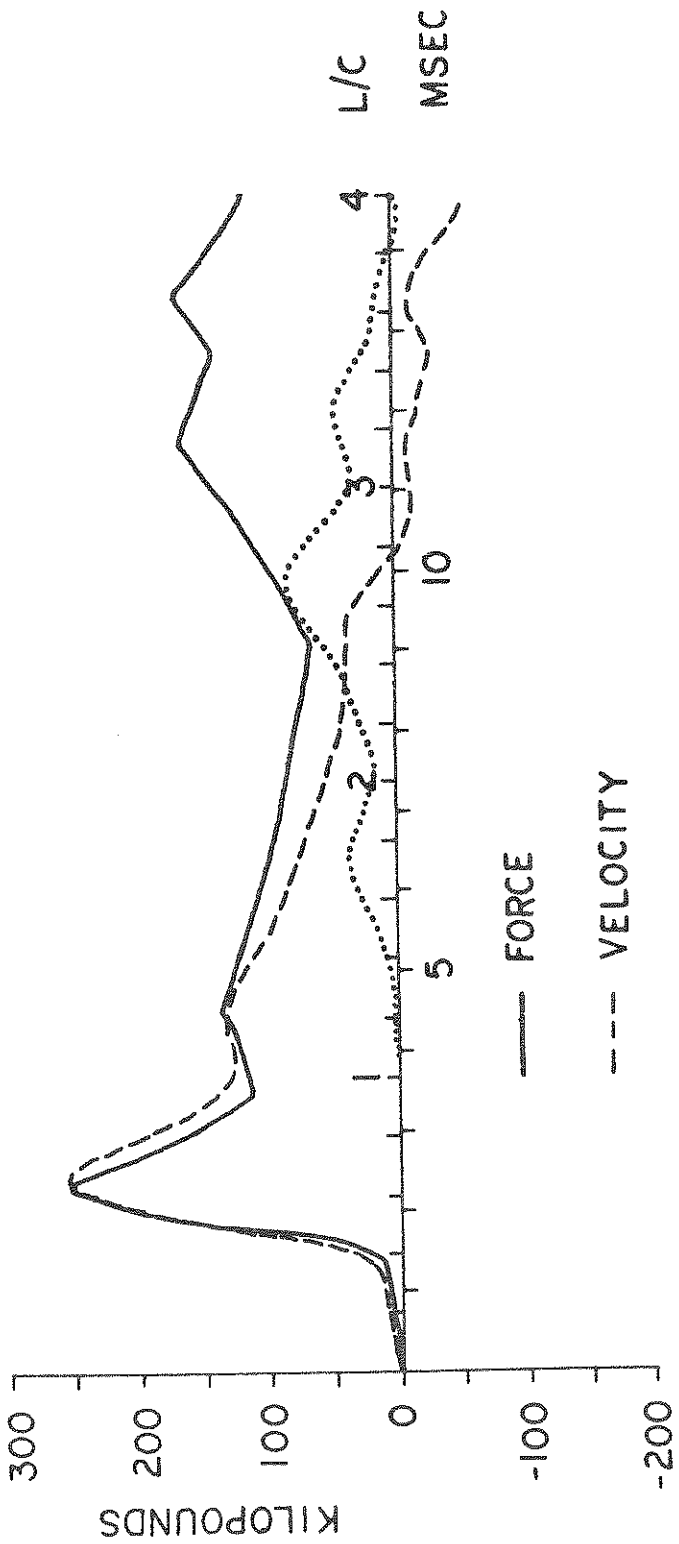

FIGURE 2.12: MEASURED FORCE AND VELOCITY AND RESISTANCE DELTA CURVE FOR DAMPER AT 0.6 L (d_i = EA/c)

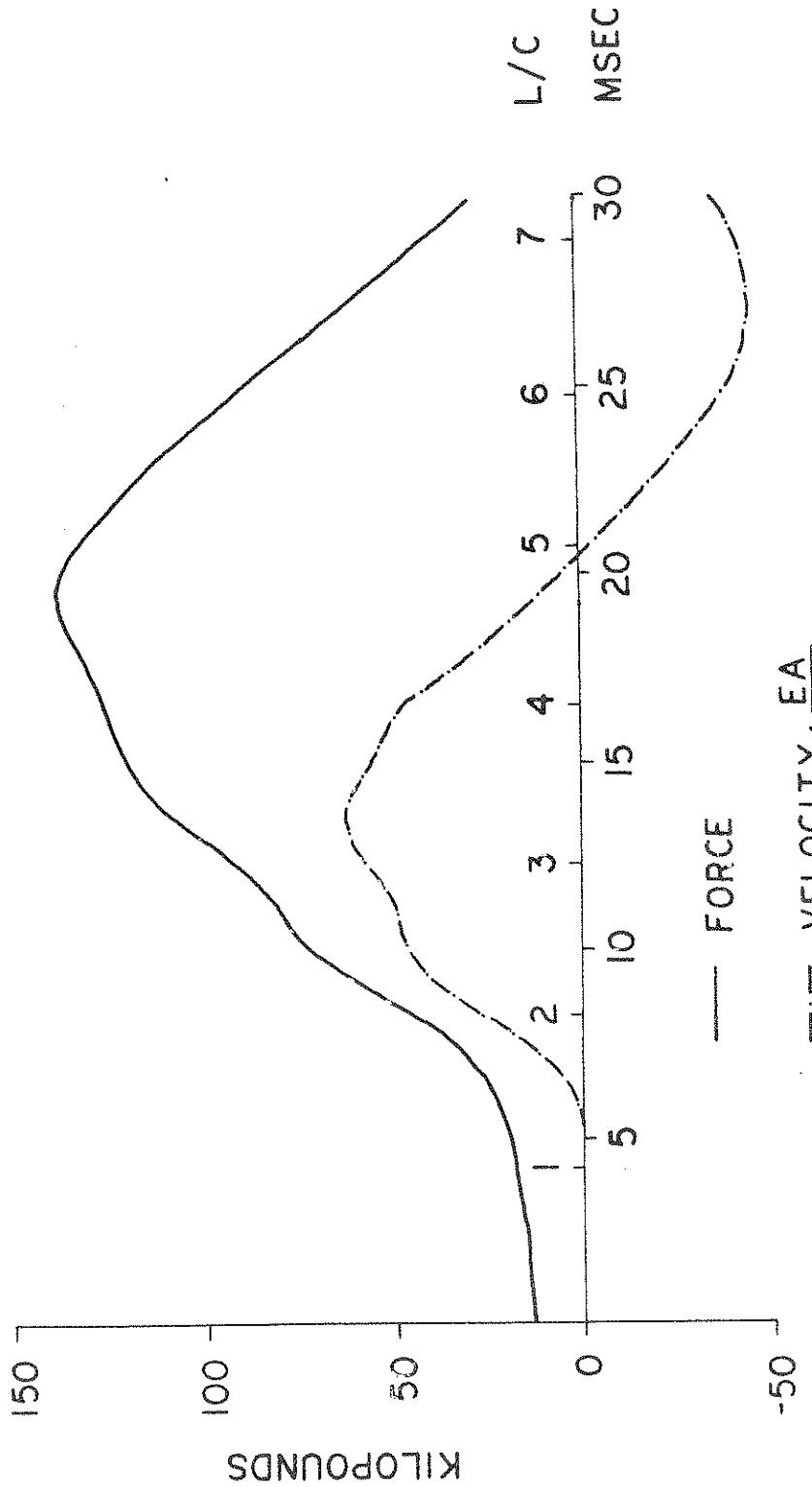

FIGURE 3.1: MEASURED TOP FORCE AND VELOCITY OF PILE 531-70 BLOW NO. 13-A

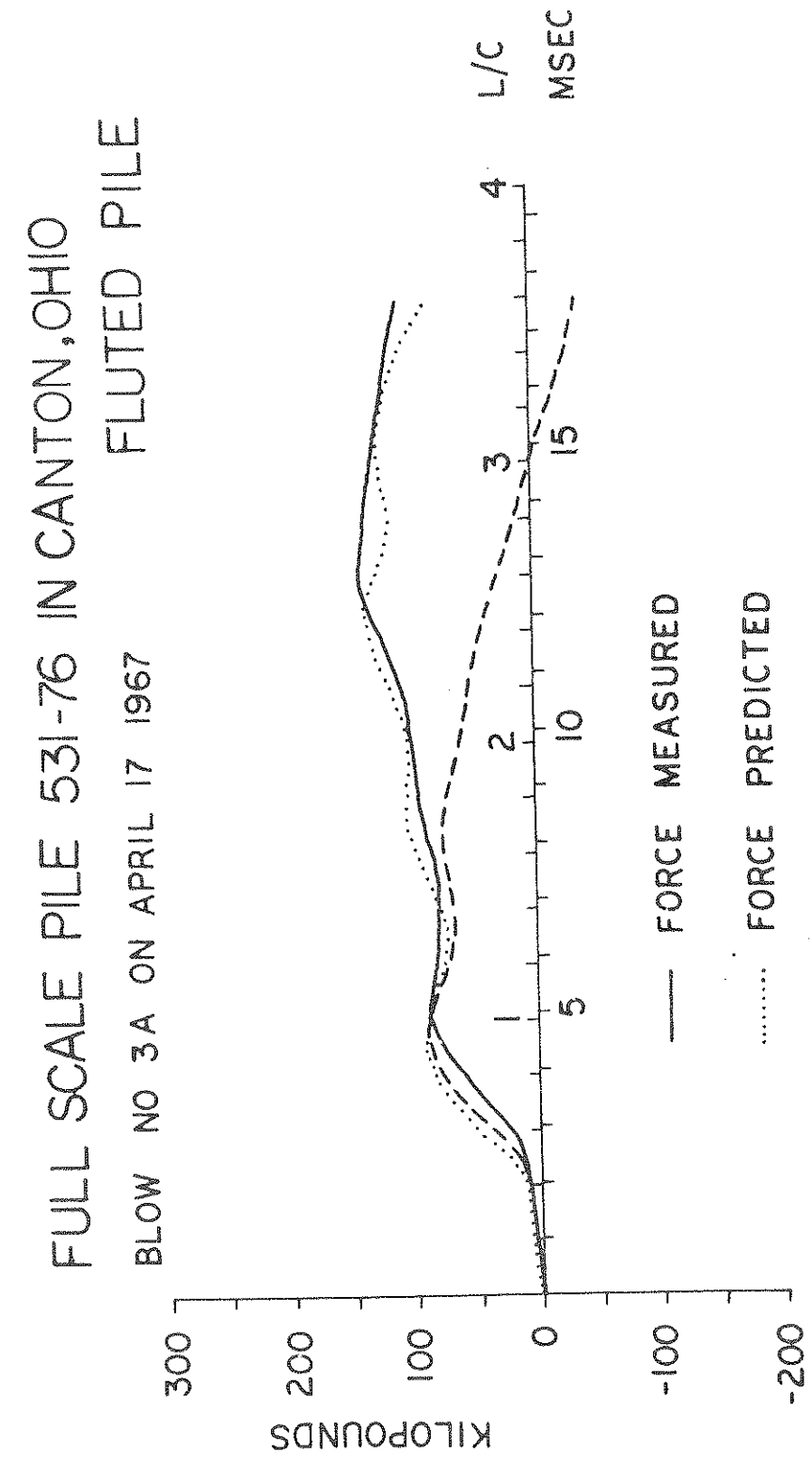

FIGURE 3.2: COMPARISON OF PREDICTED WITH MEASURED PILE TOP FORCE FOR DATA SET NO. 3

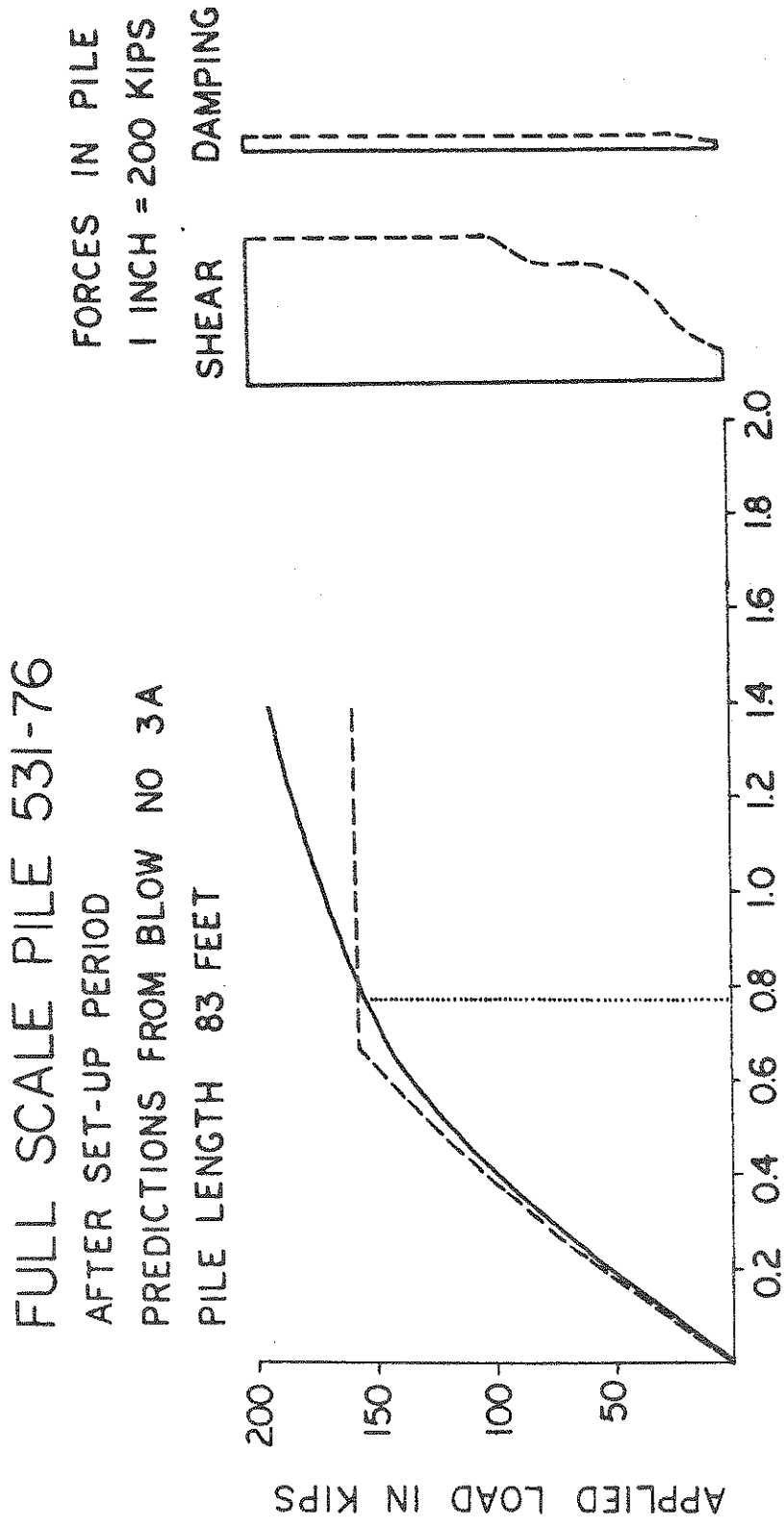

FIGURE 3.3: COMPARISON OF PREDICTED STATIC RESULTS WITH LOAD TEST AND PREDICTED FORCES IN PILE

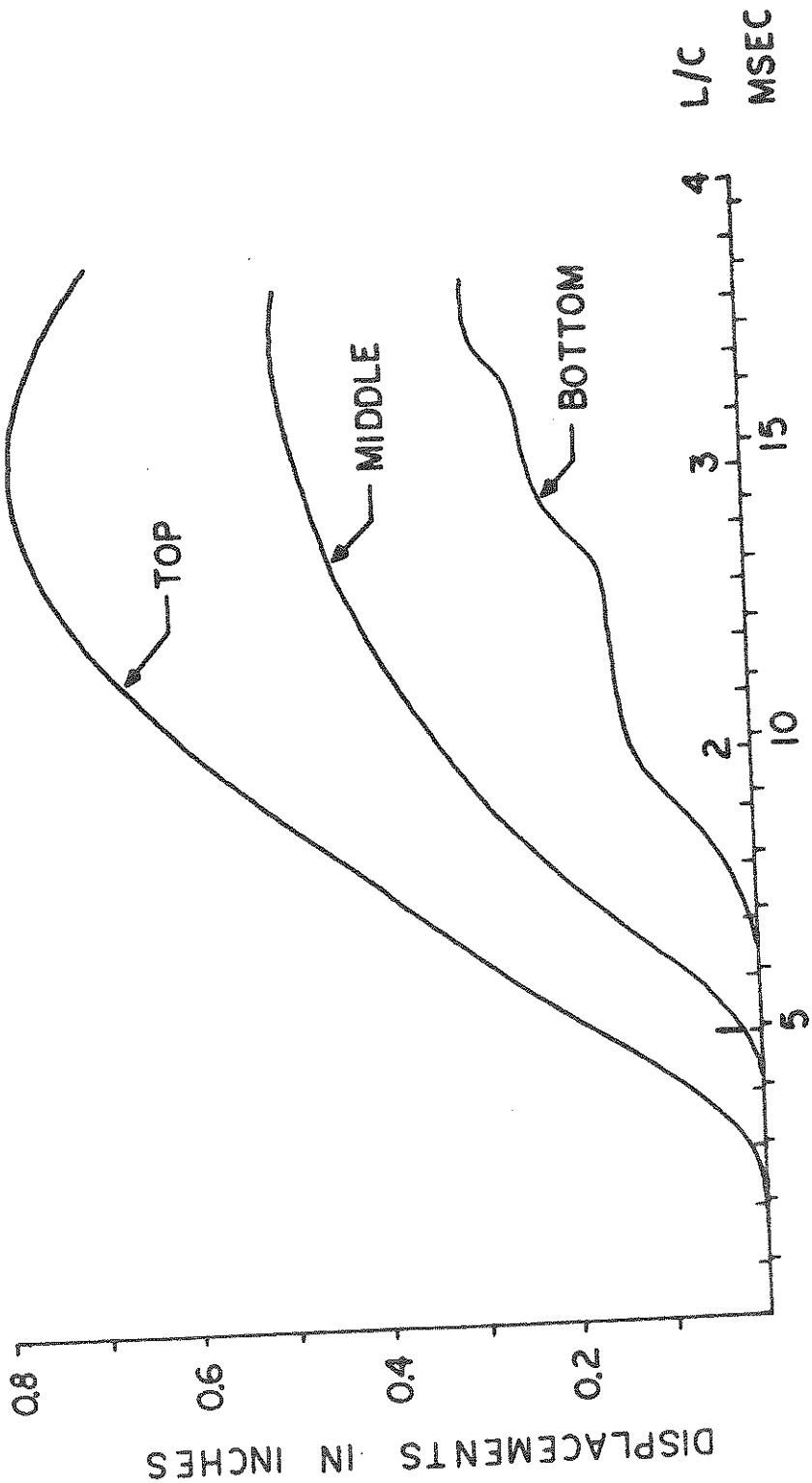

FIGURE 3.4: DISPLACEMENT AT TOP, MIDDLE, AND BOTTOM AS OBTAINED FROM DYNAMIC ANALYSIS
(Pile 531-76, BLOW NO. 3-A)

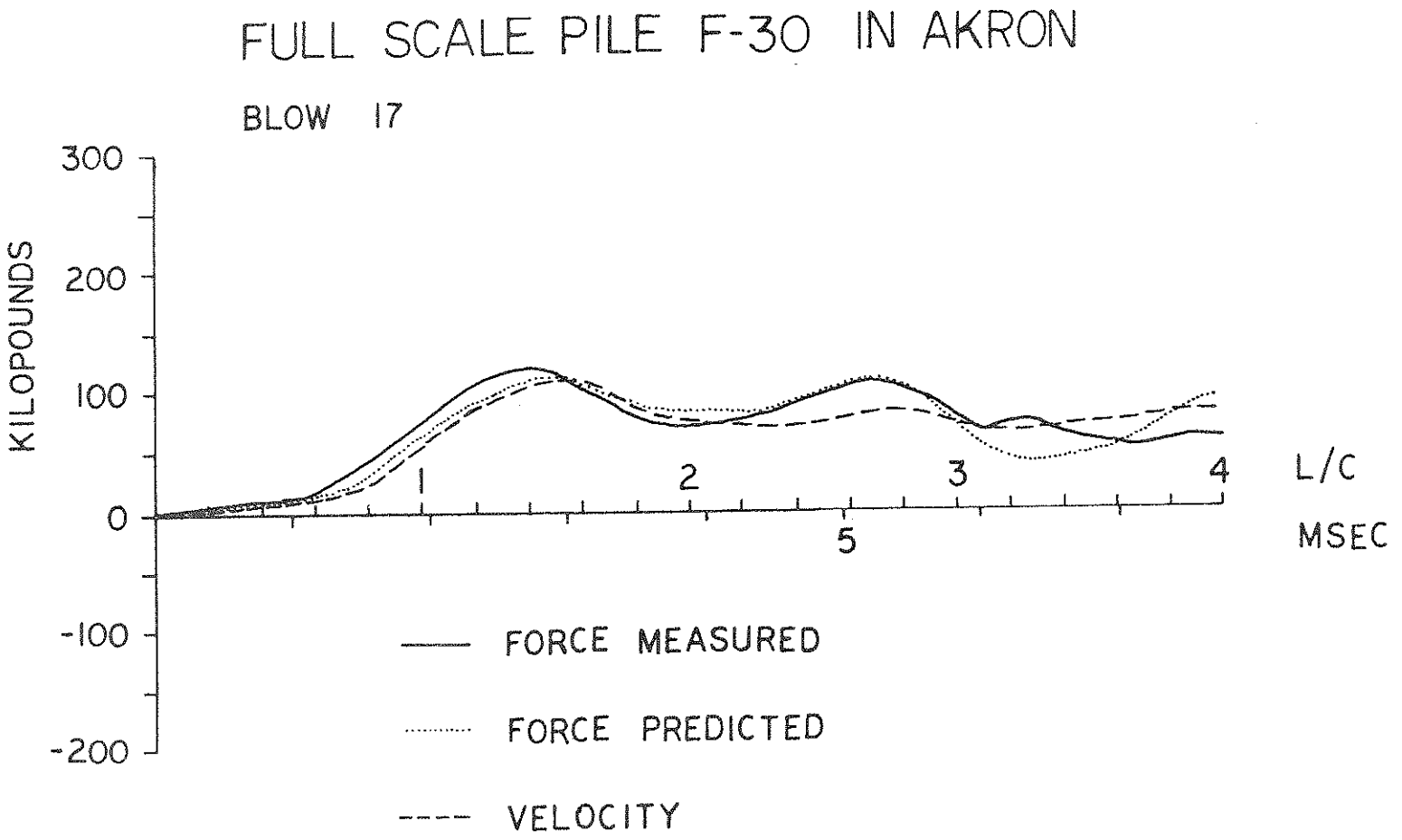

FIGURE 3.5: COMPARISON OF PREDICTED WITH MEASURED PILE TOP FORCE FOR DATA SET NO. 5

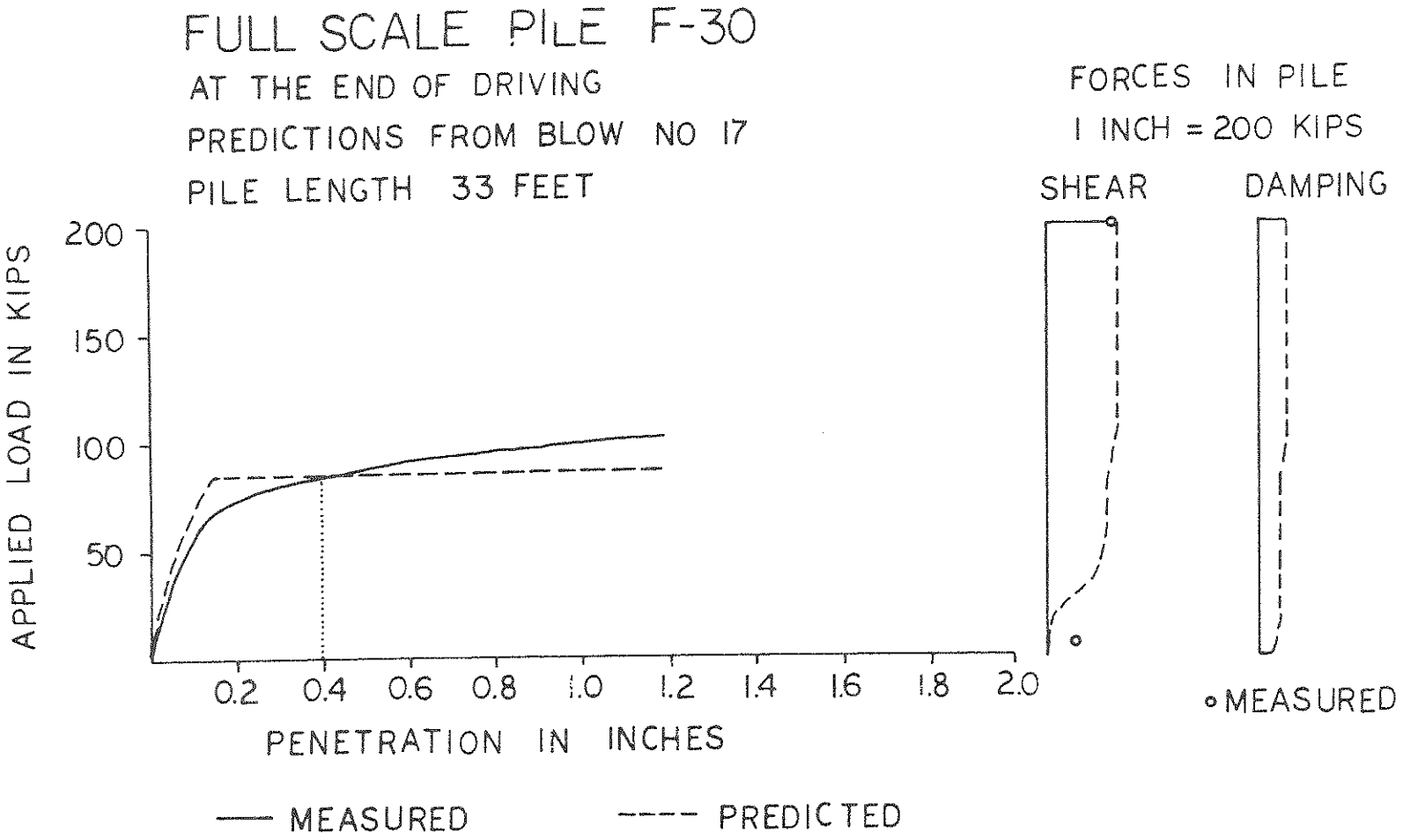

FIGURE 3.6: COMPARISON OF PREDICTED STATIC RESULTS WITH FIELD LOAD TEST AND FORCES IN PILE

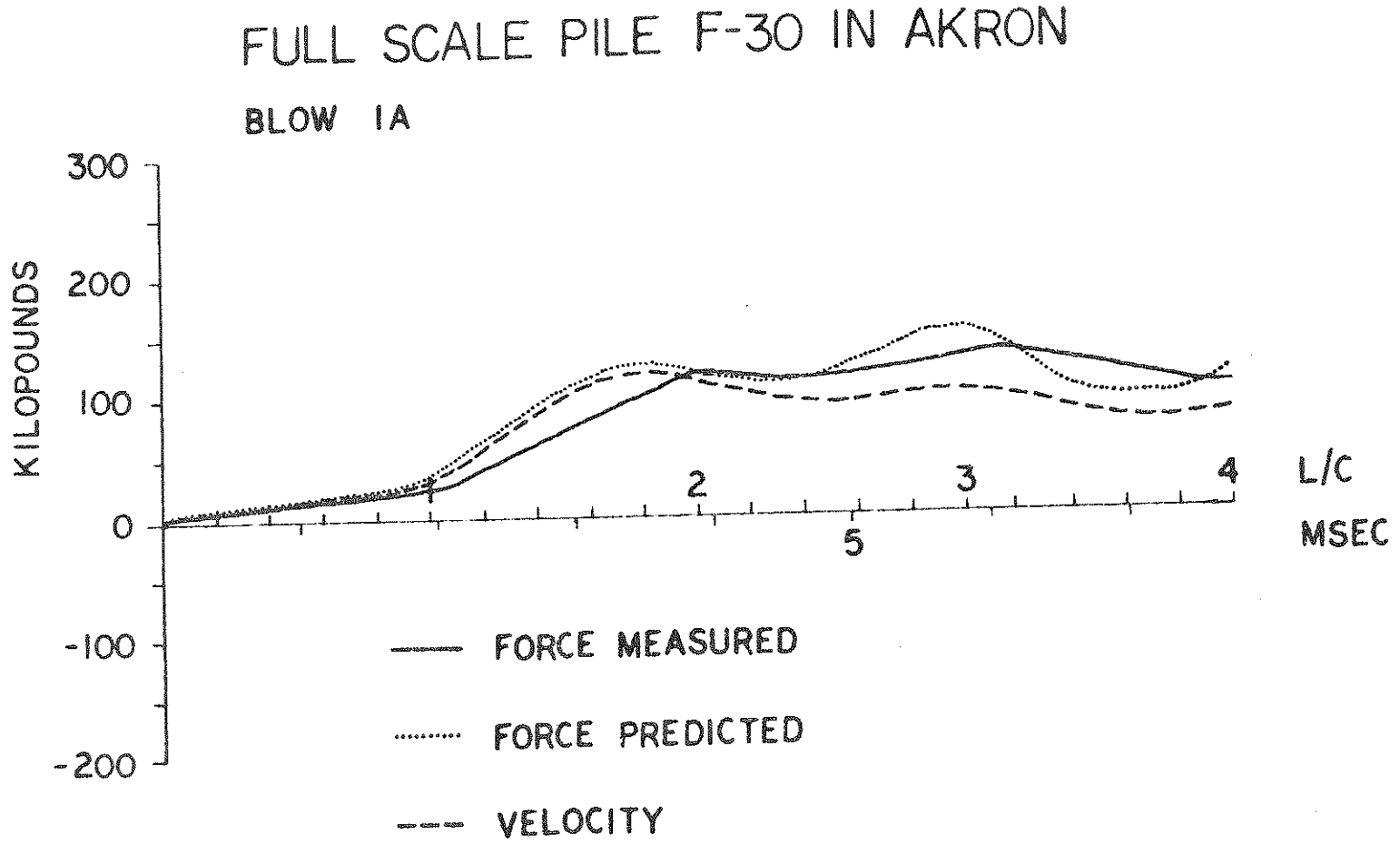

FIGURE 3.7: COMPARISON OF PREDICTED WITH MEASURED PILE TOP FORCE FOR DATA SET NO. 6

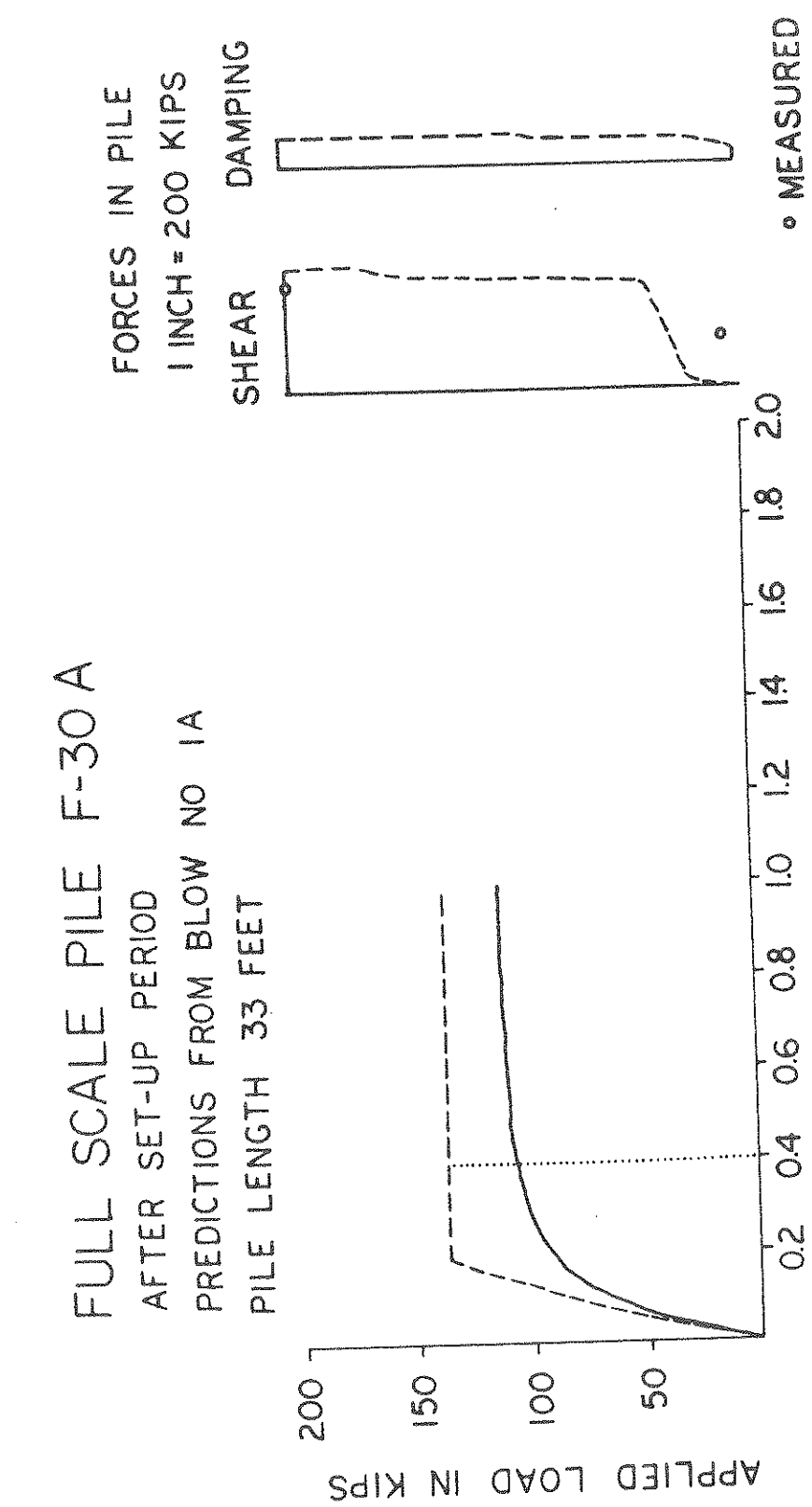

FIGURE 3.8: COMPARISON OF PREDICTED STATIC RESULTS WITH FIELD LOAD TEST AND PREDICTED FORCES IN PILE

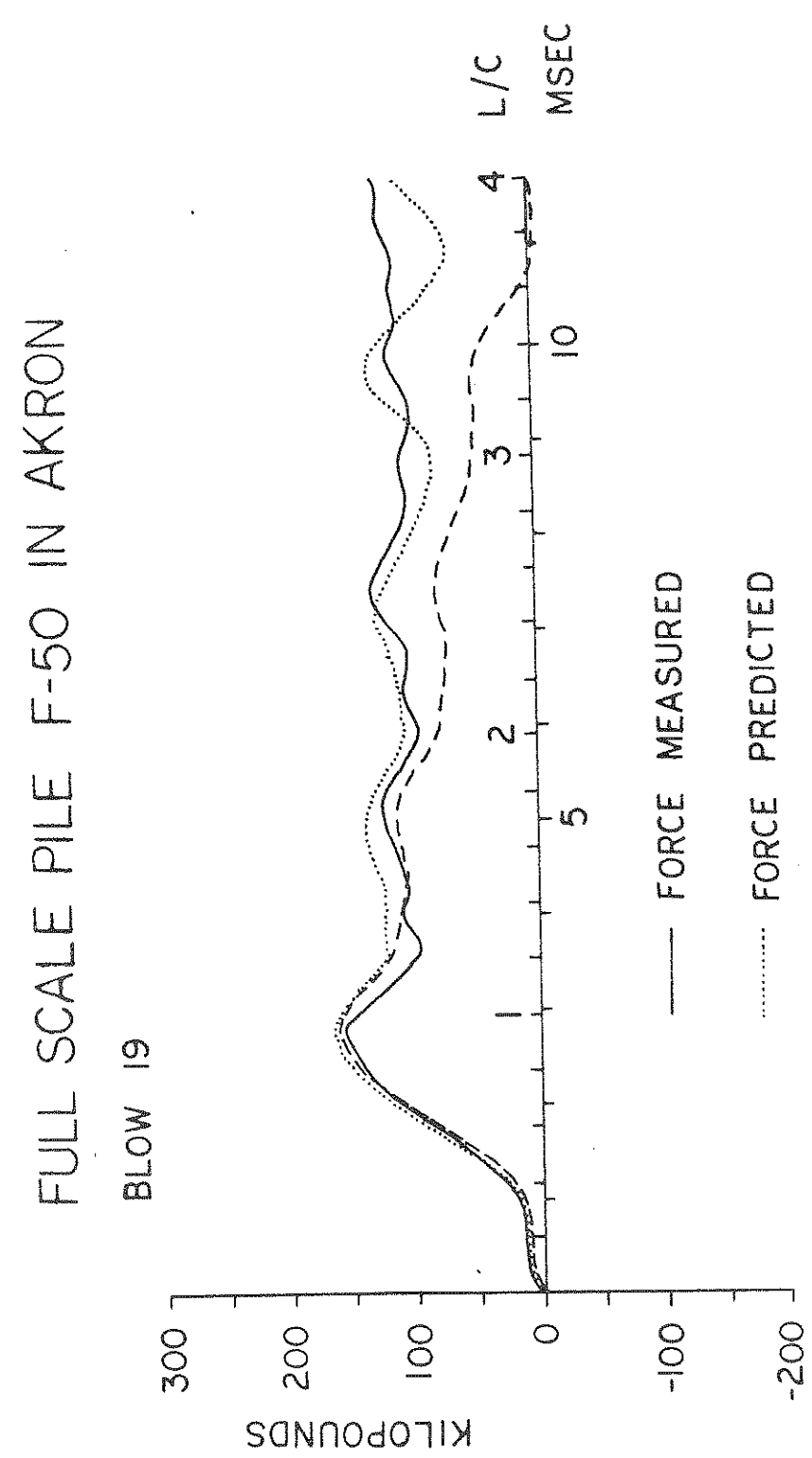

FIGURE 3.9: COMPARISON OF PREDICTED WITH MEASURED PILE TOP FORCE FOR DATA SET NO. 7

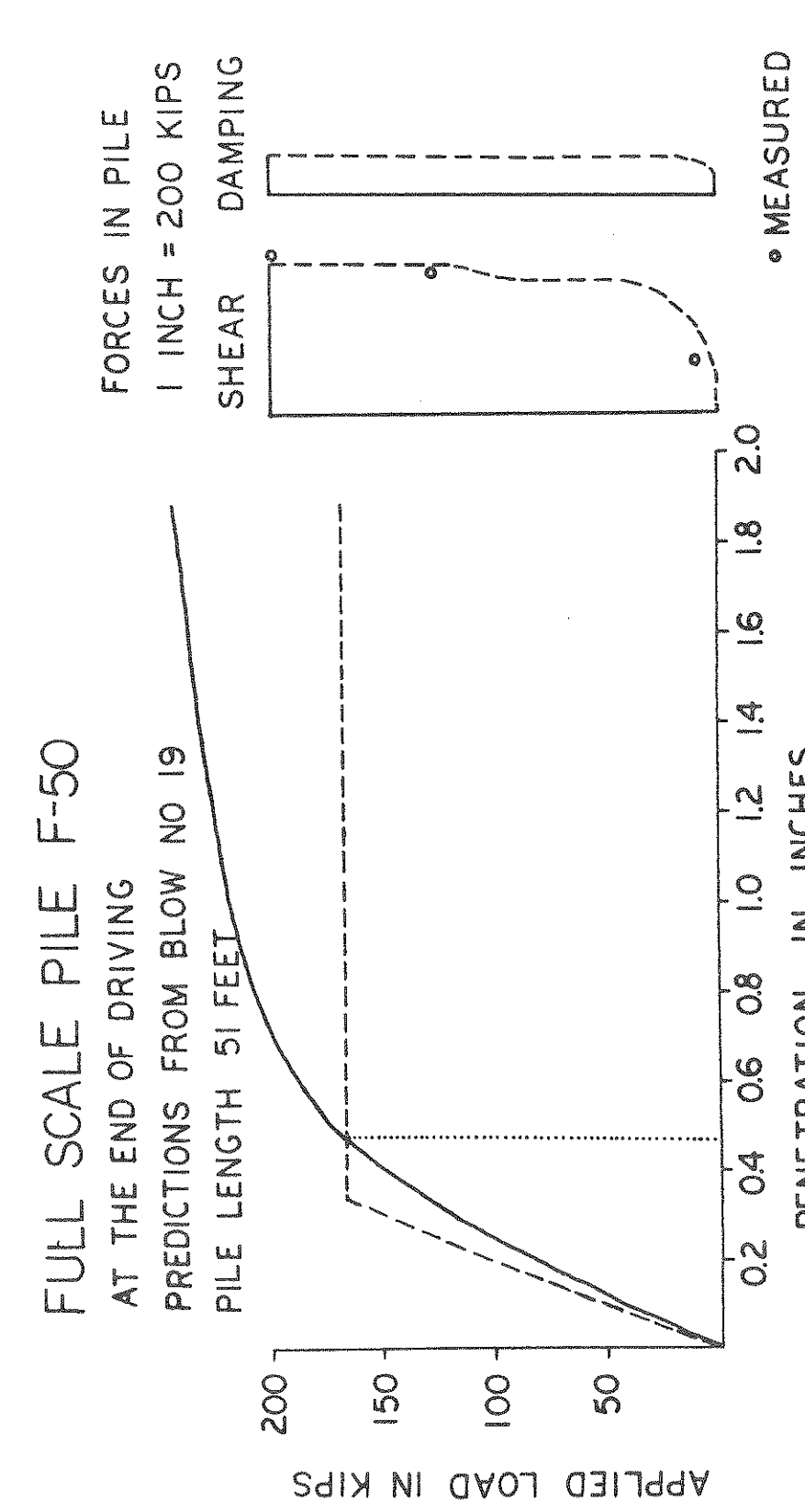

FIGURE 3.10: COMPARISON OF PREDICTED STATIC RESULTS WITH FIELD LOAD TEST AND PREDICTED FORCES IN PILE

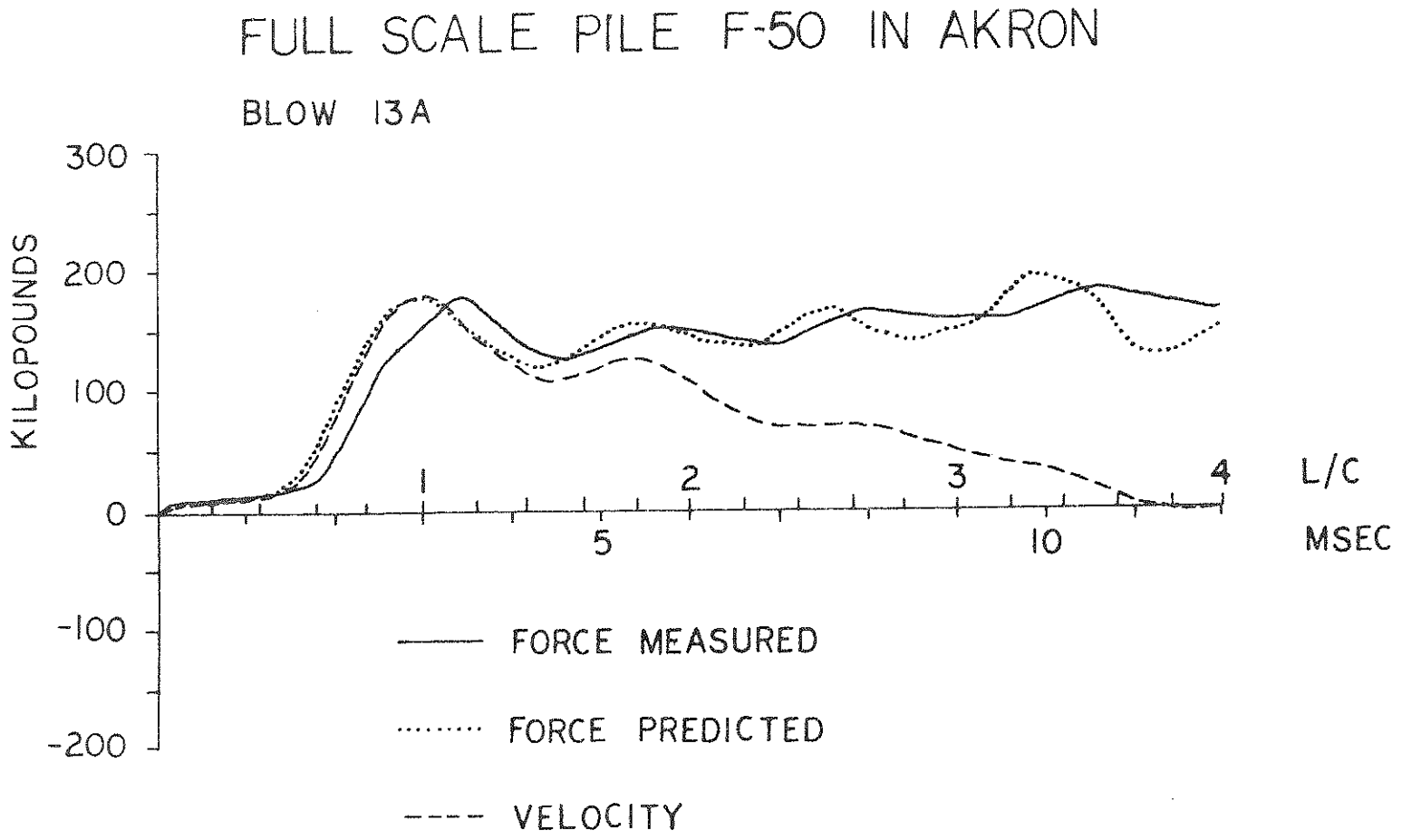

FIGURE 3.11: COMPARISON OF PREDICTED WITH MEASURED PILE TOP FORCE FOR DATA SET NO. 8

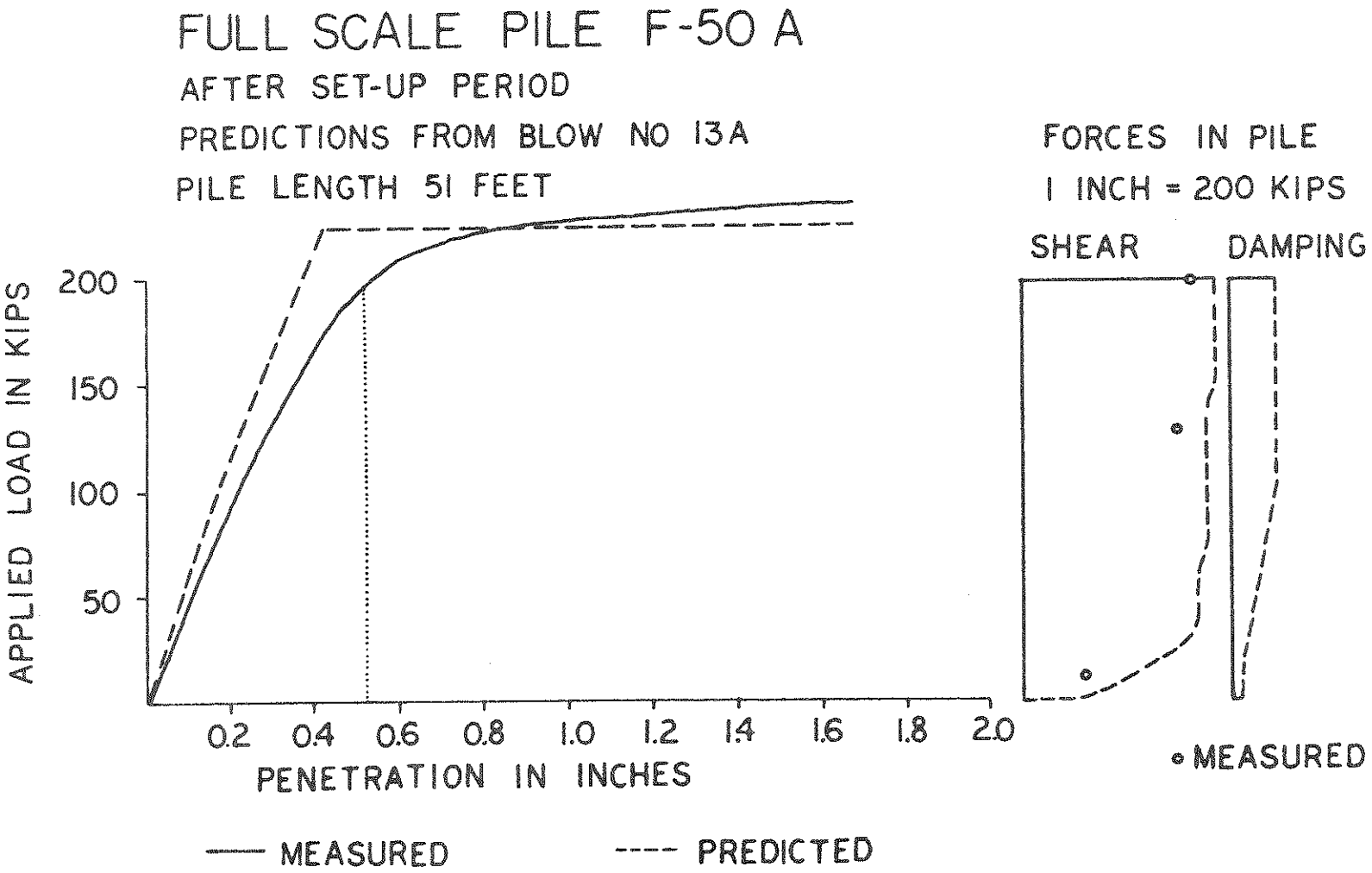

FIGURE 3.12: COMPARISON OF PREDICTED STATIC RESULT WITH FIELD LOAD TEST AND PREDICTED FORCES IN PILE

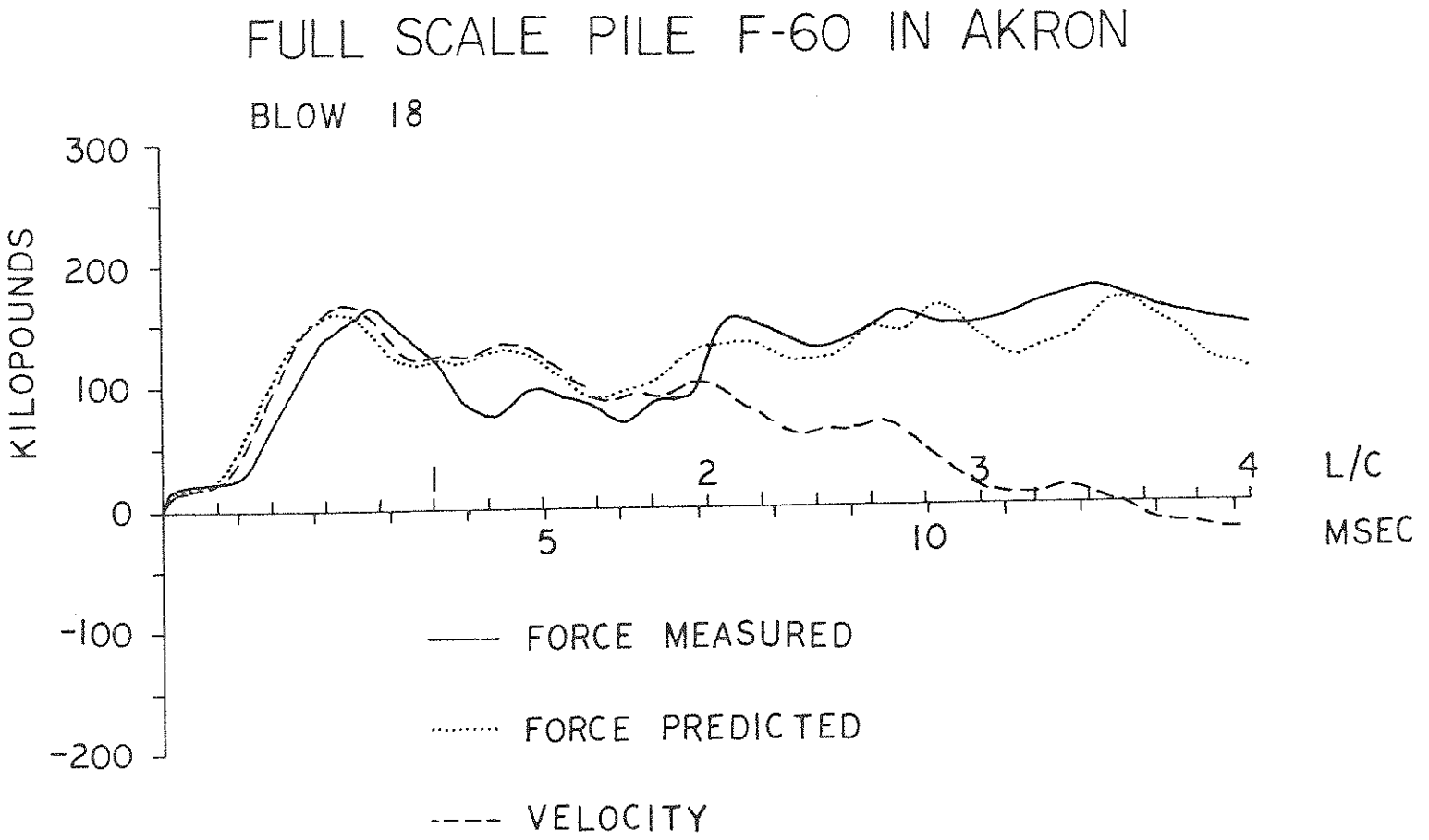

FIGURE 3.13: COMPARISON OF PREDICTED WITH MEASURED PILE TOP FORCE FOR DATA SET NO. 9

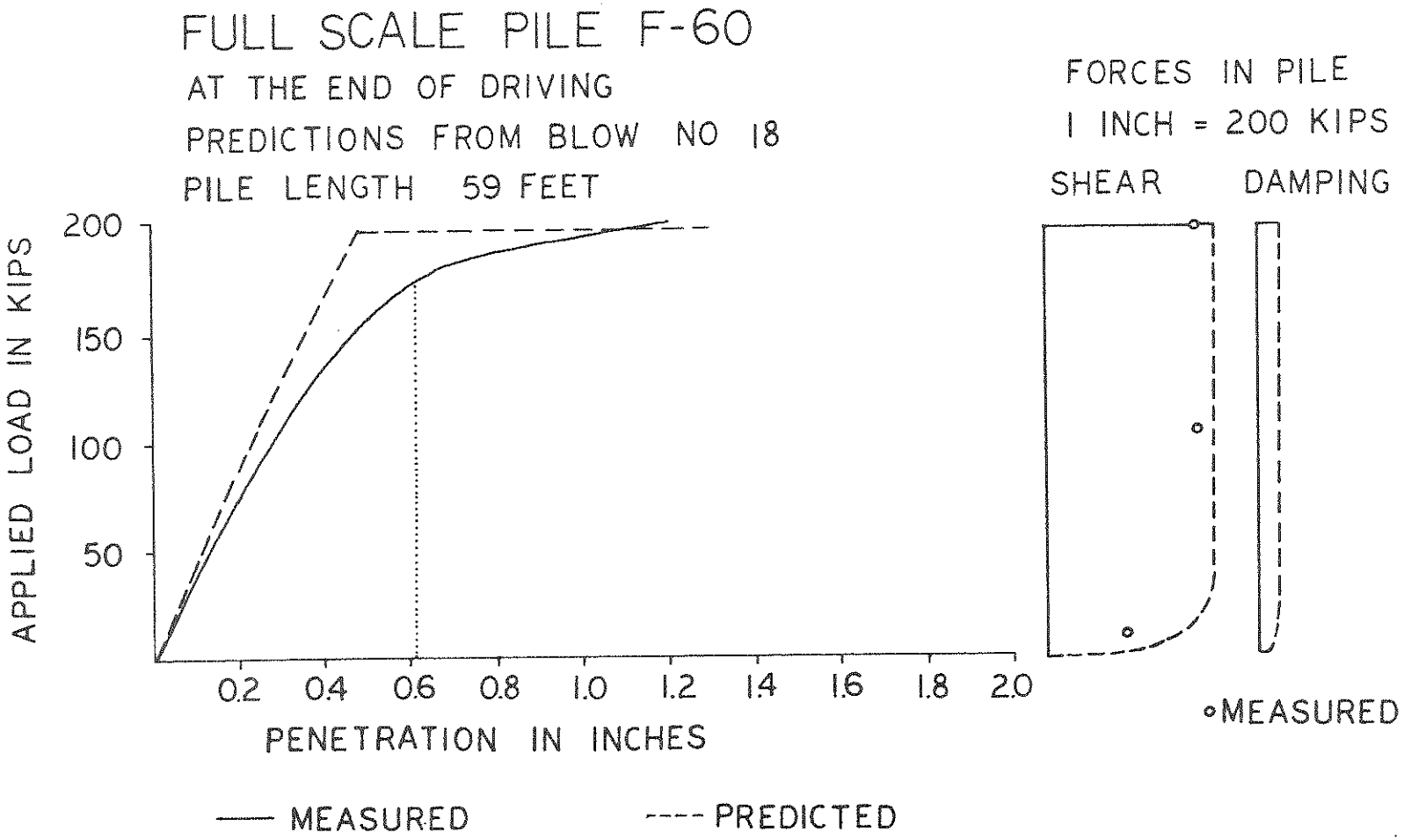

FIGURE 3.14: COMPARISON OF PREDICTED STATIC RESULT WITH FIELD LOAD TEST AND FORCES IN PILE

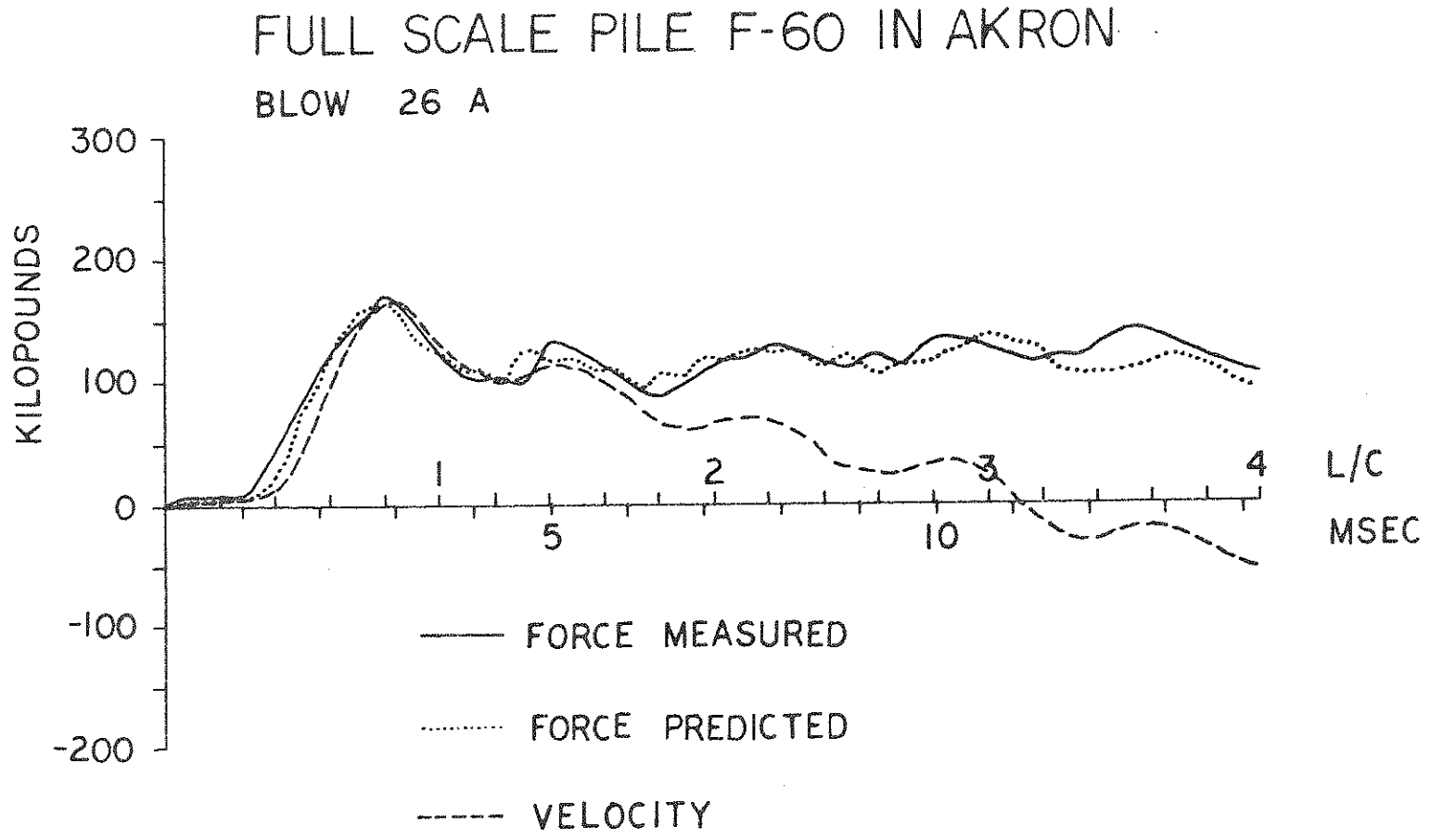

FIGURE 3.15: COMPARISON OF PREDICTED WITH MEASURED PILE TOP FORCE FOR DATA SET NO. 10

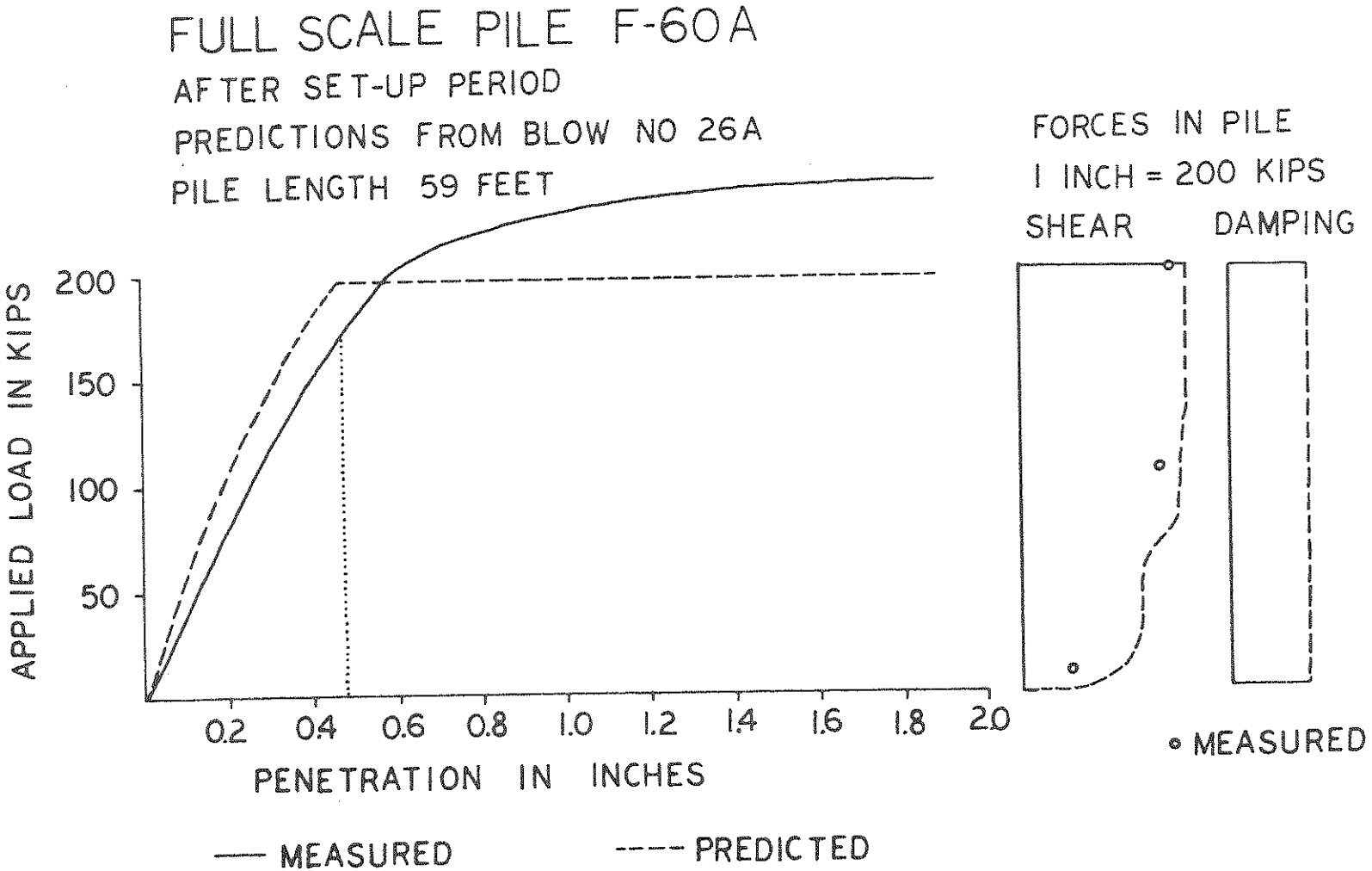

FIGURE 3.16: COMPARISON OF PREDICTED STATIC RESULT WITH FIELD LOAD TEST AND FORCES IN PILE

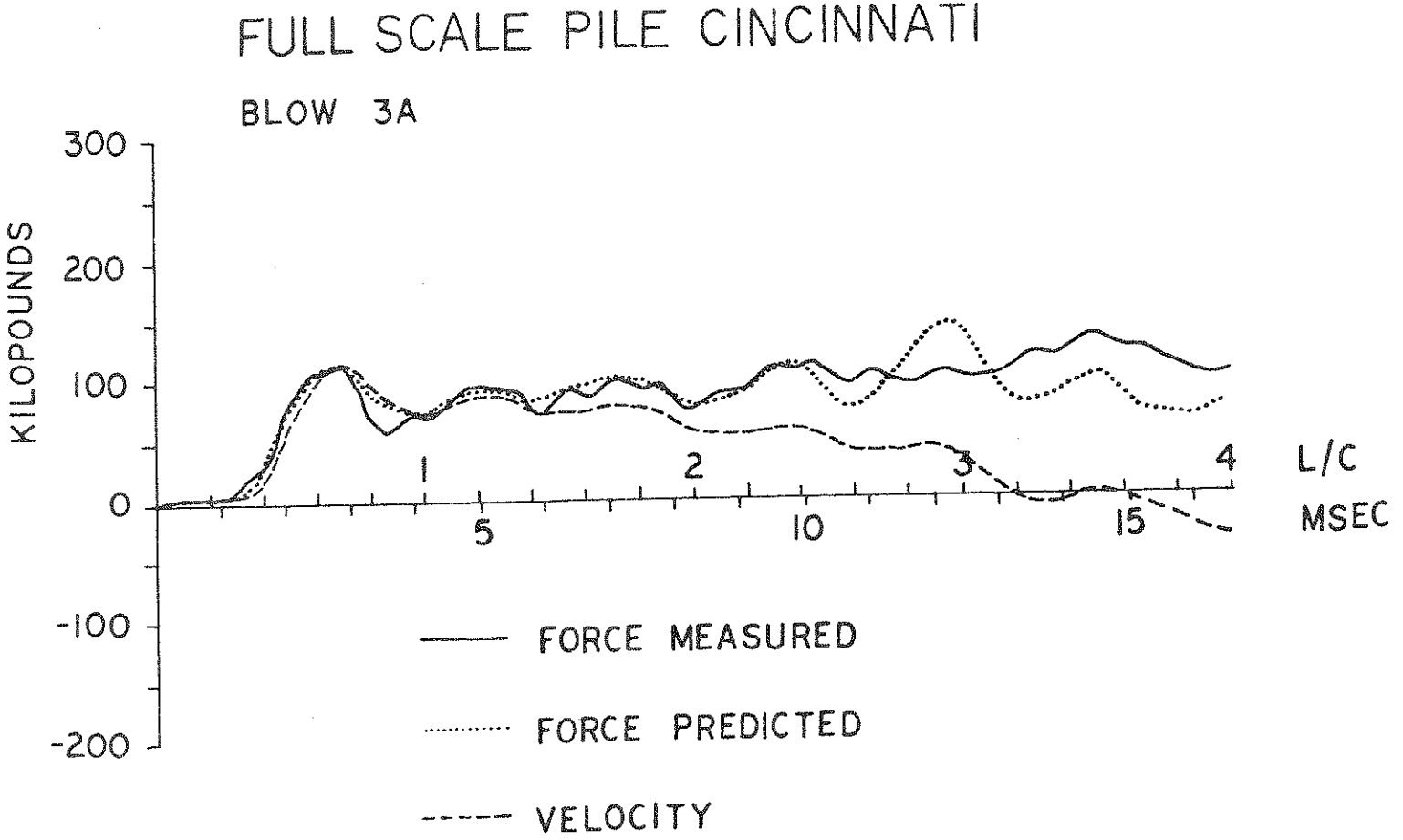

FIGURE 3.17: COMPARISON OF PREDICTED WITH MEASURED PILE TOP FORCE FOR DATA SET NO. 11

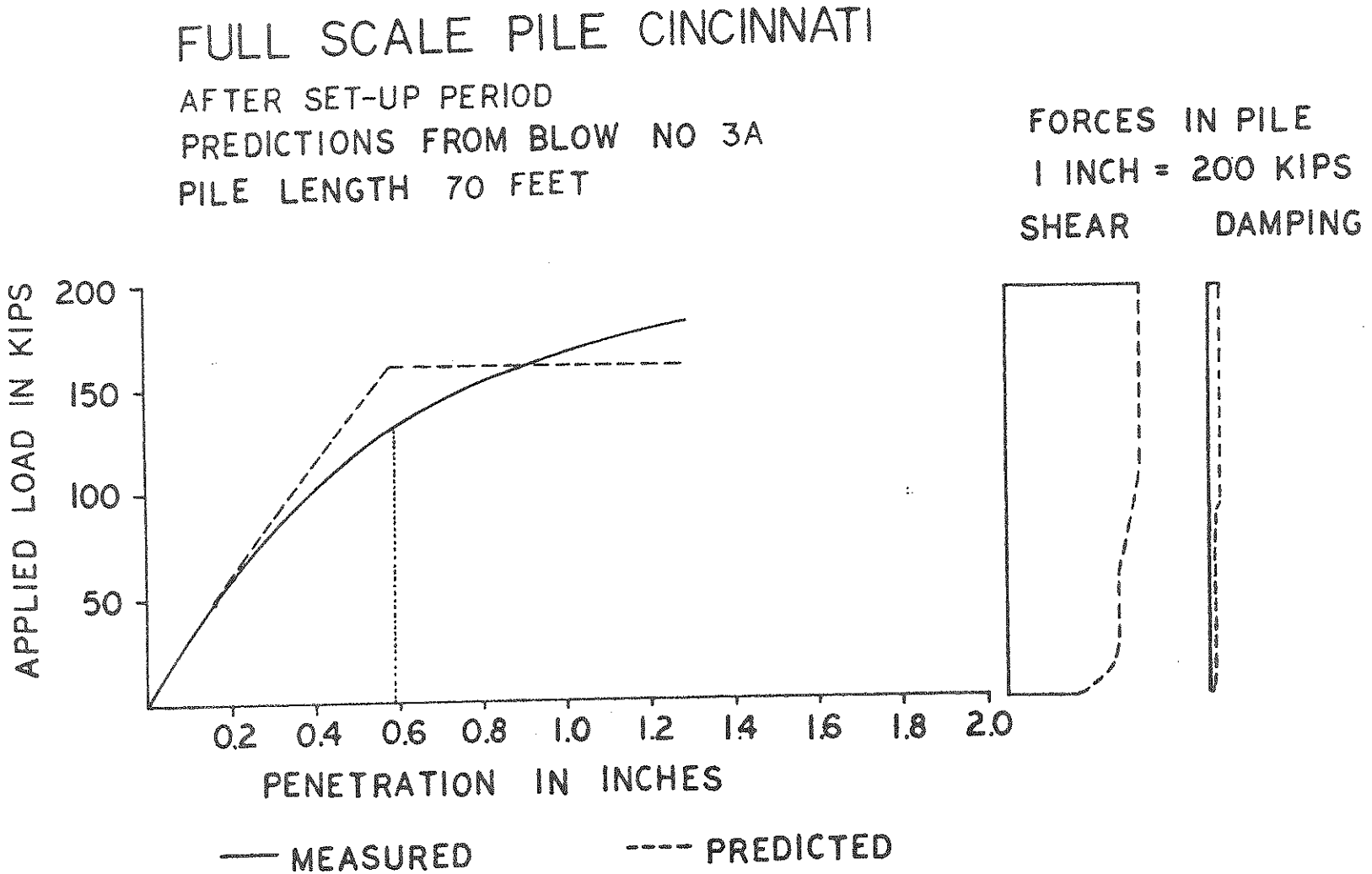

FIGURE 3.18: COMPARISON OF PREDICTED STATIC RESULTS WITH FIELD LOAD TEST AND FORCES IN PILE

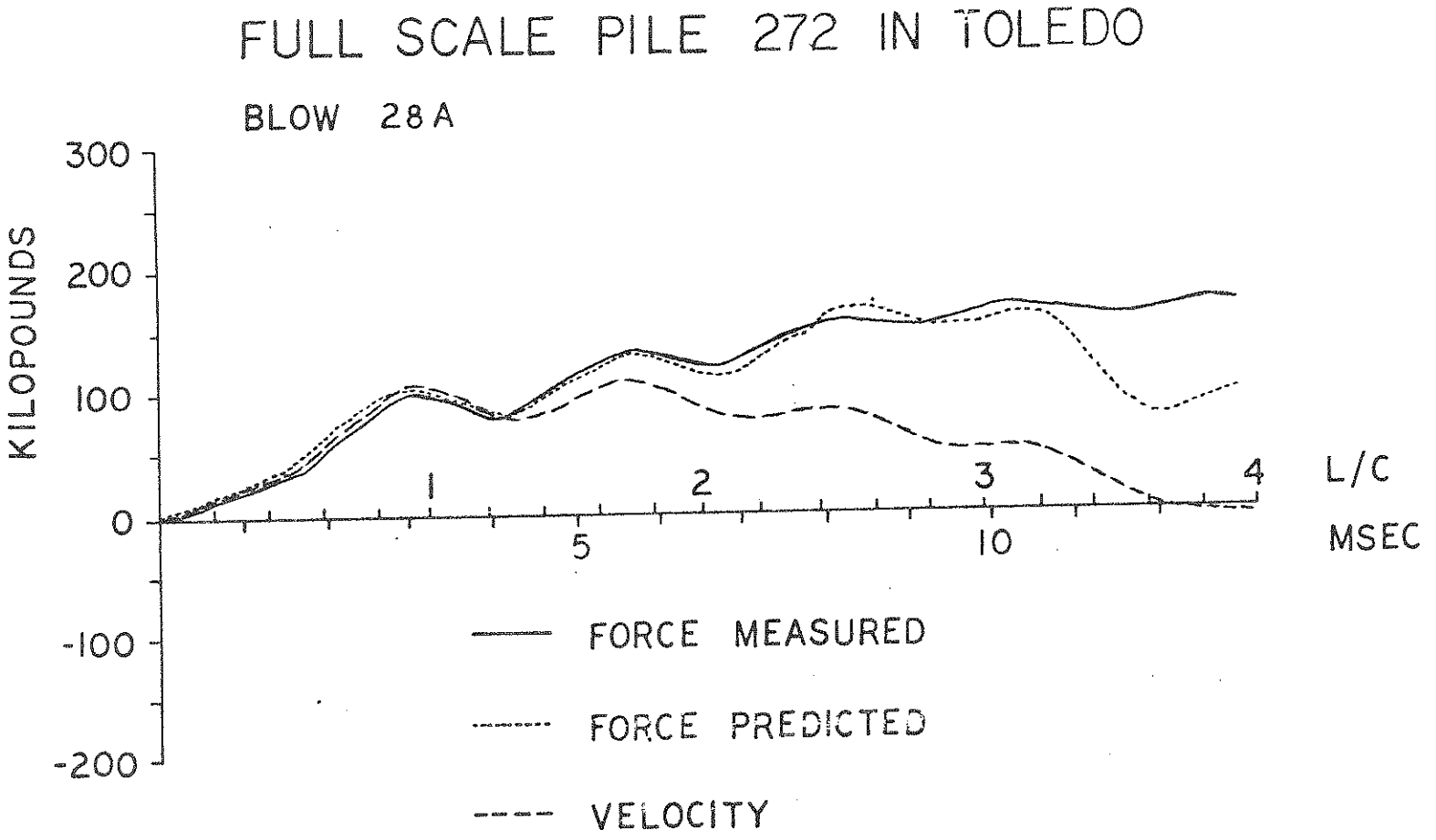

FIGURE 3.19: COMPARISON OF PREDICTED WITH MEASURED PILE TOP FORCE FOR DATA SET NO. 12
PREDICTION OBTAINED BY INSPECTION

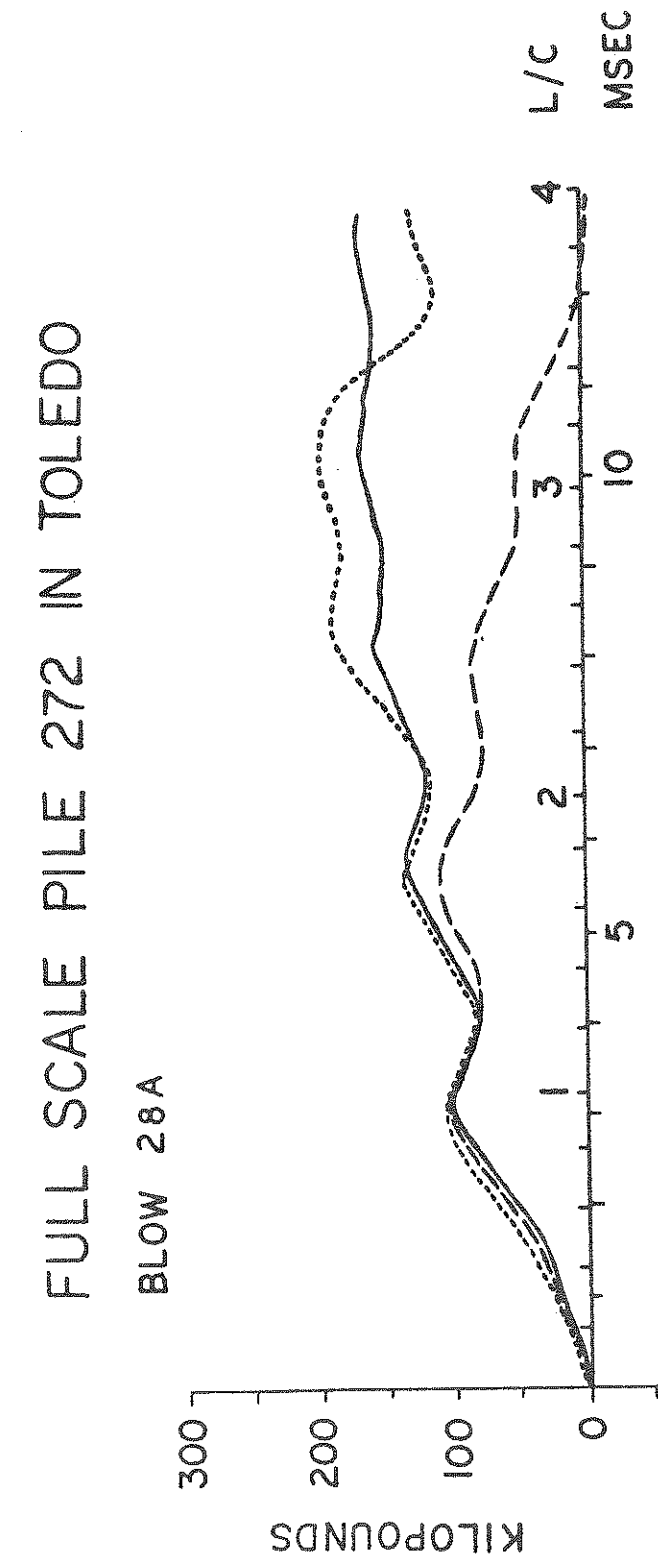

FIGURE 3.20: COMPARISON OF PREDICTED WITH MEASURED PILE TOP FORCE FOR DATA SET NO. 12 PREDICTION FROM AUTOMATED ROUTINE

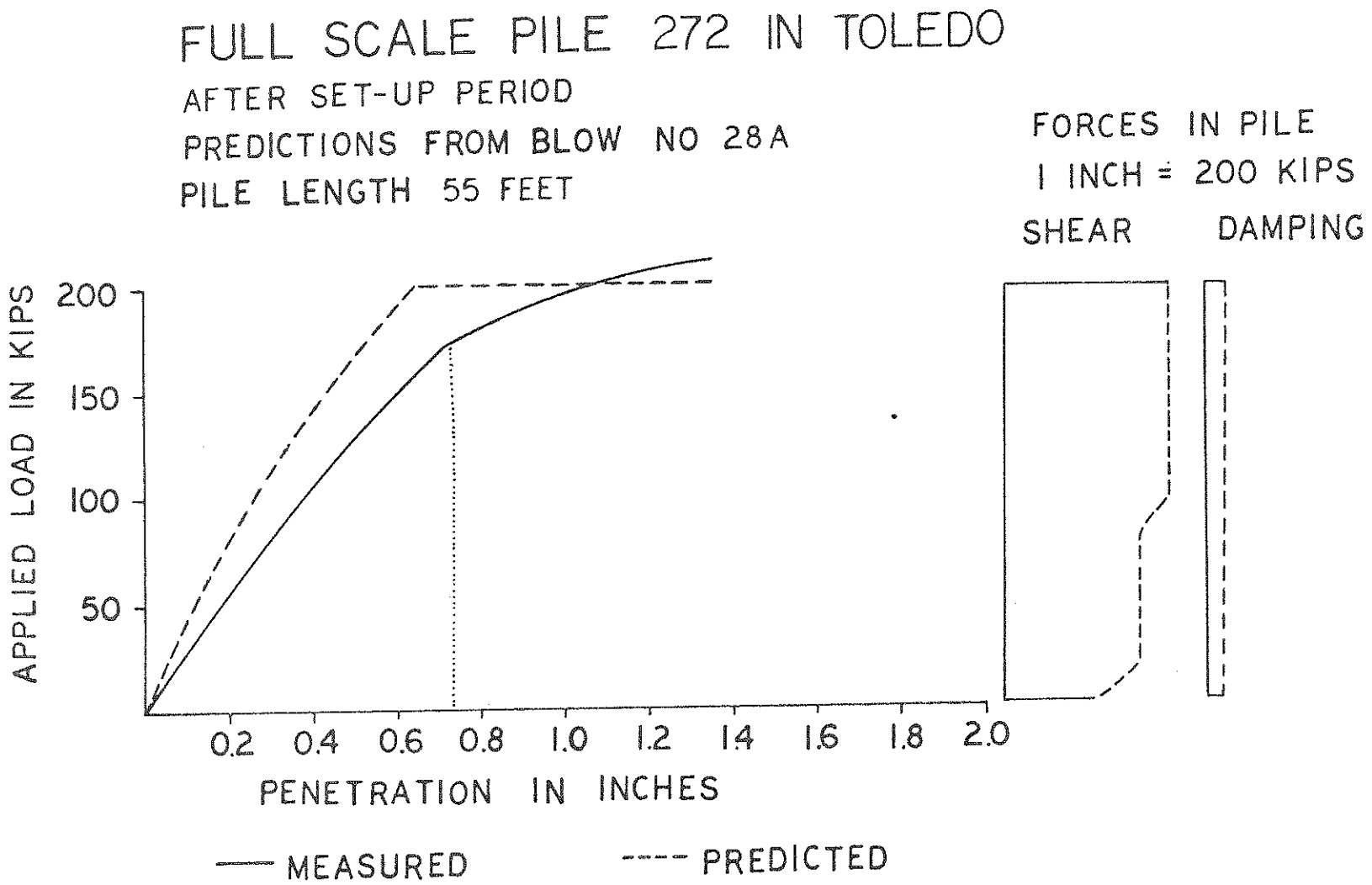

FIGURE 3.21: COMPARISON OF PREDICTED STATIC RESULTS WITH FIELD LOAD TEST AND FORCES IN PILE PREDICTION OBTAINED BY INSPECTION

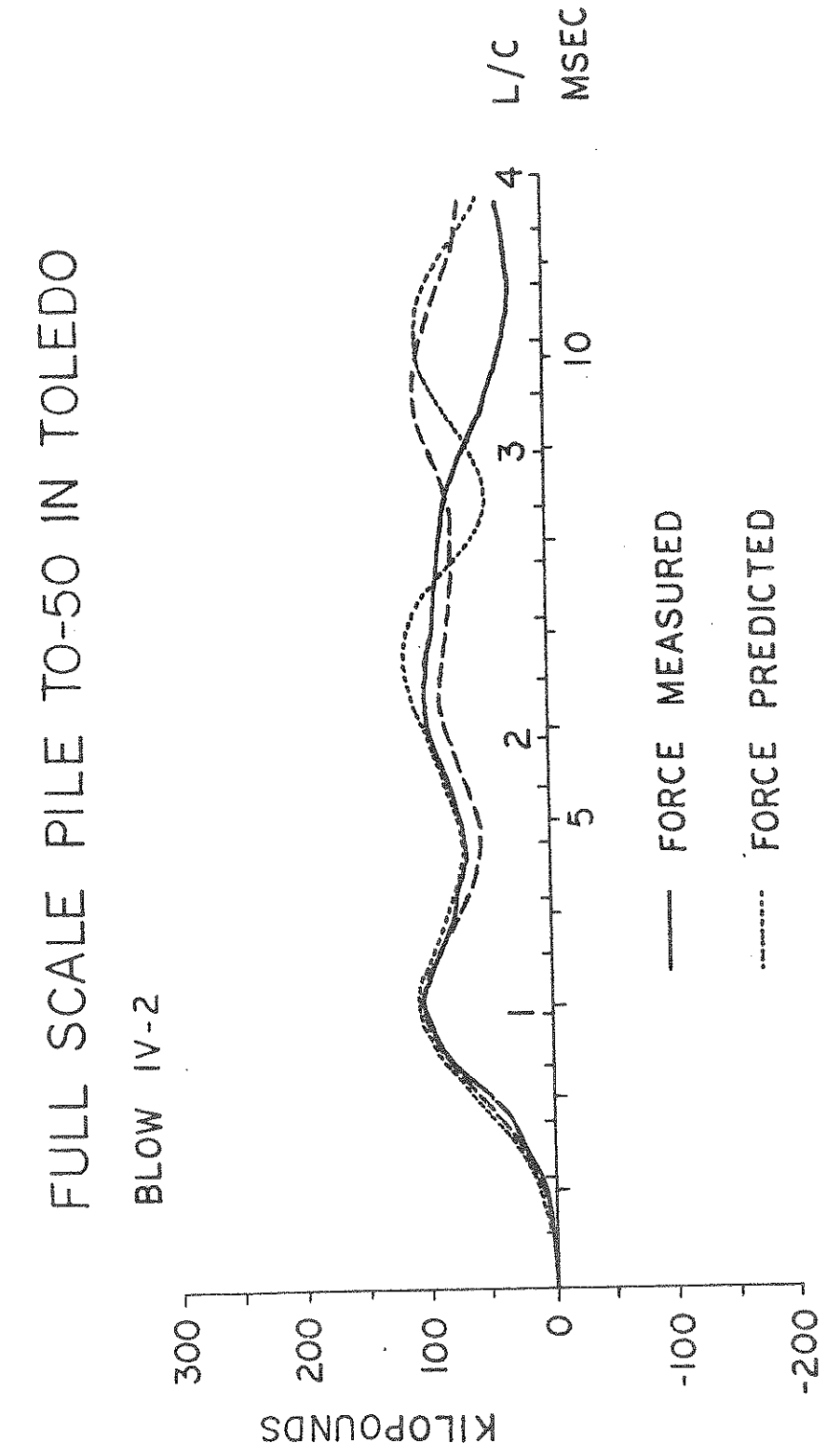

FIGURE 3.22: COMPARISON OF PREDICTED WITH MEASURED PILE TOP FORCE FOR DATA SET NO. 13

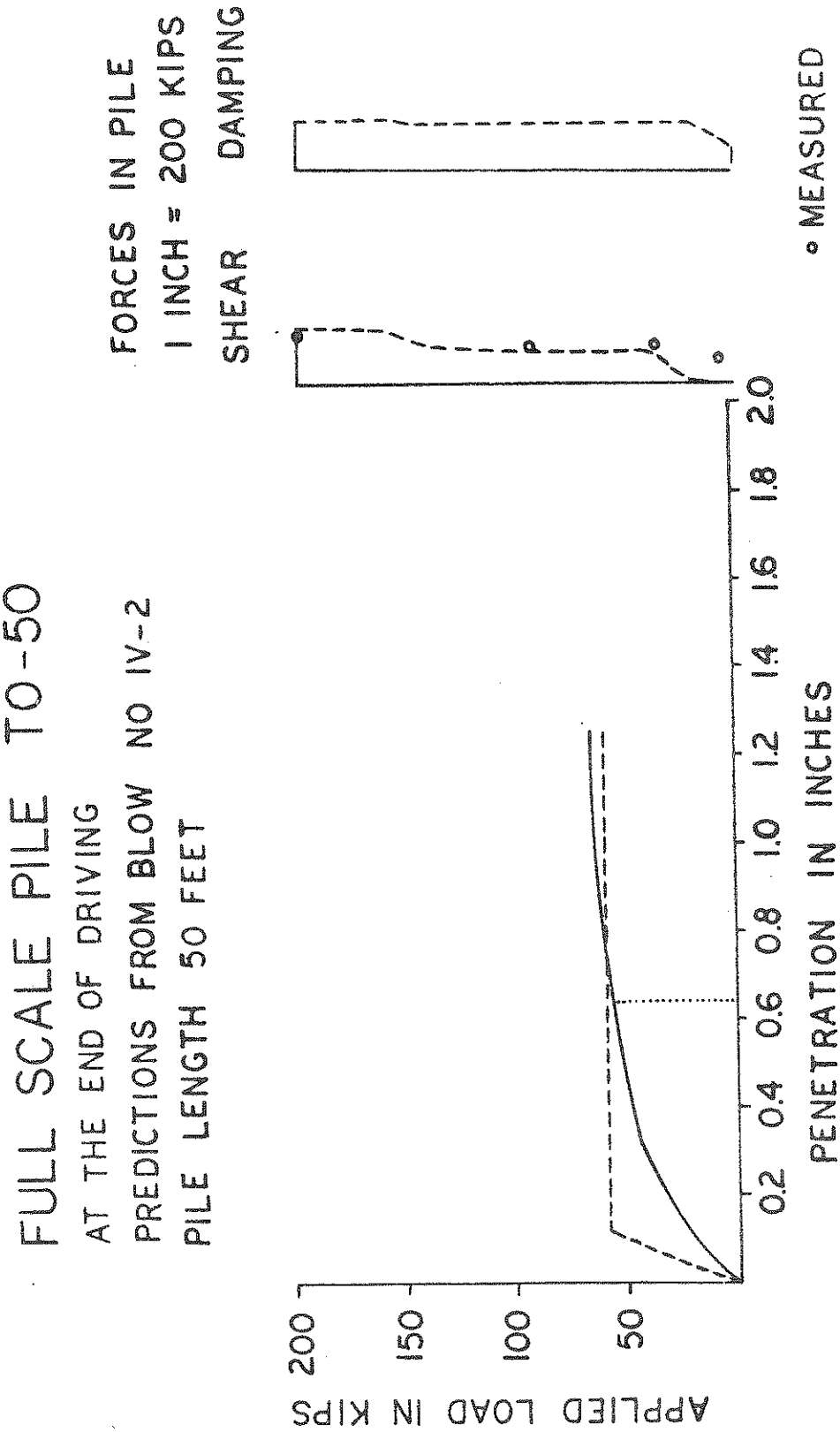

FIGURE 3.23: COMPARISON OF PREDICTED STATIC RESULTS WITH FIELD LOAD TEST AND FORCES IN PILE

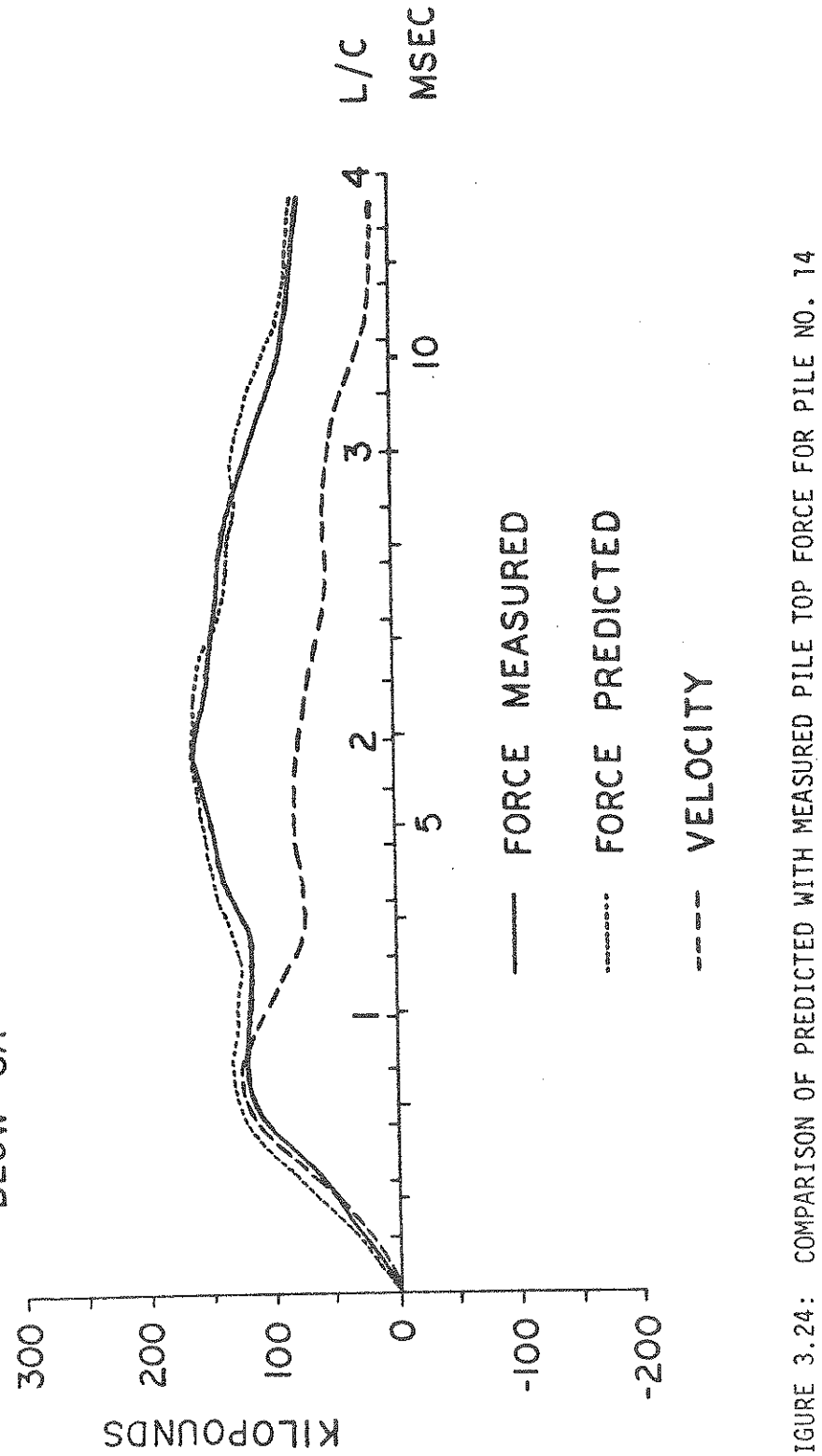

FIGURE 3.24: COMPARISON OF PREDICTED WITH MEASURED PILE TOP FORCE FOR PILE NO. 14

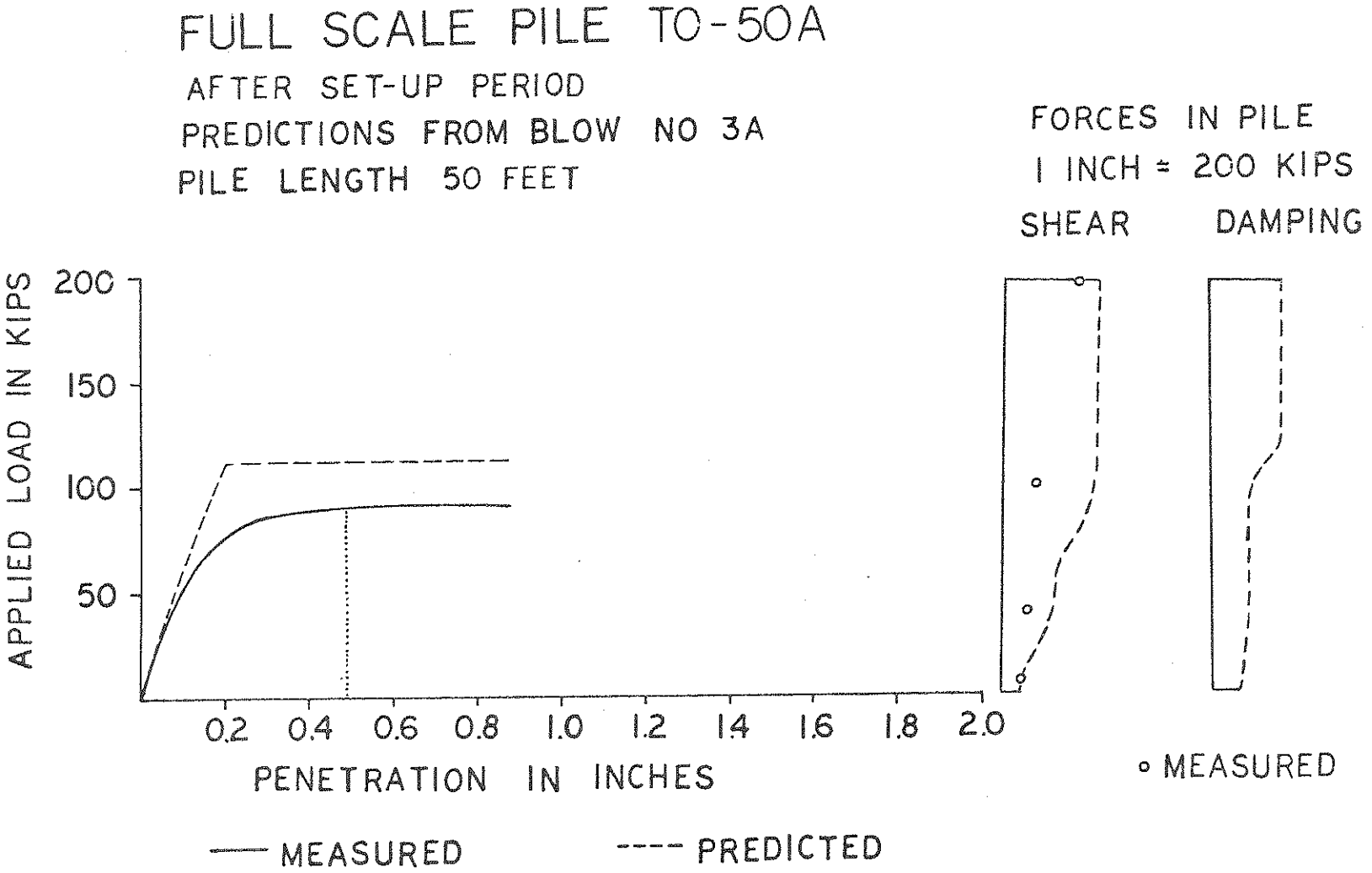

FIGURE 3.25: COMPARISON OF PREDICTED STATIC RESULTS WITH FIELD LOAD TEST AND FORCES IN PILE

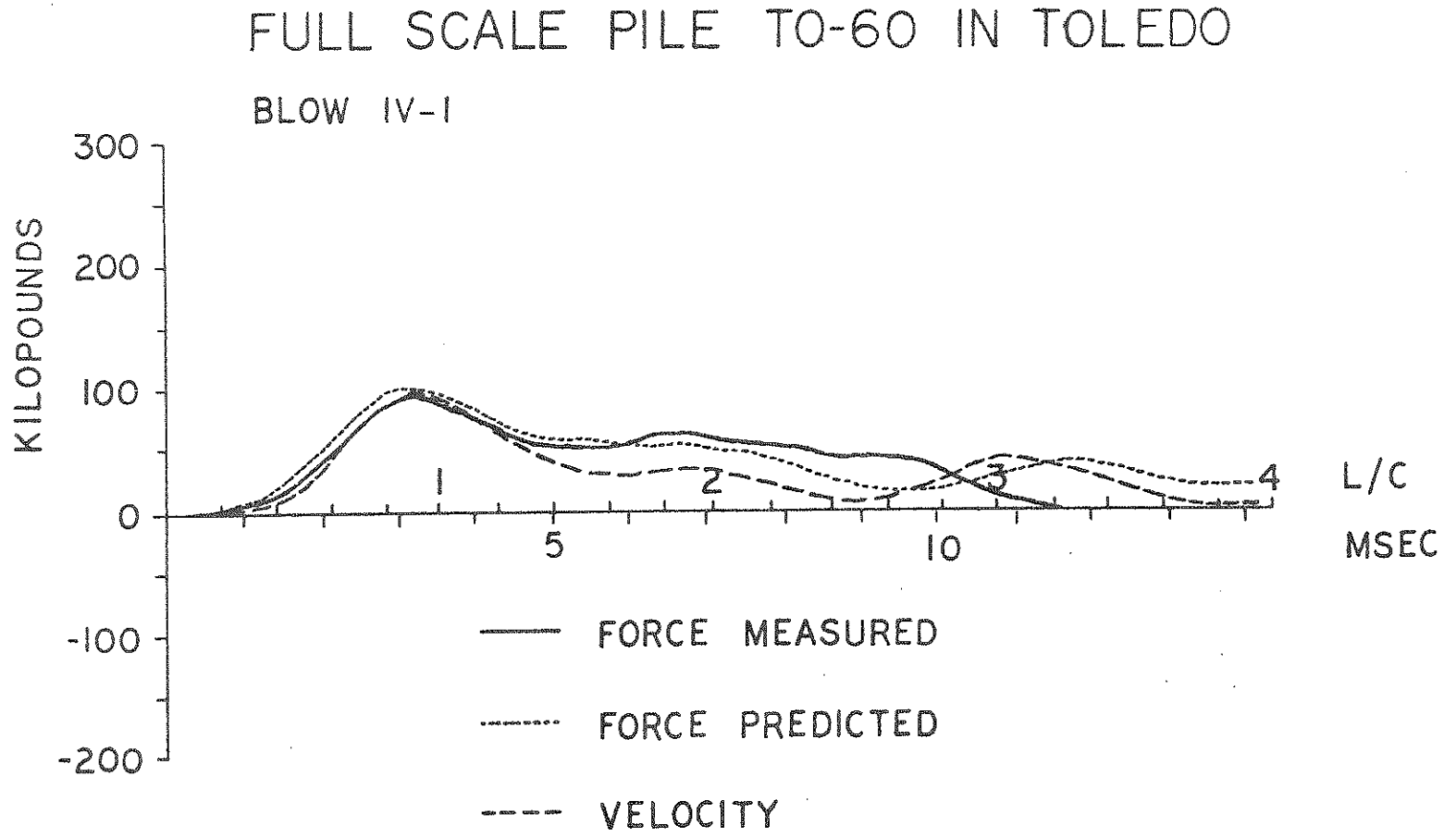

FIGURE 3.26: COMPARISON OF PREDICTED WITH MEASURED PILE TOP FORCE FOR DATA SET NO. 15

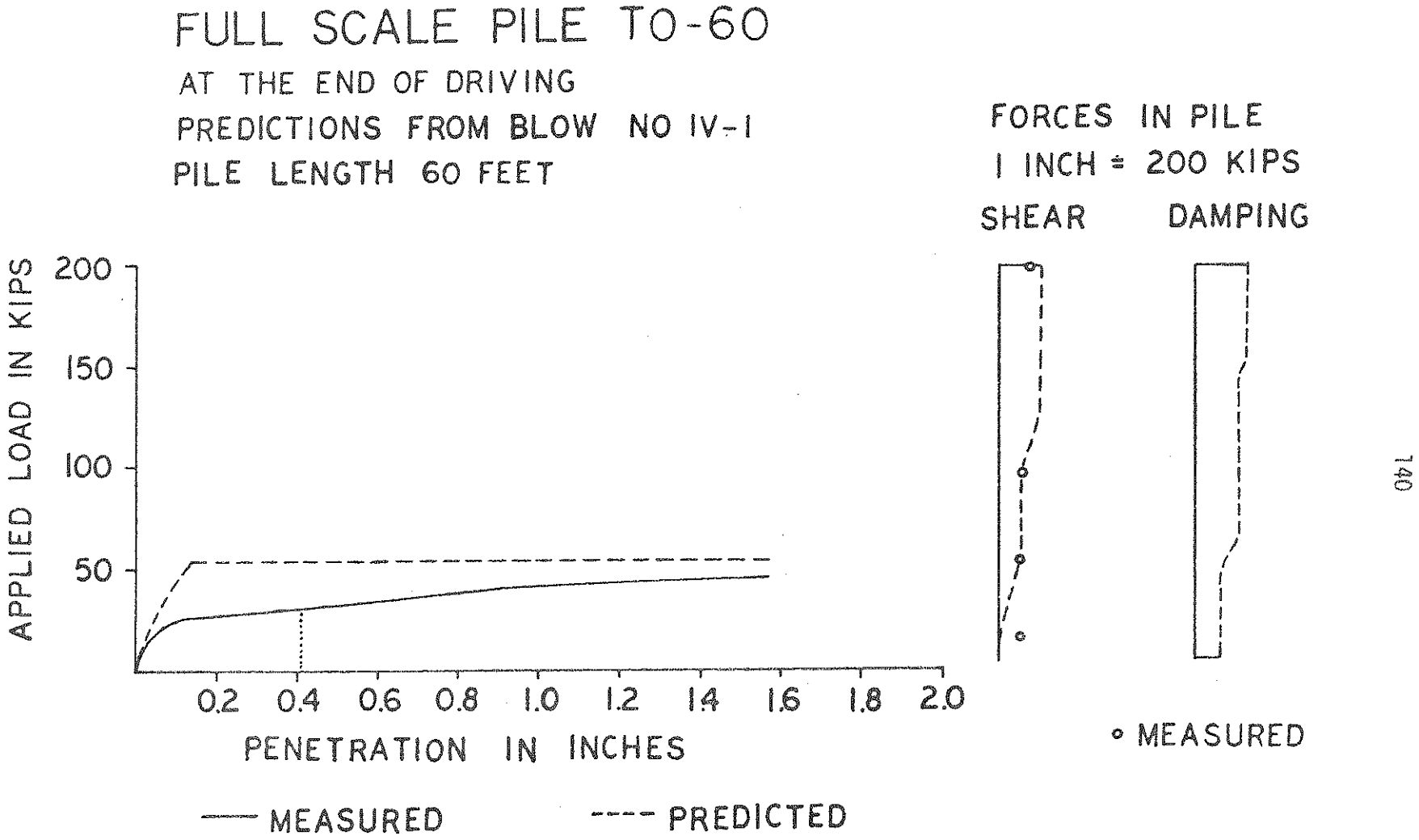

FIGURE 3.27: COMPARISON OF PREDICTED STATIC RESULT WITH FIELD LOAD TEST AND FORCES IN PILE

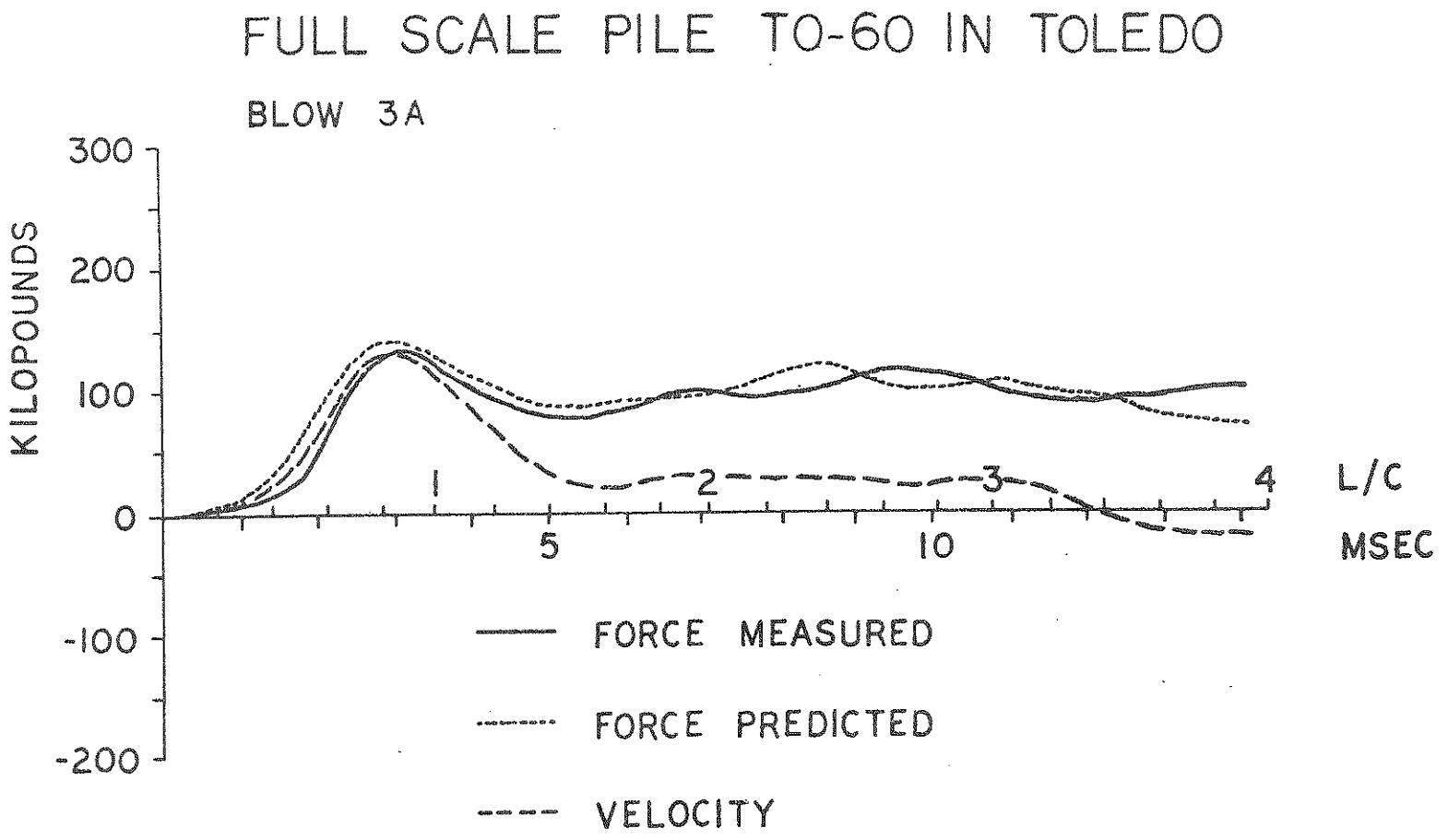

FIGURE 3.28: COMPARISON OF PREDICTED WITH MEASURED PILE TOP FORCE FOR DATA SET NO. 16

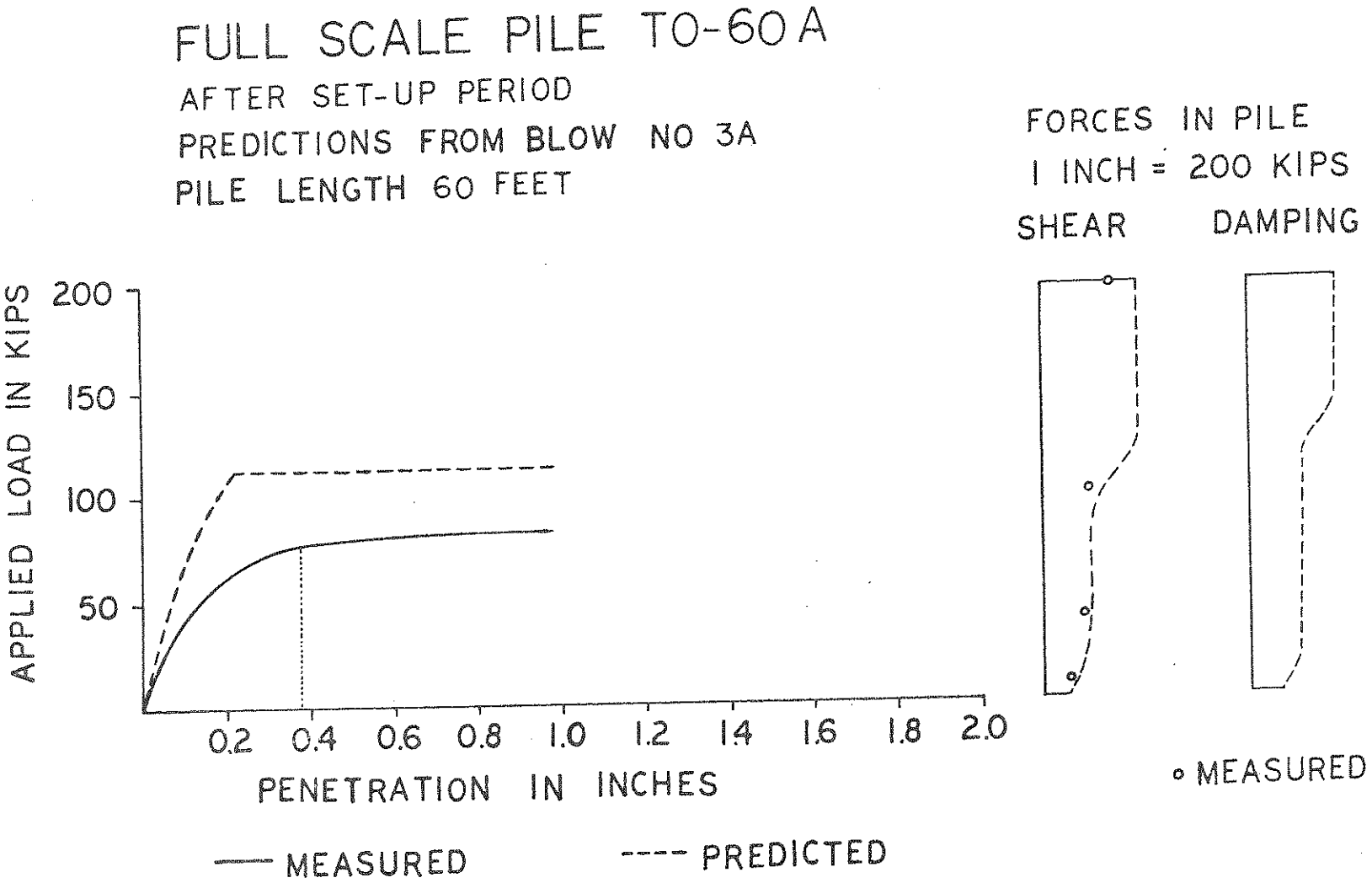

FIGURE 3.29: COMPARISON OF PREDICTED STATIC RESULTS WITH FIELD LOAD TEST AND FORCES IN PILE

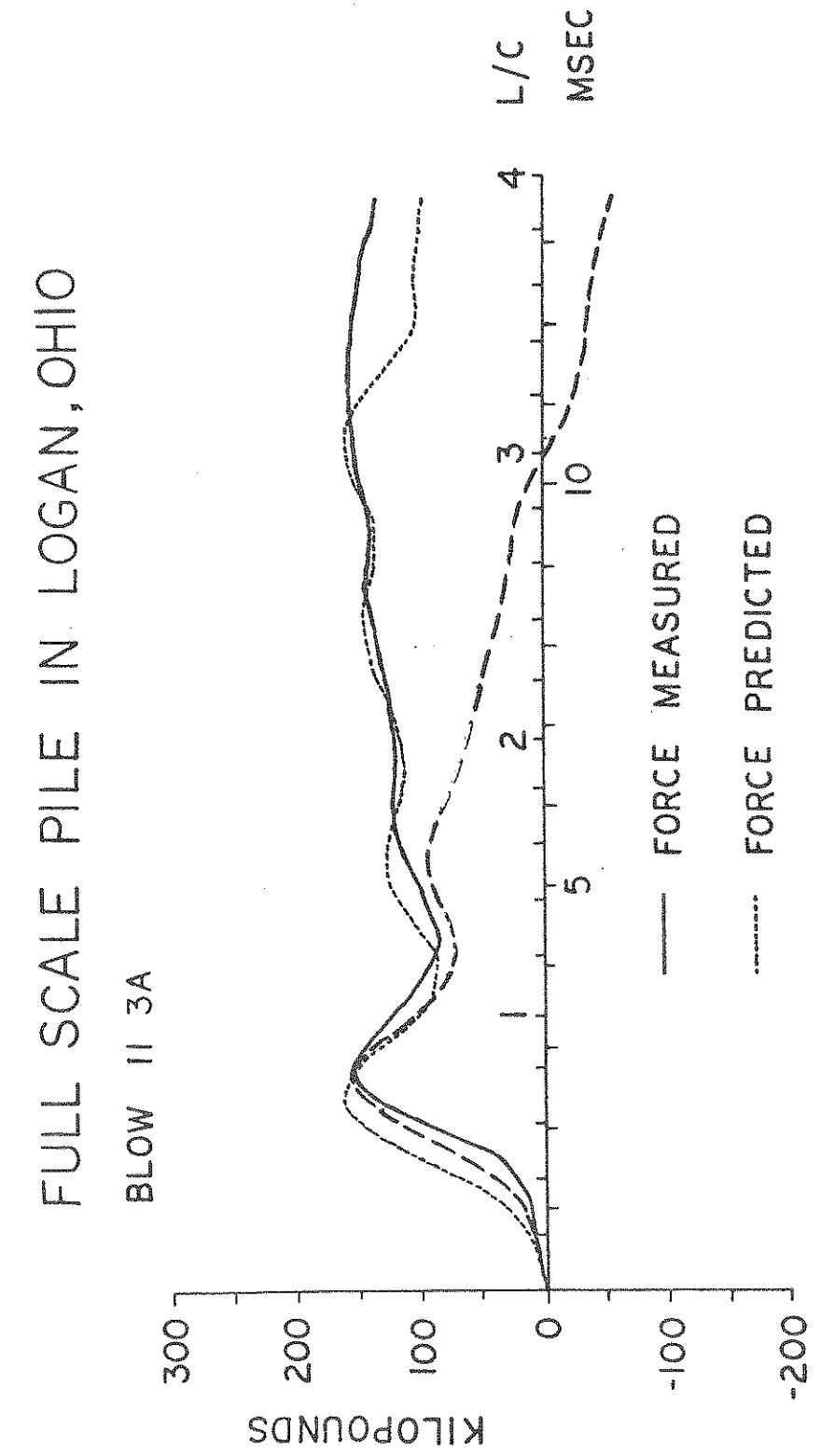

FIGURE 3.30: COMPARISON OF PREDICTED WITH MEASURED PILE TOP FORCE FOR DATA SET NO. 17

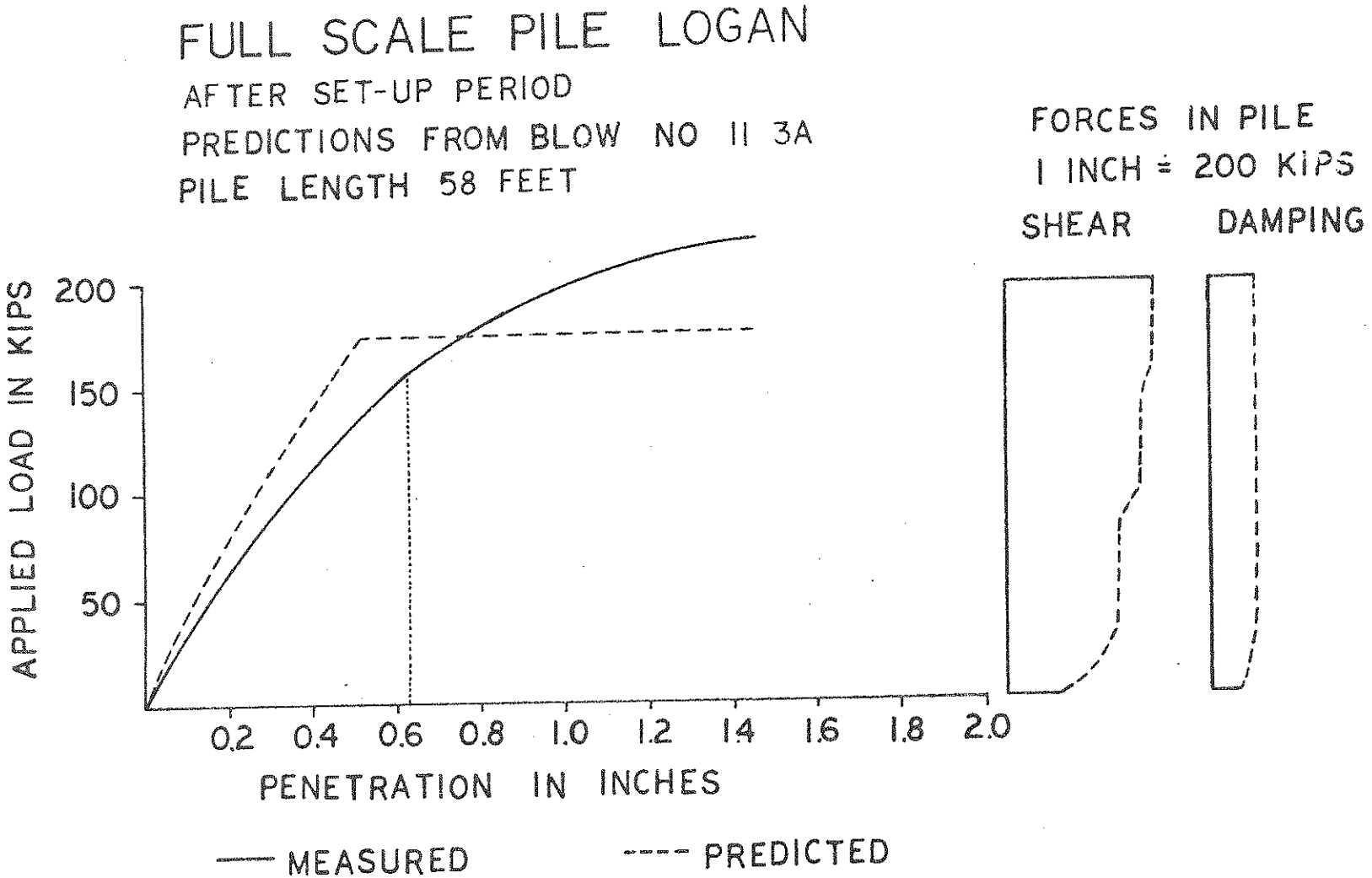

FIGURE 3.31: COMPARISON OF PREDICTED STATIC RESULTS WITH FIELD LOAD TEST AND FORCES IN PILE

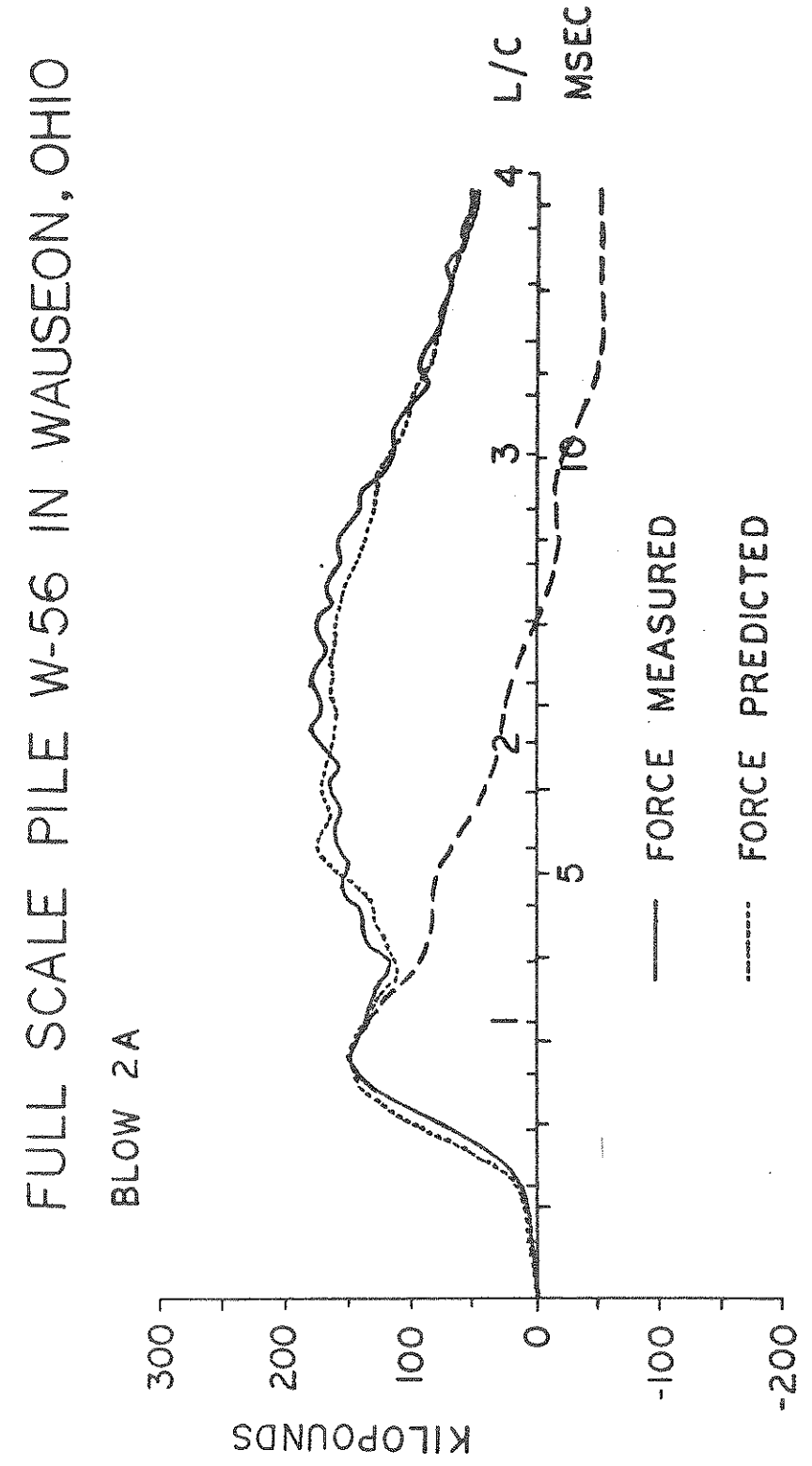

FIGURE 3.32: COMPARISON OF PREDICTED WITH MEASURED PILE TOP FORCE FOR DATA SET NO. 18

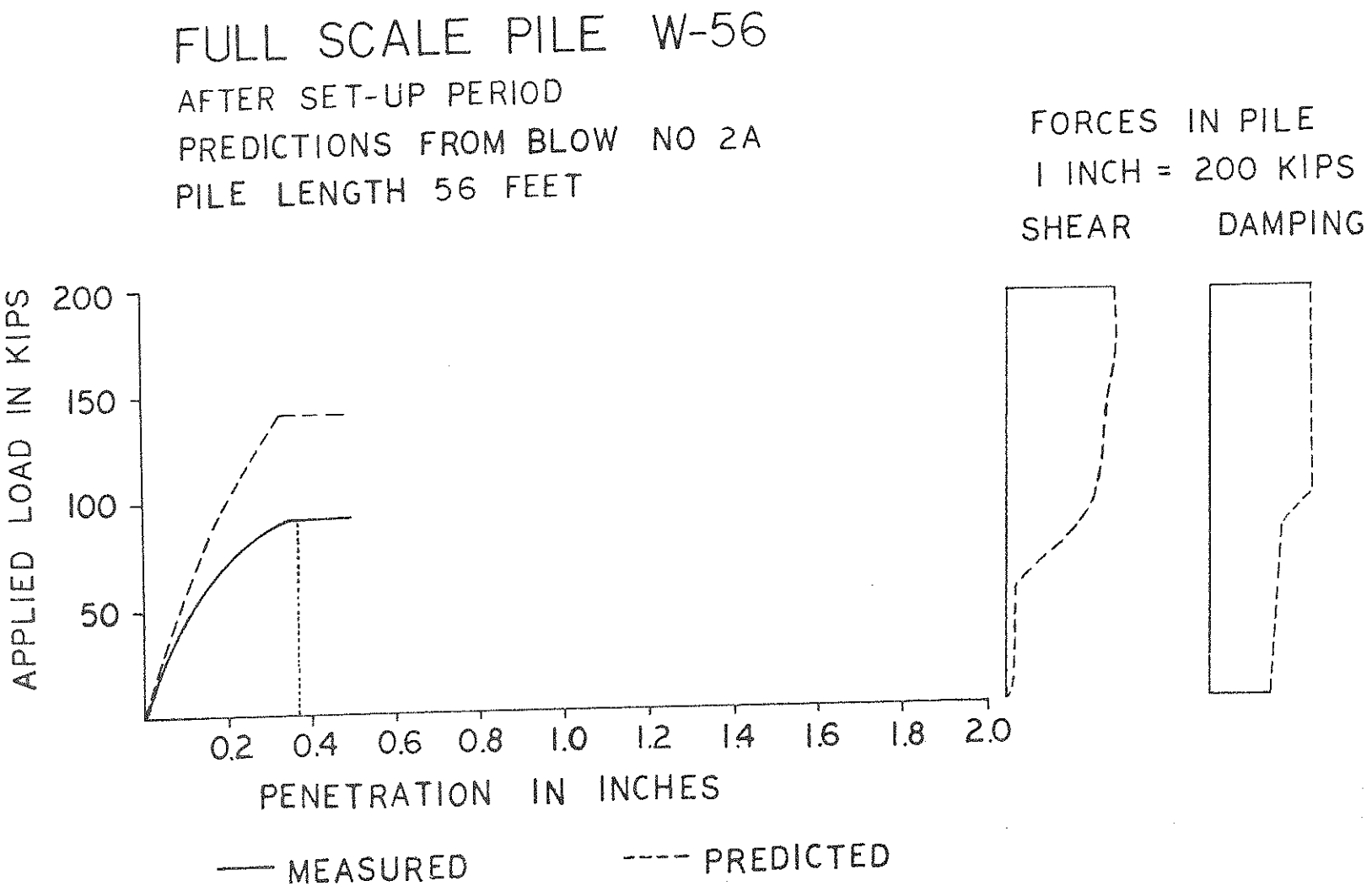

FIGURE 3.33: COMPARISON OF PREDICTED STATIC RESULTS WITH MEASURED LOAD TEST AND FORCES IN PILE

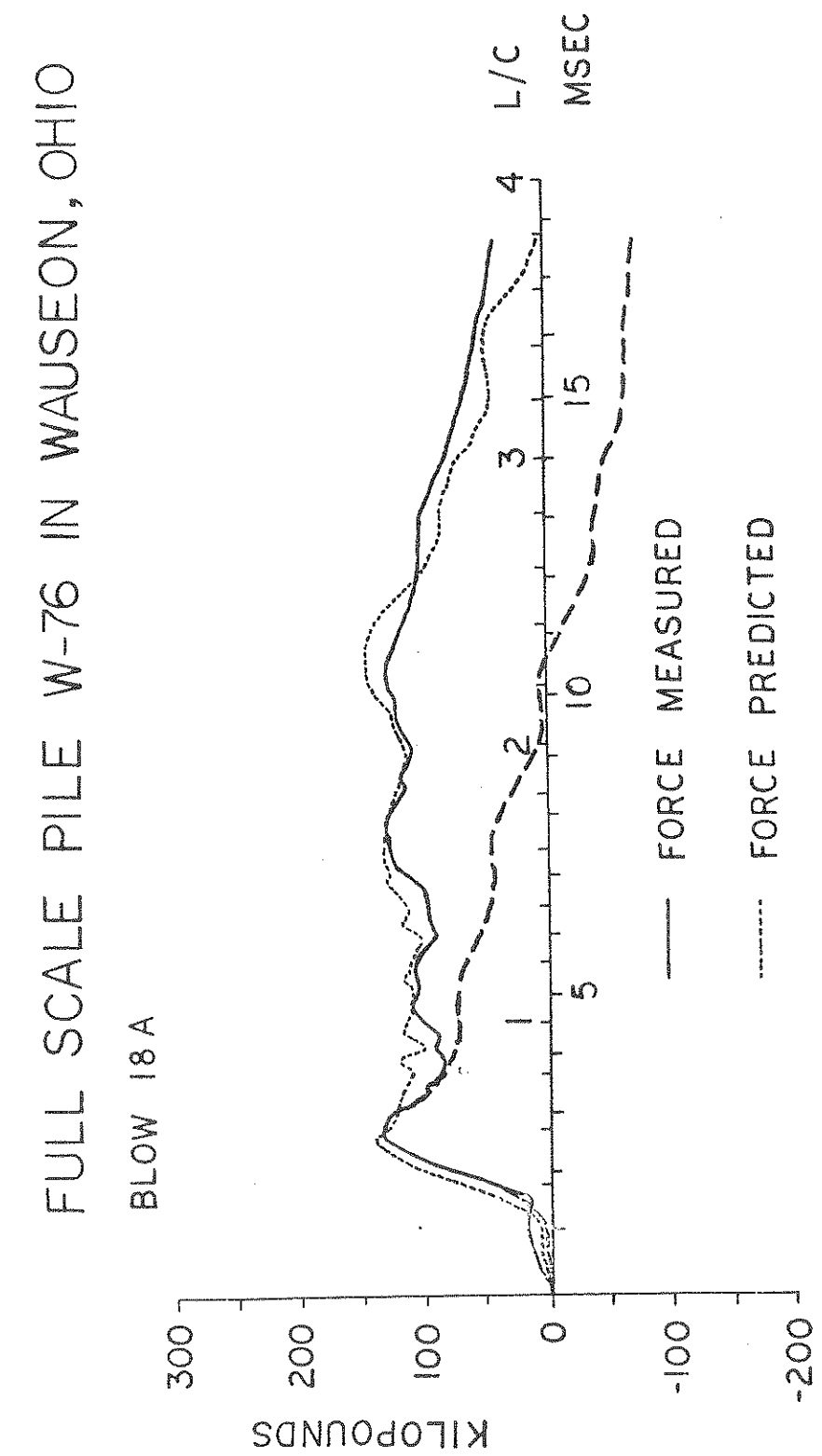

FIGURE 3.34: COMPARISON OF PREDICTED WITH MEASURED PILE TOP FORCE FOR DATA SET NO. 19 PREDICTION FROM AUTOMATED ROUTINE

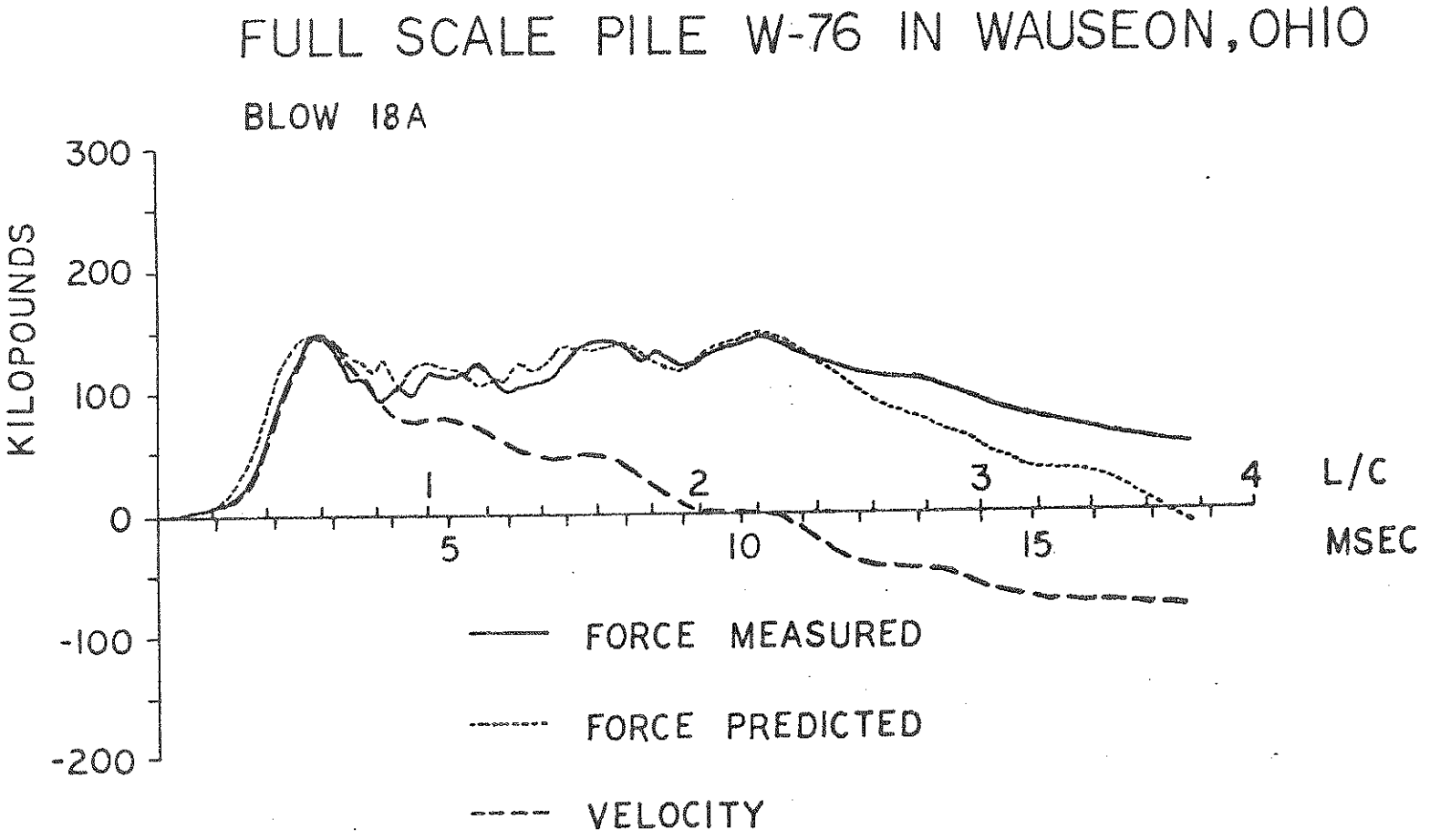

FIGURE 3.35: COMPARISON OF PREDICTED WITH MEASURED PILE TOP FORCE FOR DATA SET NO. 19
PREDICTION BY INSPECTION

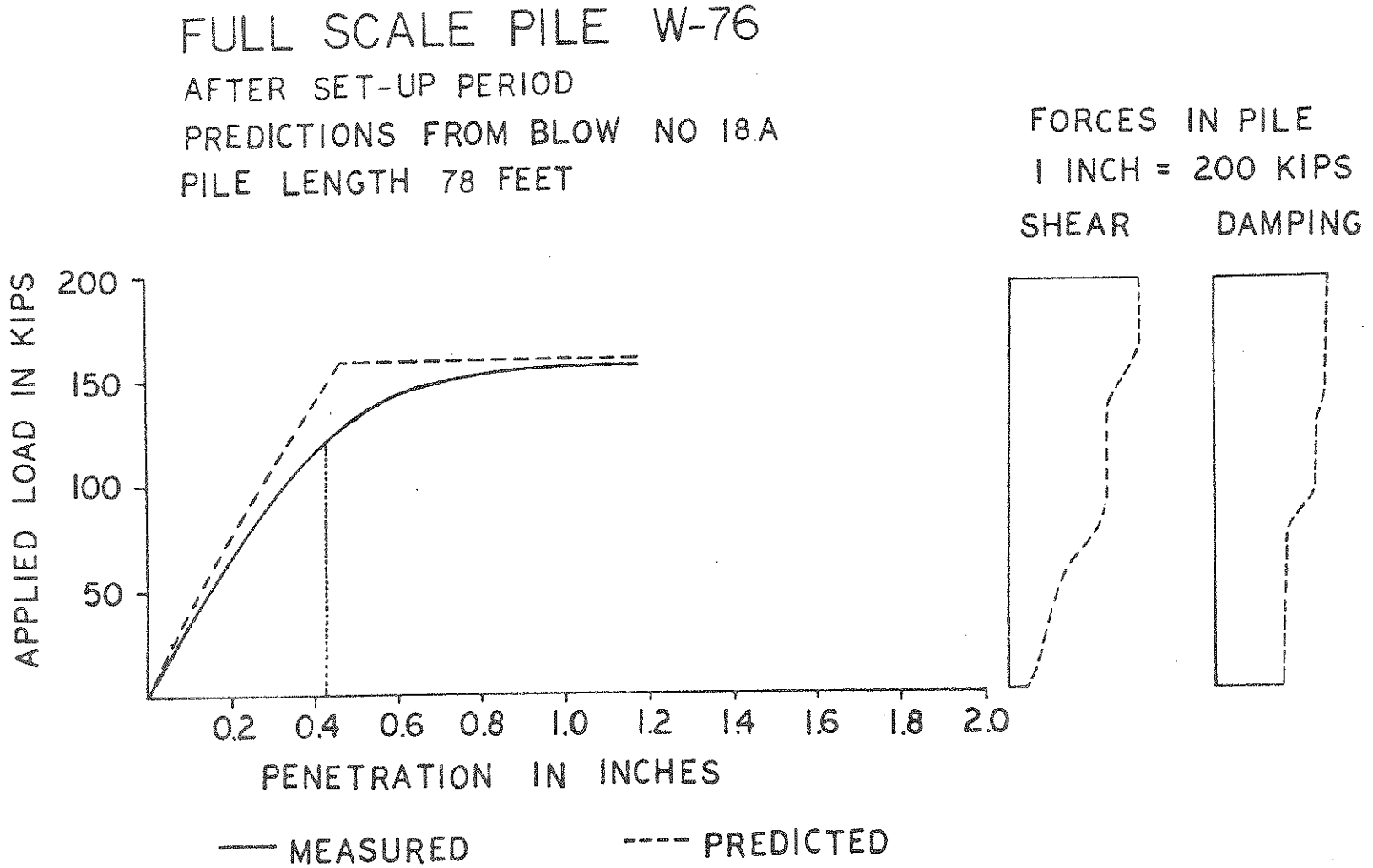

FIGURE 3.36: COMPARISON OF PREDICTED STATIC RESULTS WITH FIELD LOAD TEST AND FORCES IN PILE PREDICTIONS FROM COMPUTER ROUTINE

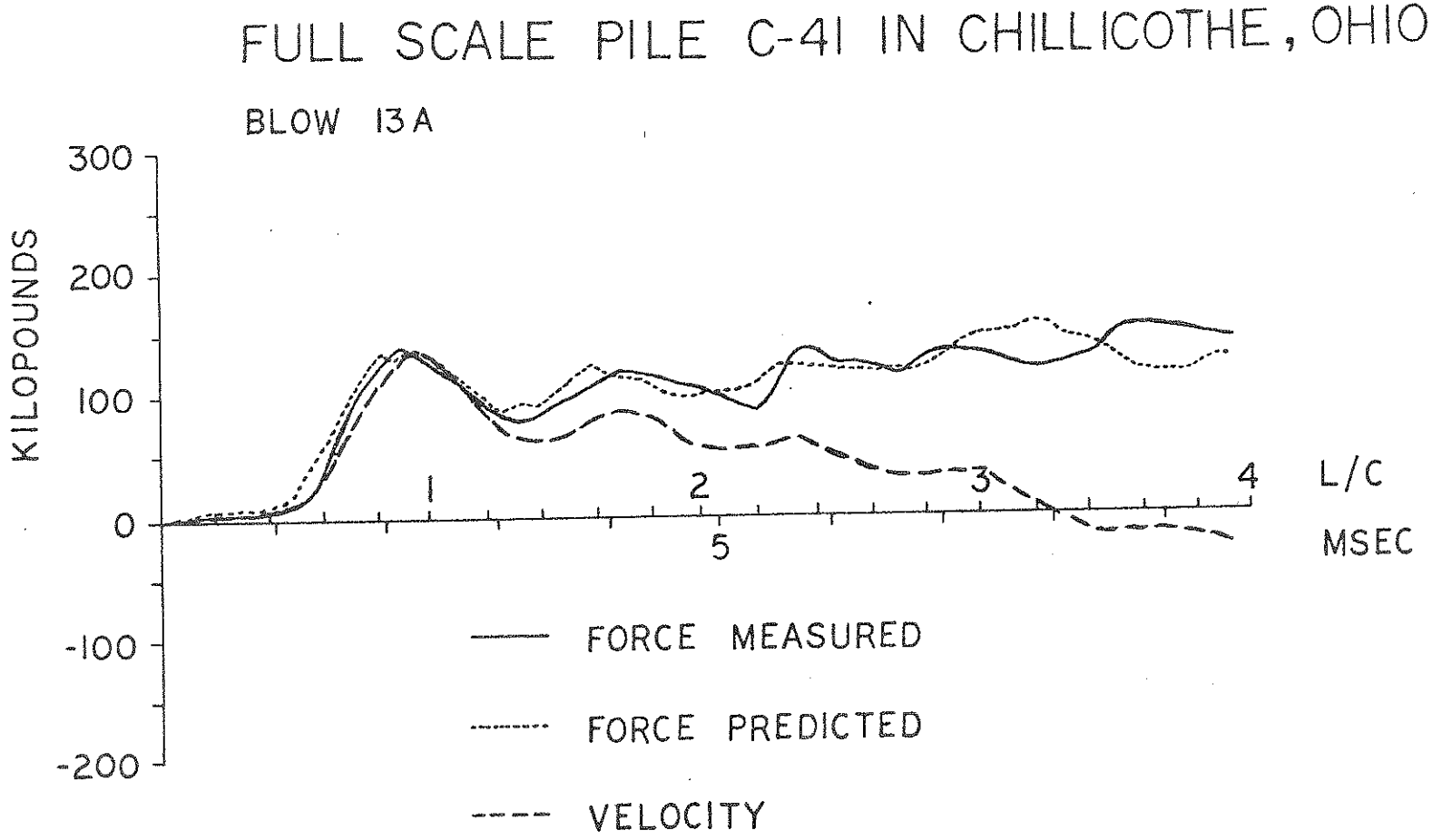

FIGURE 3.37: COMPARISON OF PREDICTED WITH MEASURED PILE TOP FORCE FOR DATA SET NO. 19

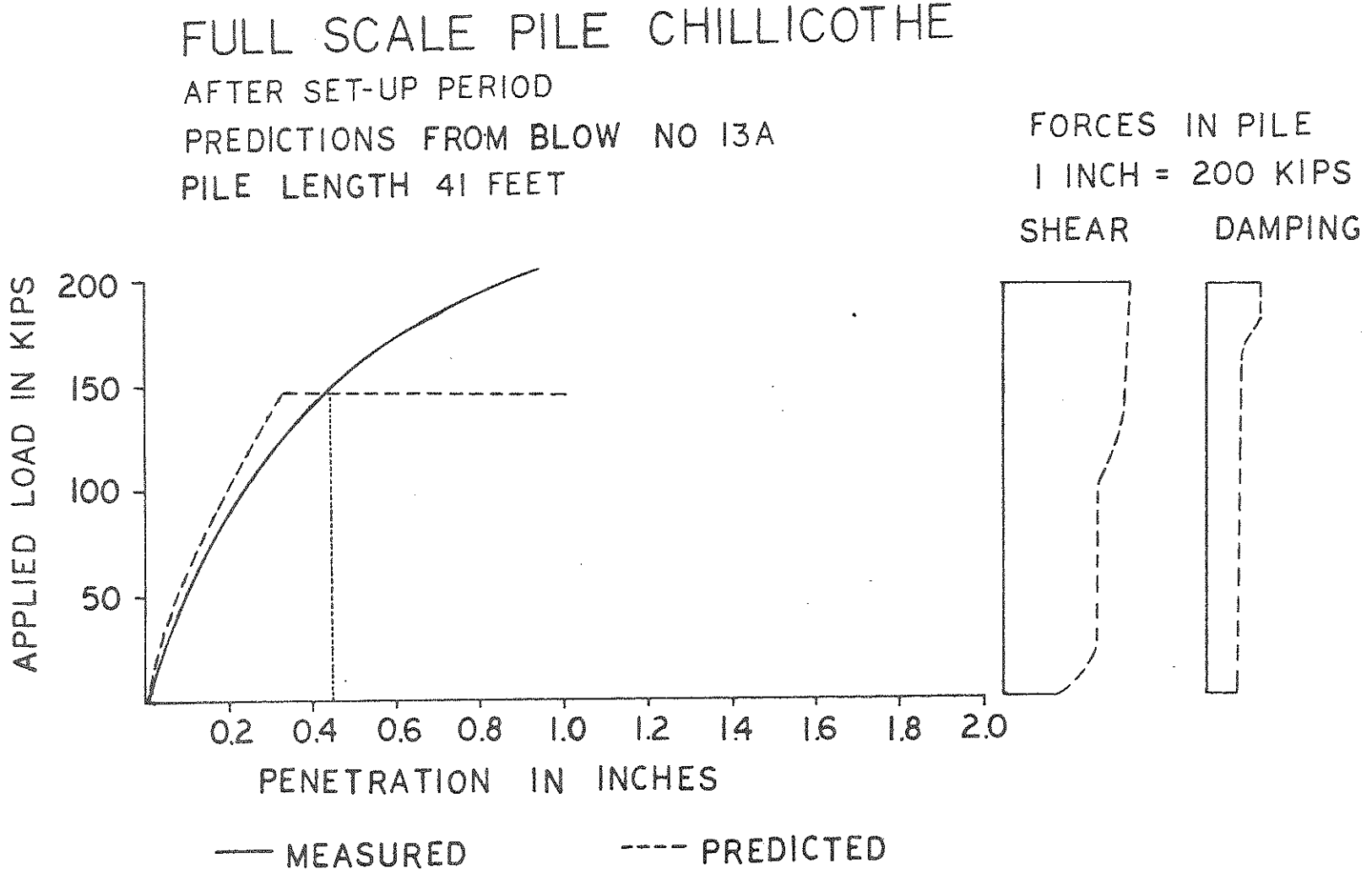

FIGURE 3.38: COMPARISON OF PREDICTED STATIC RESULTS WITH FIELD TEST AND FORCES IN PILE

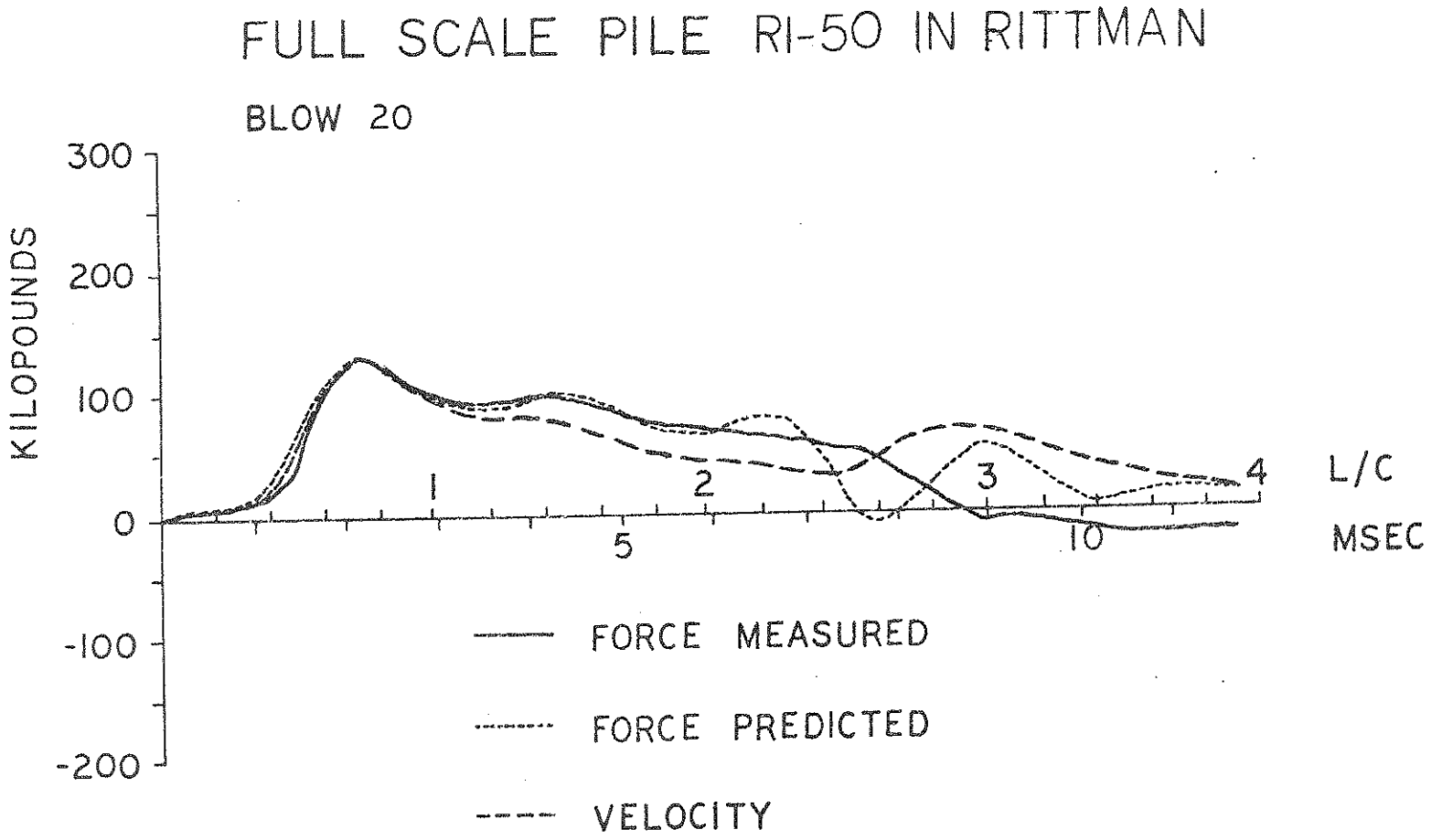

FIGURE 3.39: COMPARISON OF PREDICTED WITH MEASURED PILE TOP FORCE FOR DATA SET NO. 21

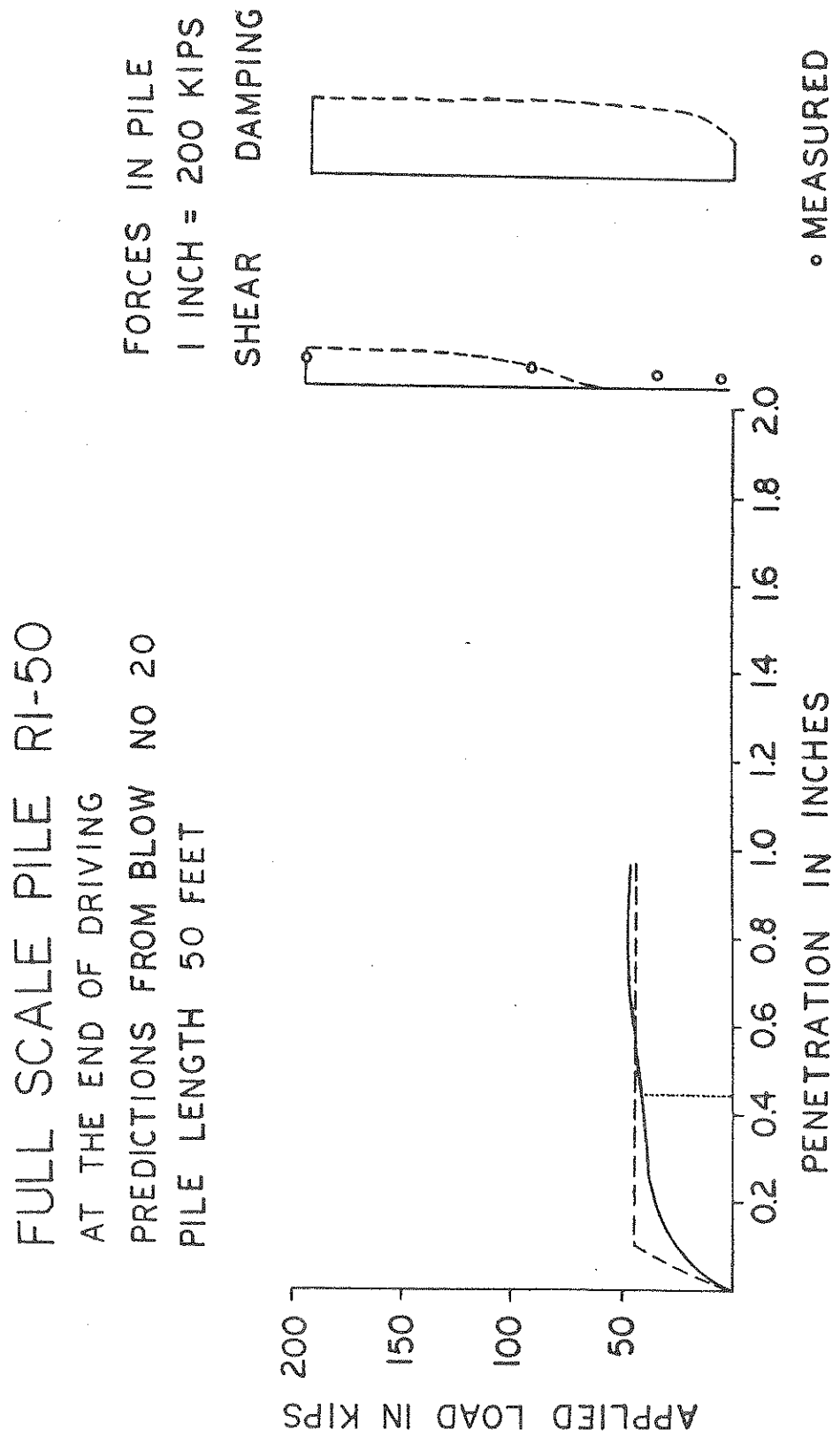

FIGURE 3.40: COMPARISON OF PREDICTED STATIC RESULTS WITH FIELD LOAD TEST AND FORCES IN PILE

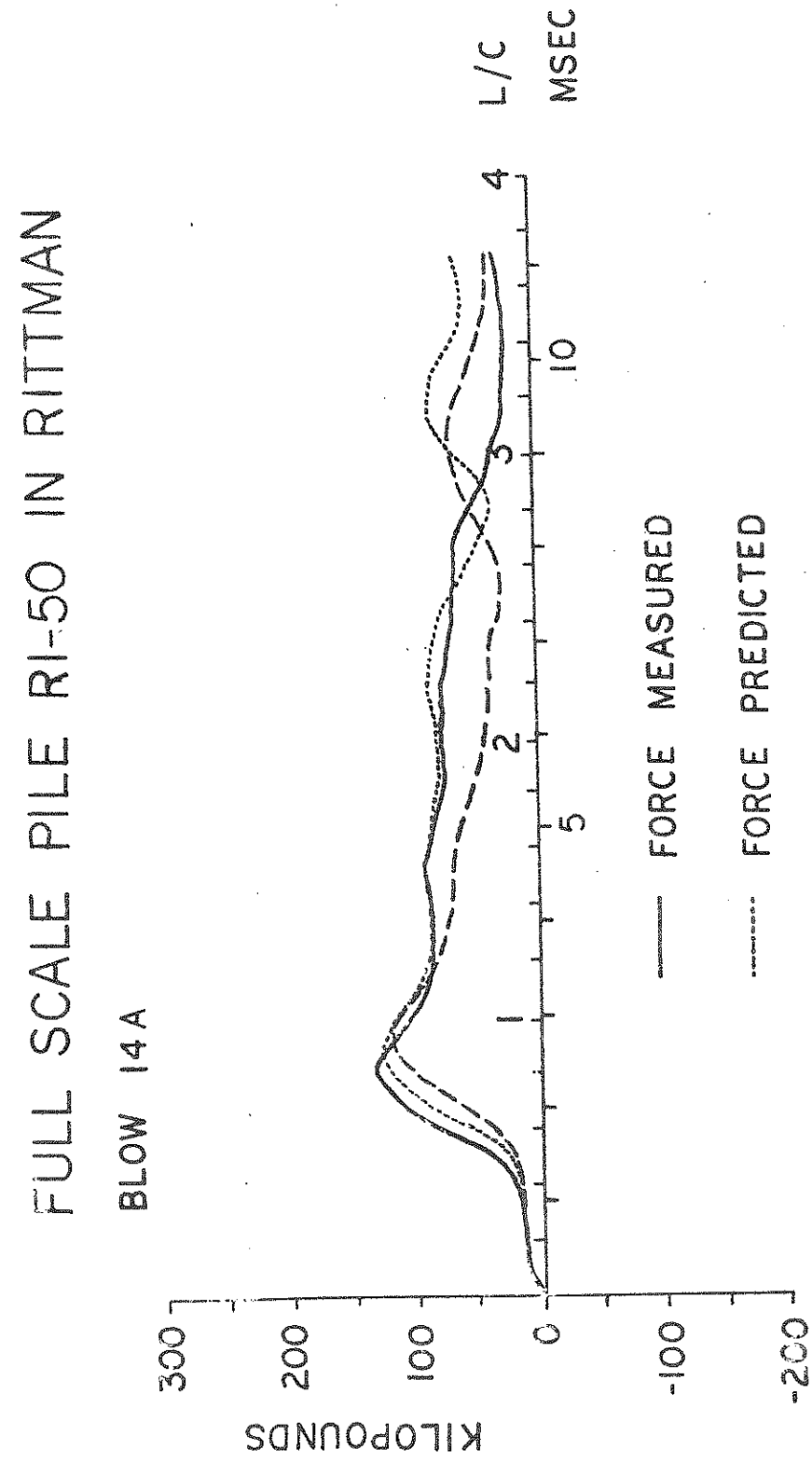

FIGURE 3.41: COMPARISON OF PREDICTED WITH MEASURED PILE TOP FORCE FOR DATA SET NO. 22

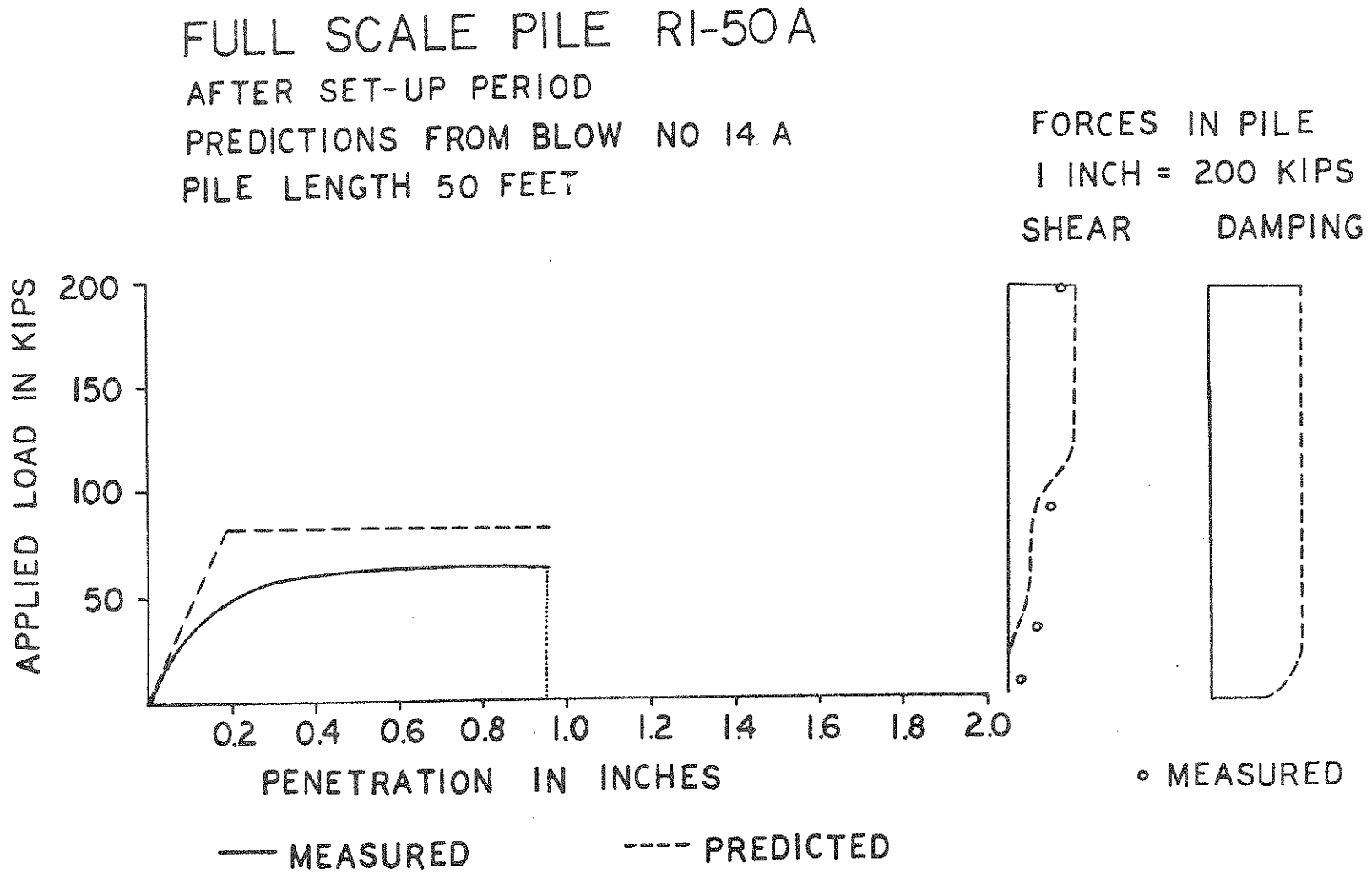

FIGURE 3.42: COMPARISON OF PREDICTED STATIC RESULTS WITH FIELD LOAD TEST AND FORCES IN PILE

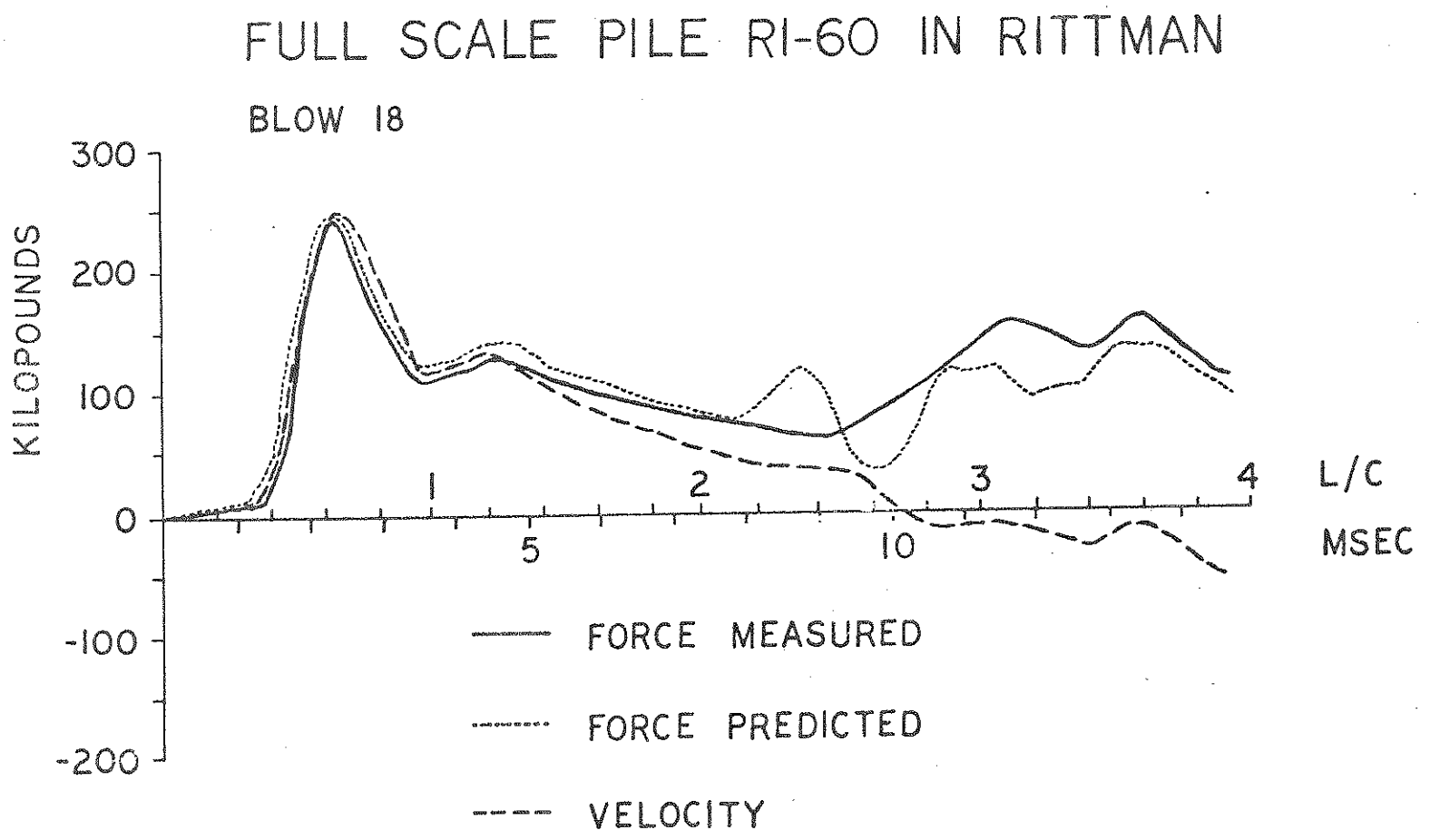

FIGURE 3.43: COMPARISON OF PREDICTED WITH MEASURED PILE TOP FORCE FOR DATA SET NO. 23

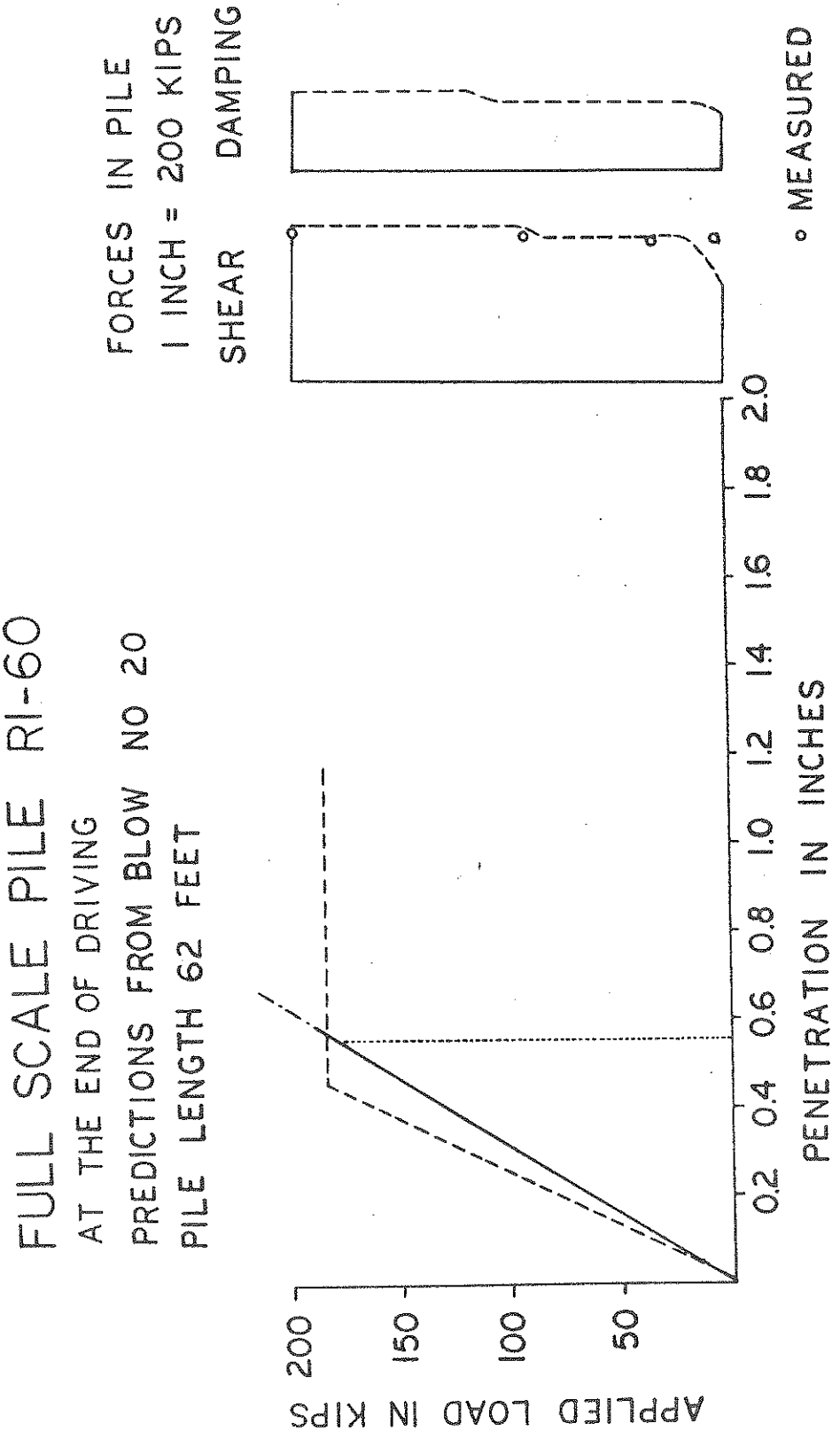

FIGURE 3.44: COMPARISON OF PREDICTED STATIC RESULTS WITH FIELD LOAD TEST AND FORCES IN PILE

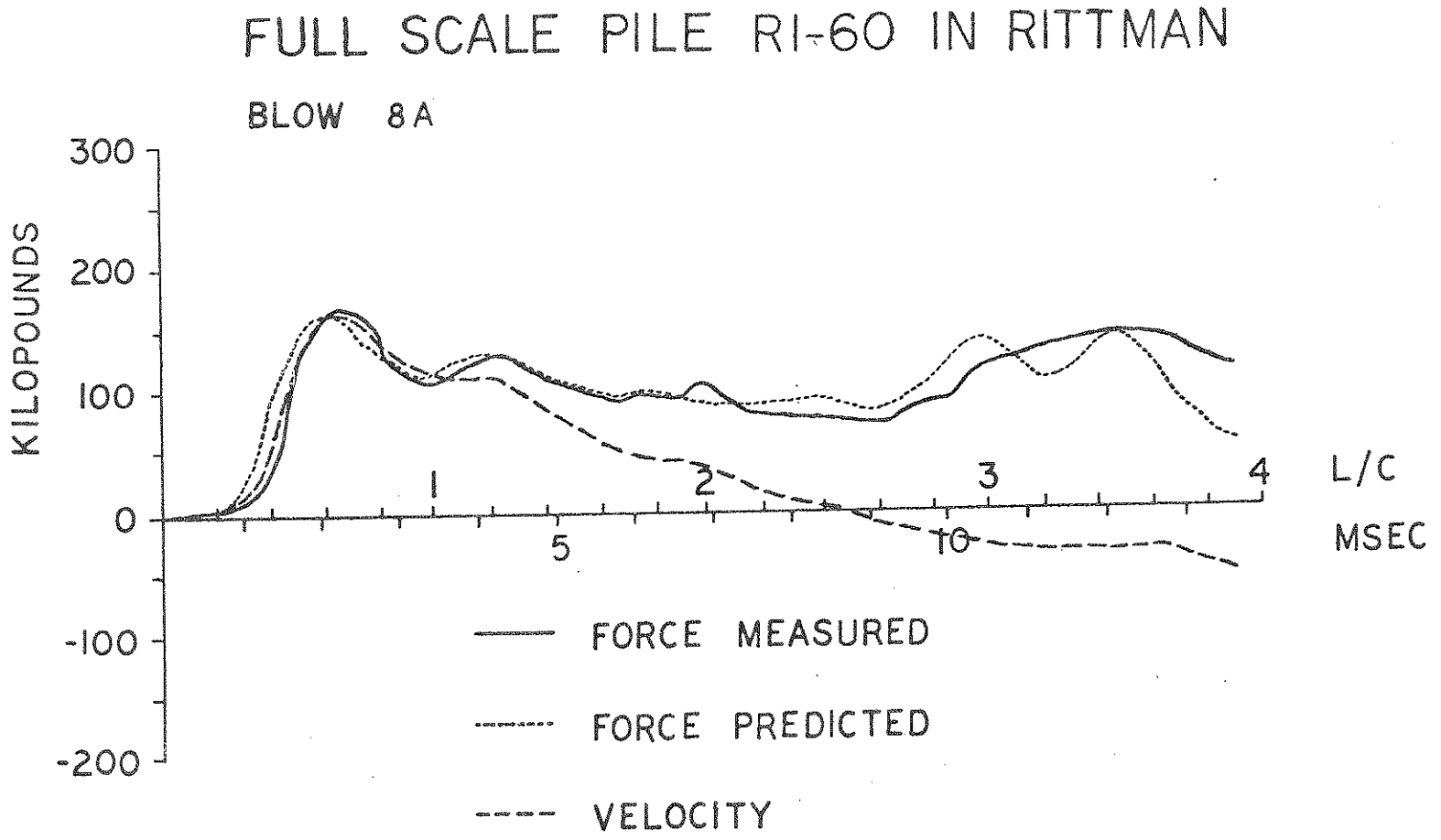

FIGURE 3.45: COMPARISON OF PREDICTED WITH MEASURED PILE TOP FORCE FOR DATA SET NO. 24

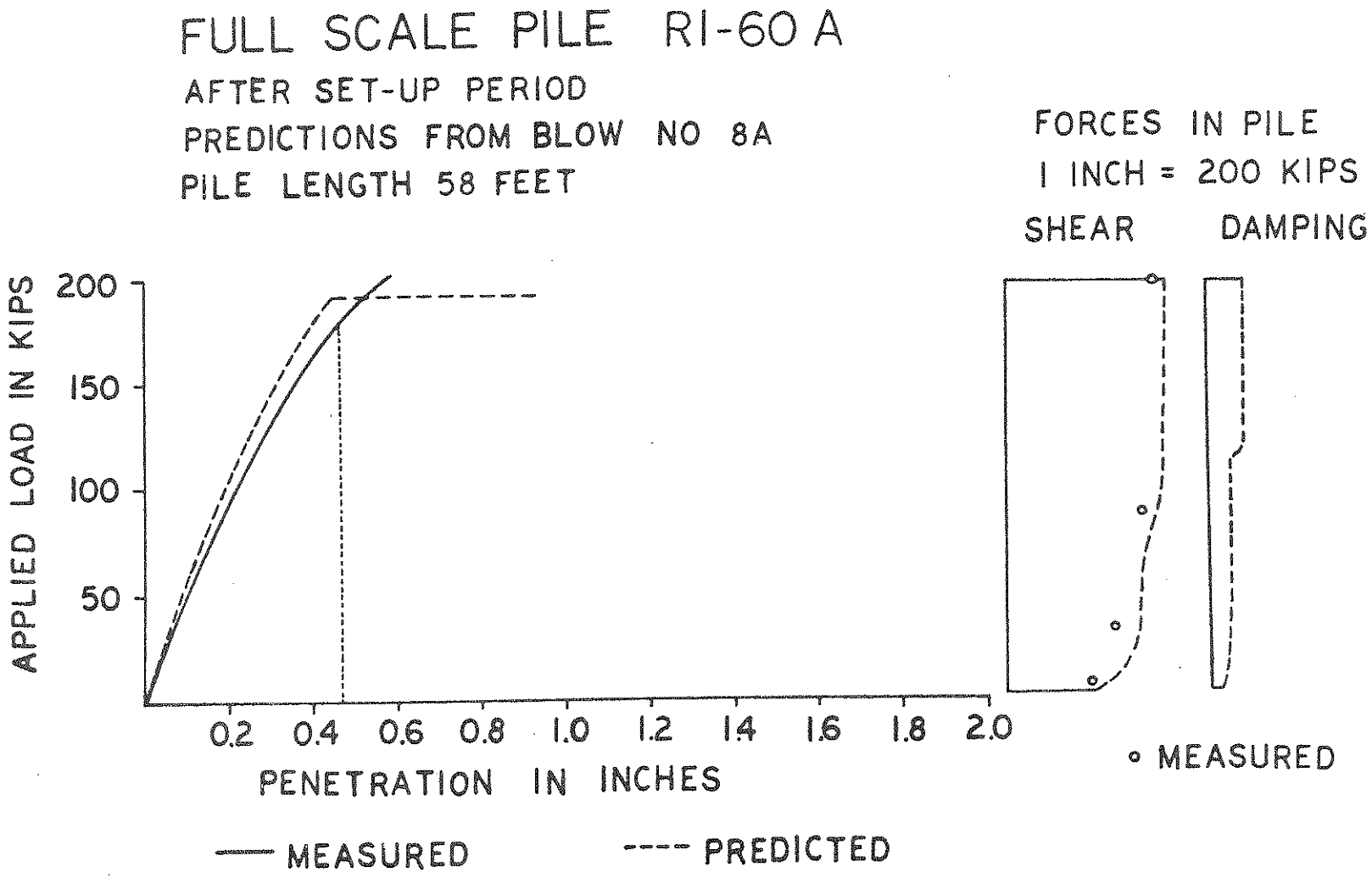

FIGURE 3.46: COMPARISON OF PREDICTED STATIC RESULTS WITH FIELD LOAD TEST AND FORCES IN PILE

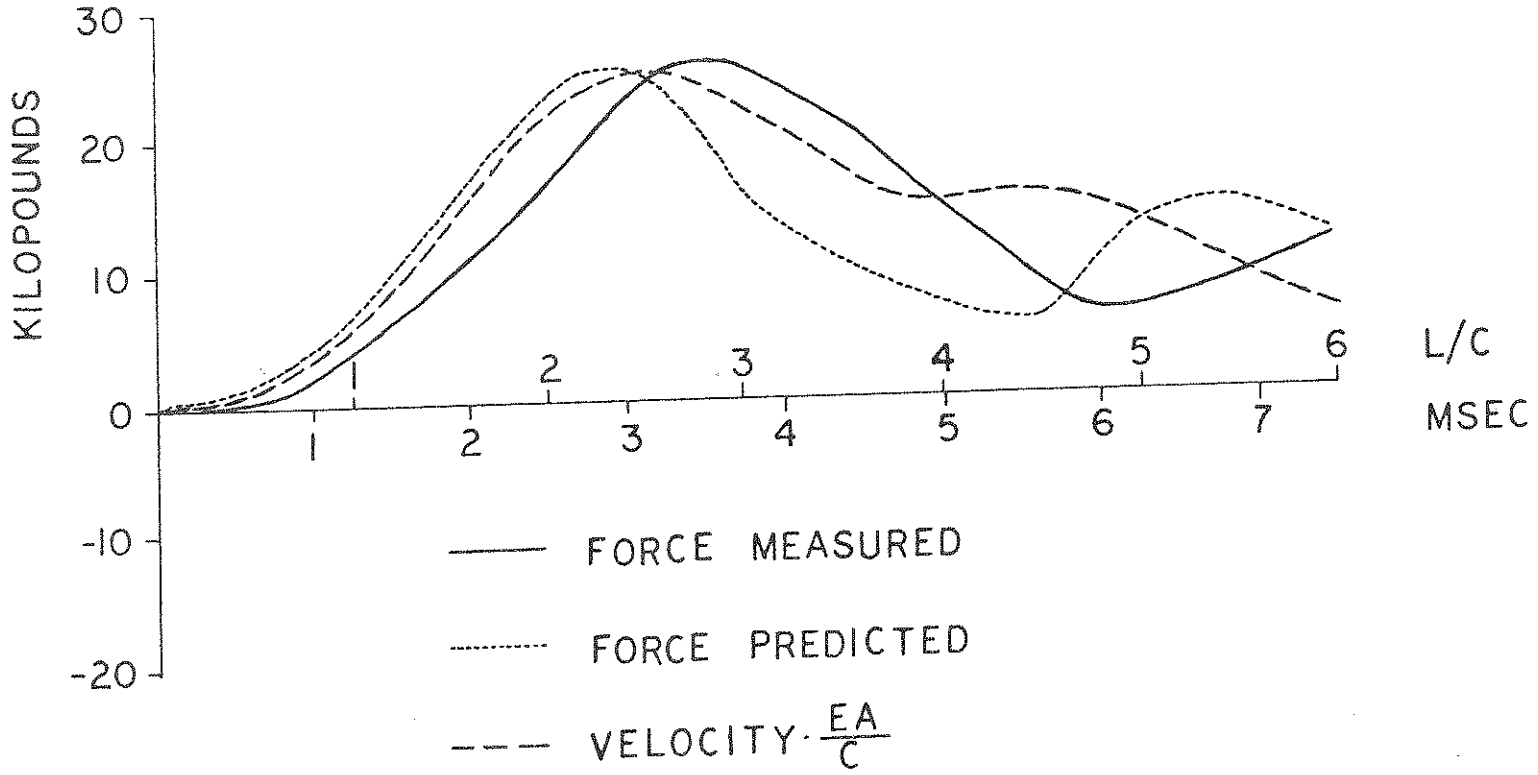

FIGURE 3.47: MEASURED FORCE AND VELOCITY AND PREDICTED PILE TOP FORCE FOR REDUCED SCALE Pile 3-R-20 (Data Set No. 12)

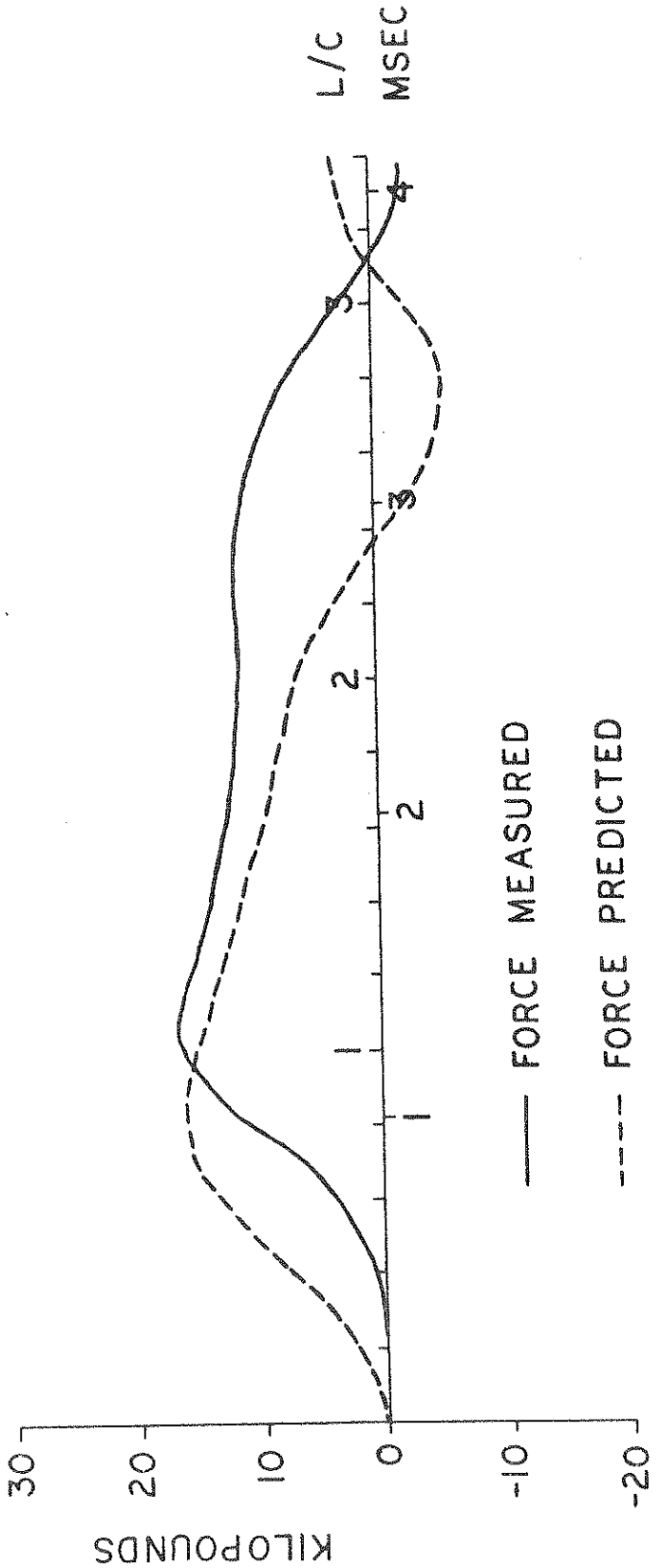

FIGURE 3.48: MEASURED AND PREDICTED PILETOP FORCE FOR REDUCED SCALE PILE 6-T-5
(Data Set No. 22)

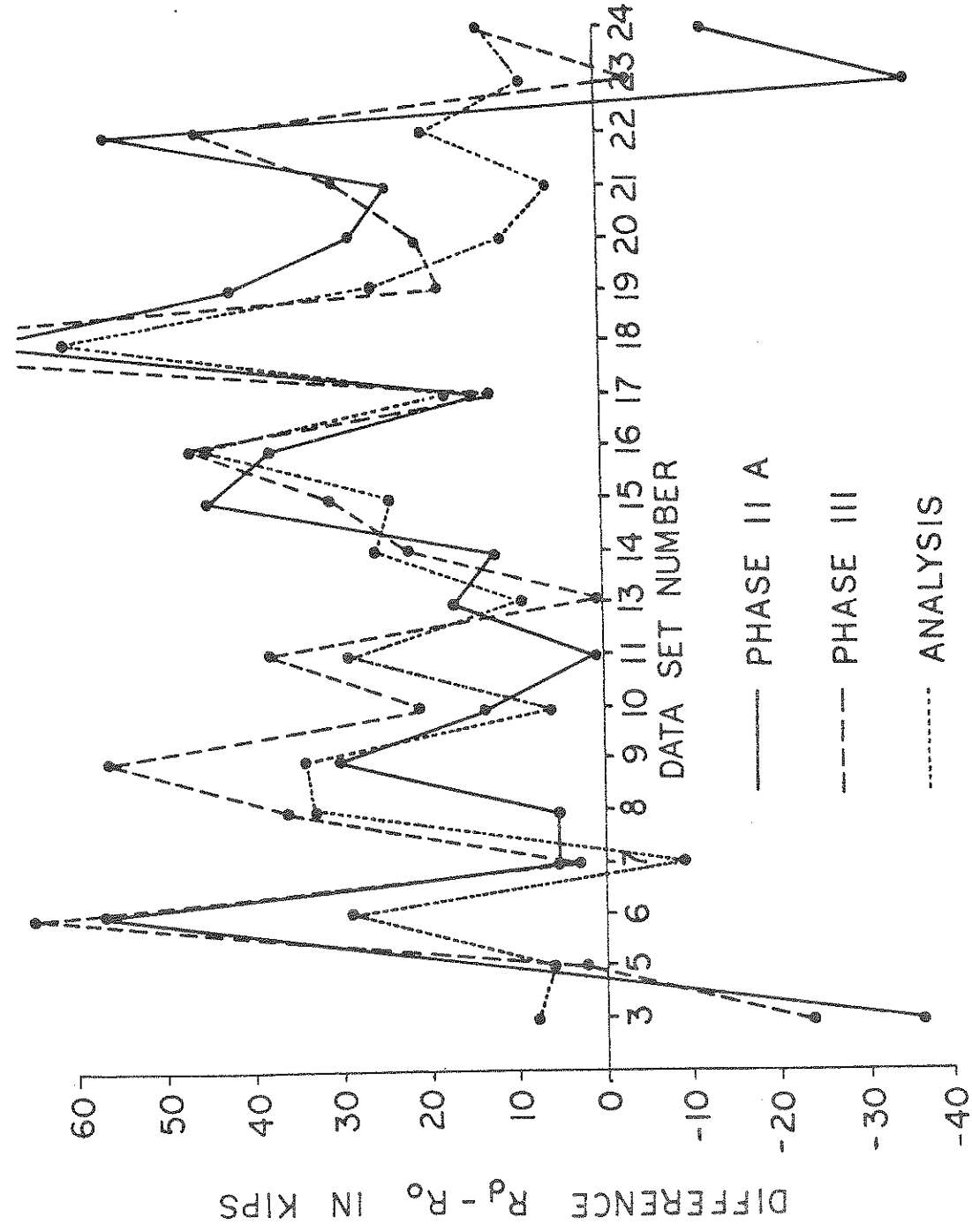

FIGURE 3.49: DIFFERENCES BETWEEN PREDICTED AND MEASURED STATIC CAPACITY

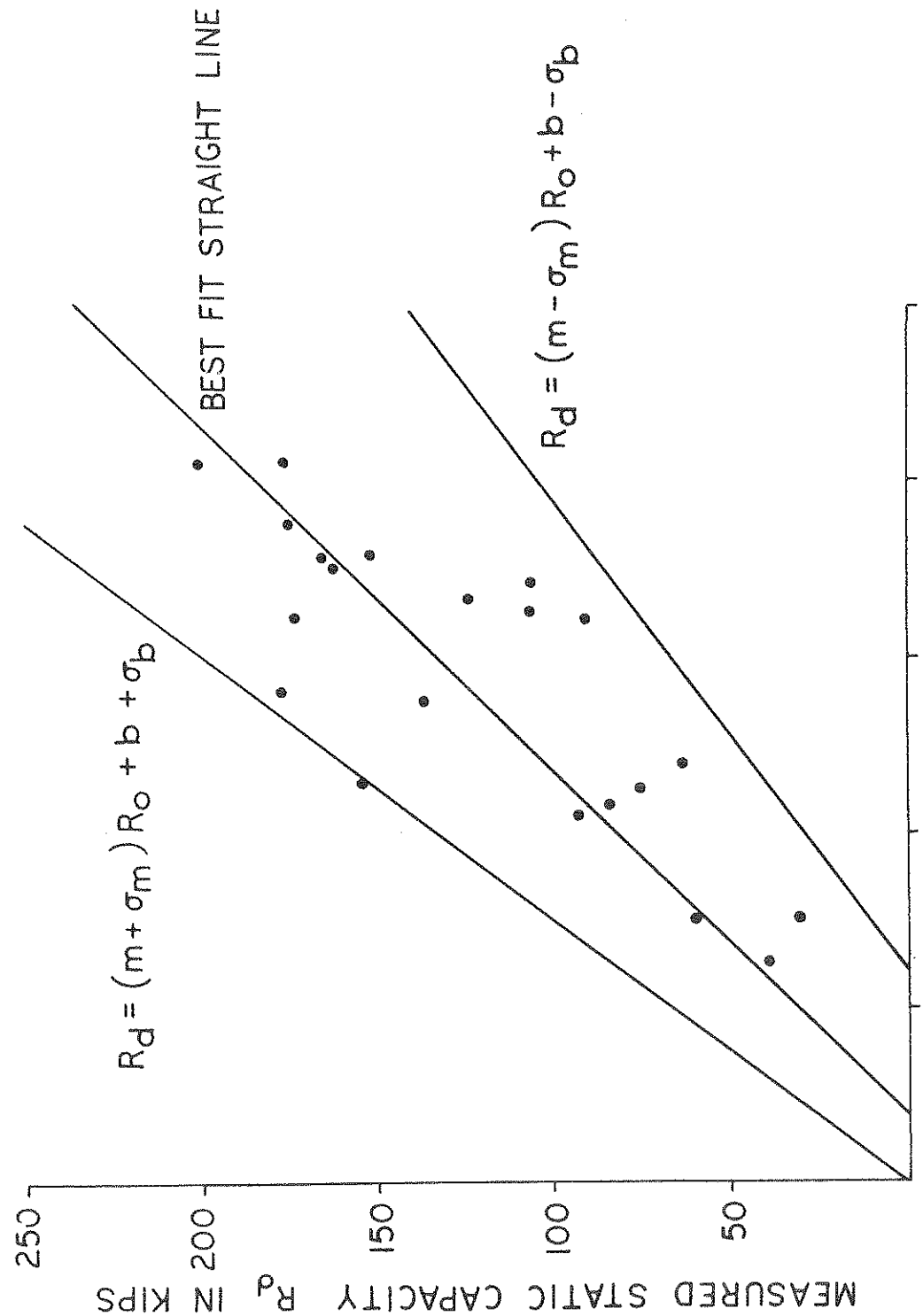

FIGURE 3.50: RESULTS FROM STATISTICAL ANALYSIS FOR PHASE IIA PREDICTION METHOD

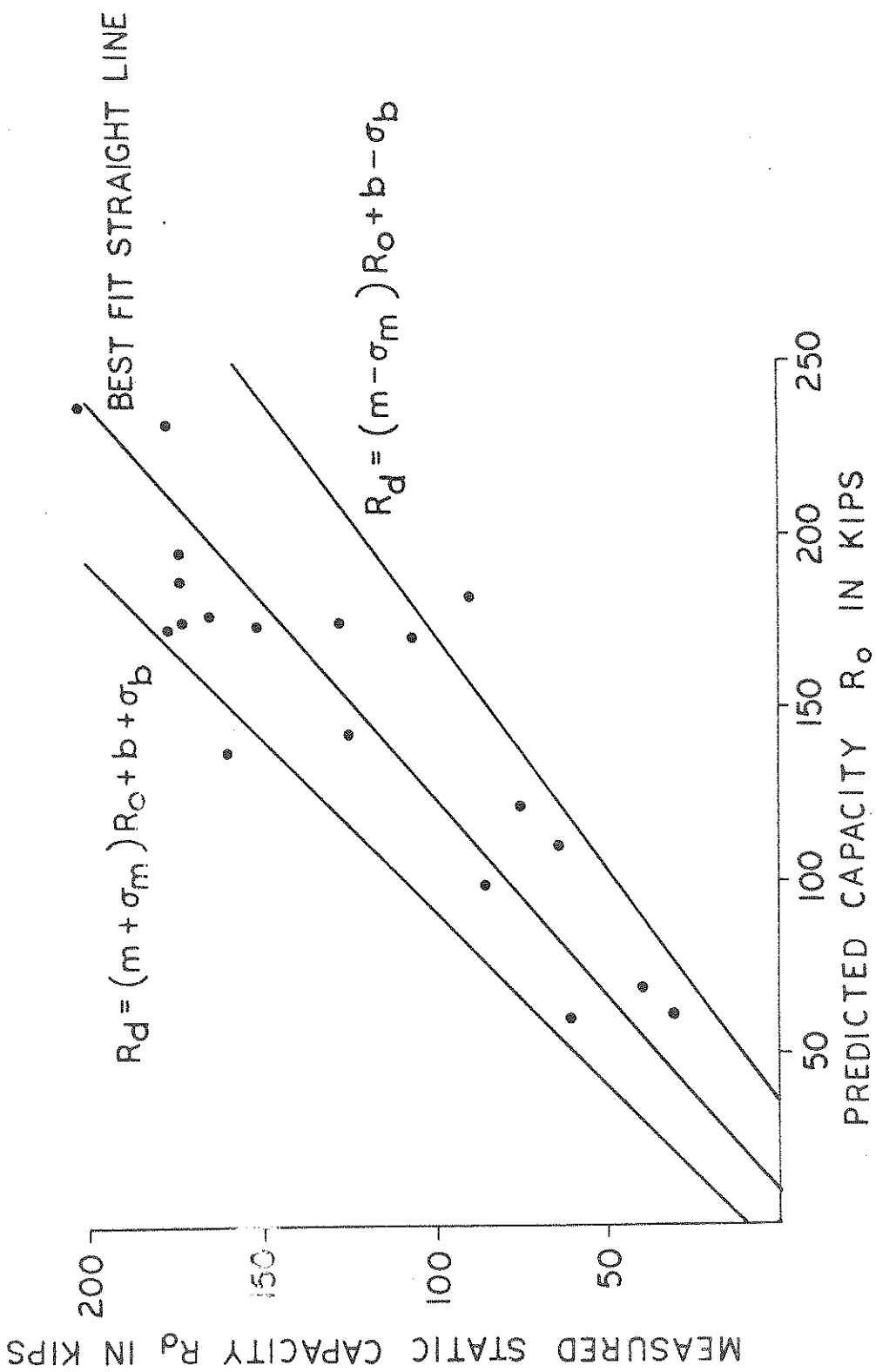

FIGURE 3.51: RESULTS FROM STATISTICAL ANALYSIS FOR PHASE III PREDICTION METHOD

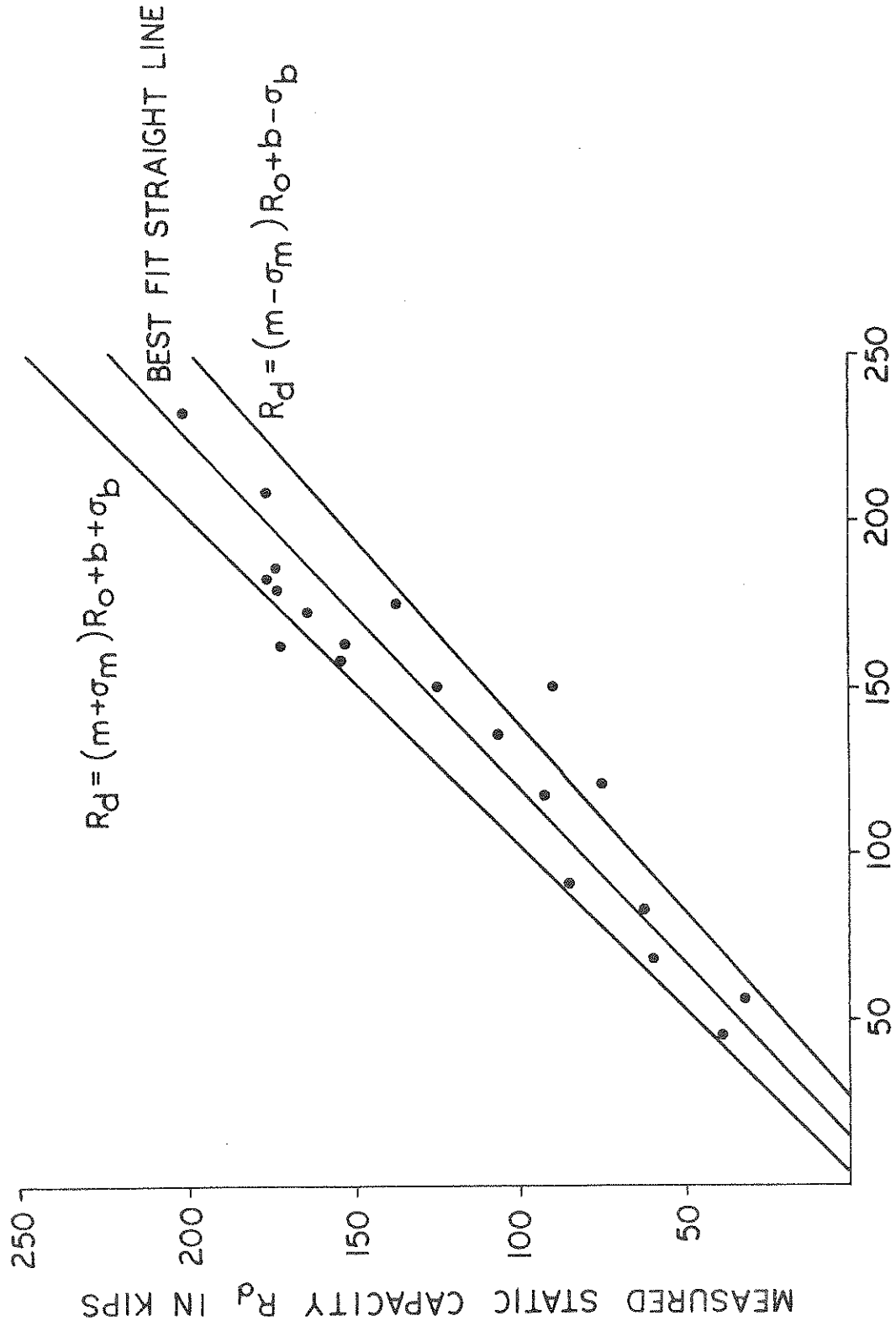

FIGURE 3.52: RESULTS FROM STATISTICAL ANALYSIS FOR PREDICTIONS FROM WAVE ANALYSIS

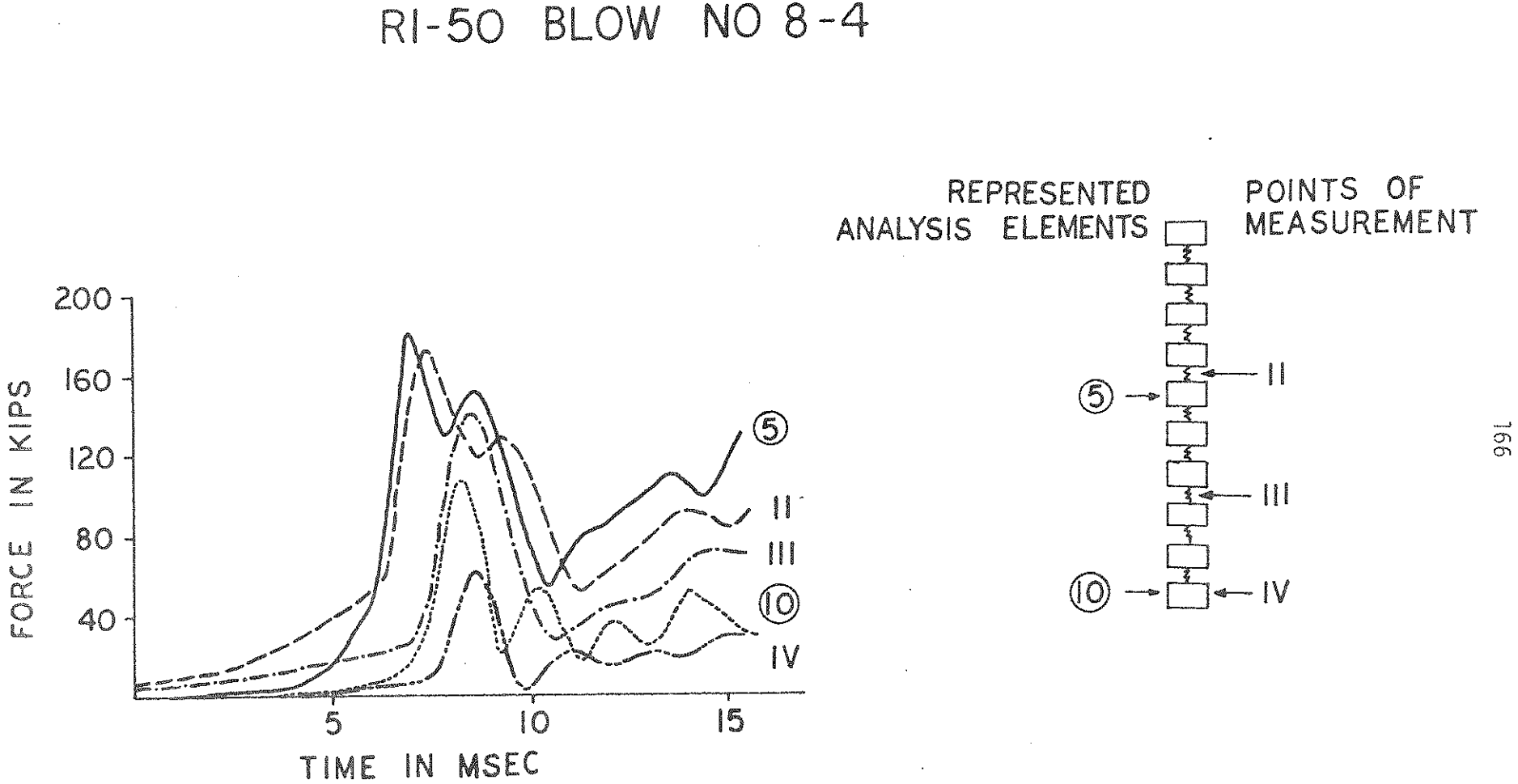

FIGURE 3.53: COMPARISON OF PREDICTED WITH MEASURED PILE FORCES DURING DRIVING

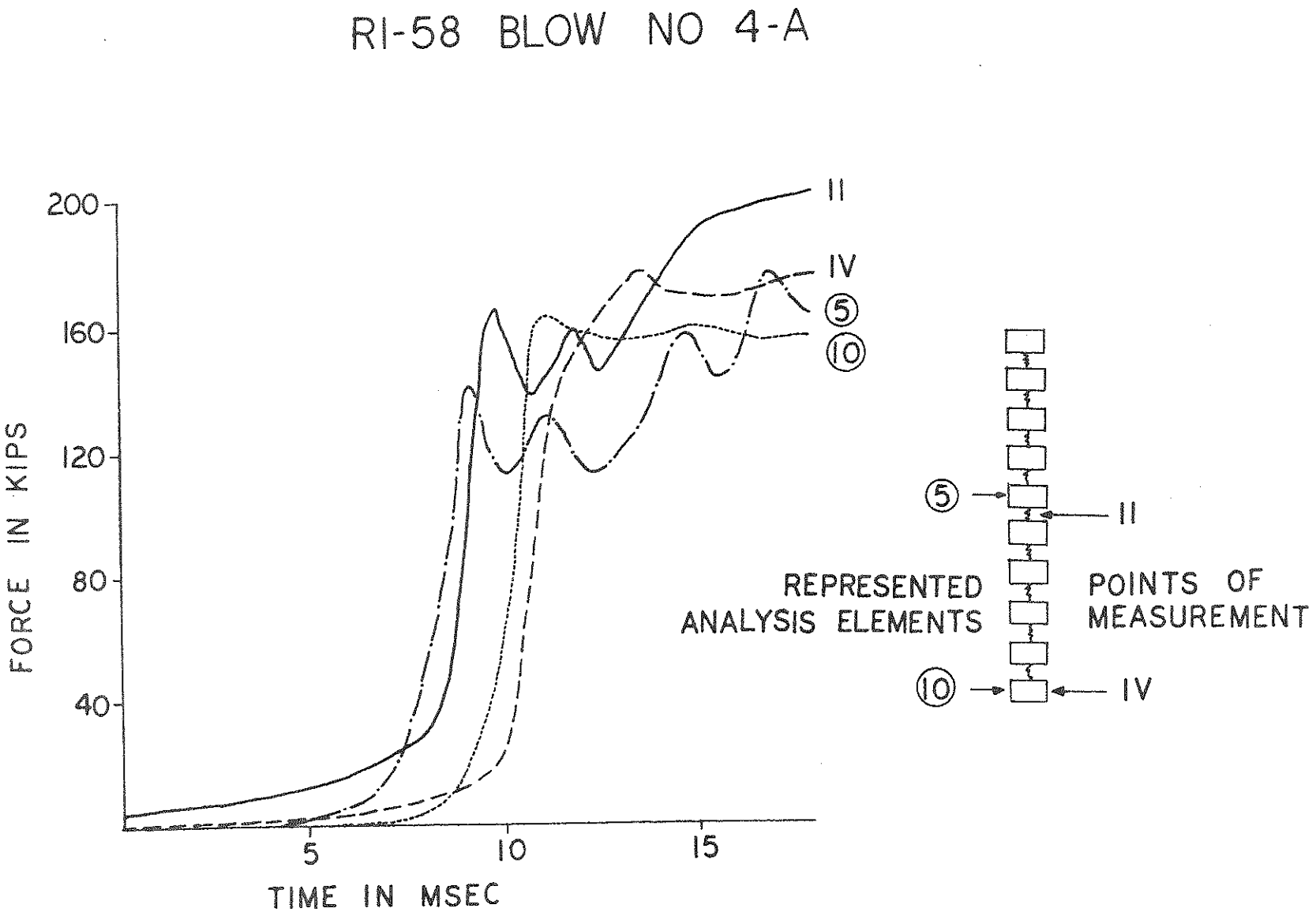

FIGURE 3.54: COMPARISON OF MEASURED WITH COMPUTED FORCES IN PILE DURING DRIVING

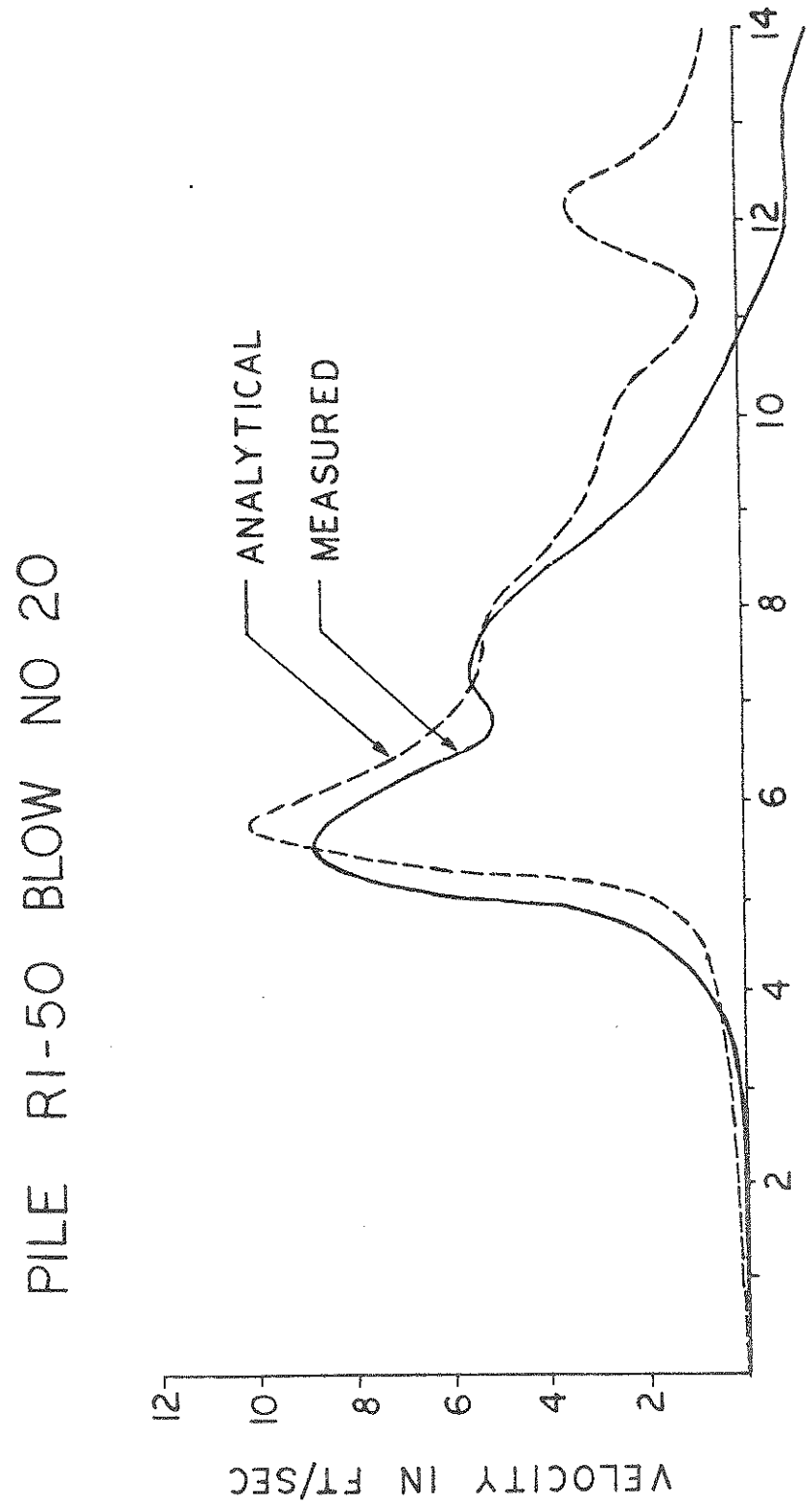

FIGURE 3.55: VELOCITY AT PILE TIP
COMPARISON BETWEEN MEASUREMENT AND ANALYSIS

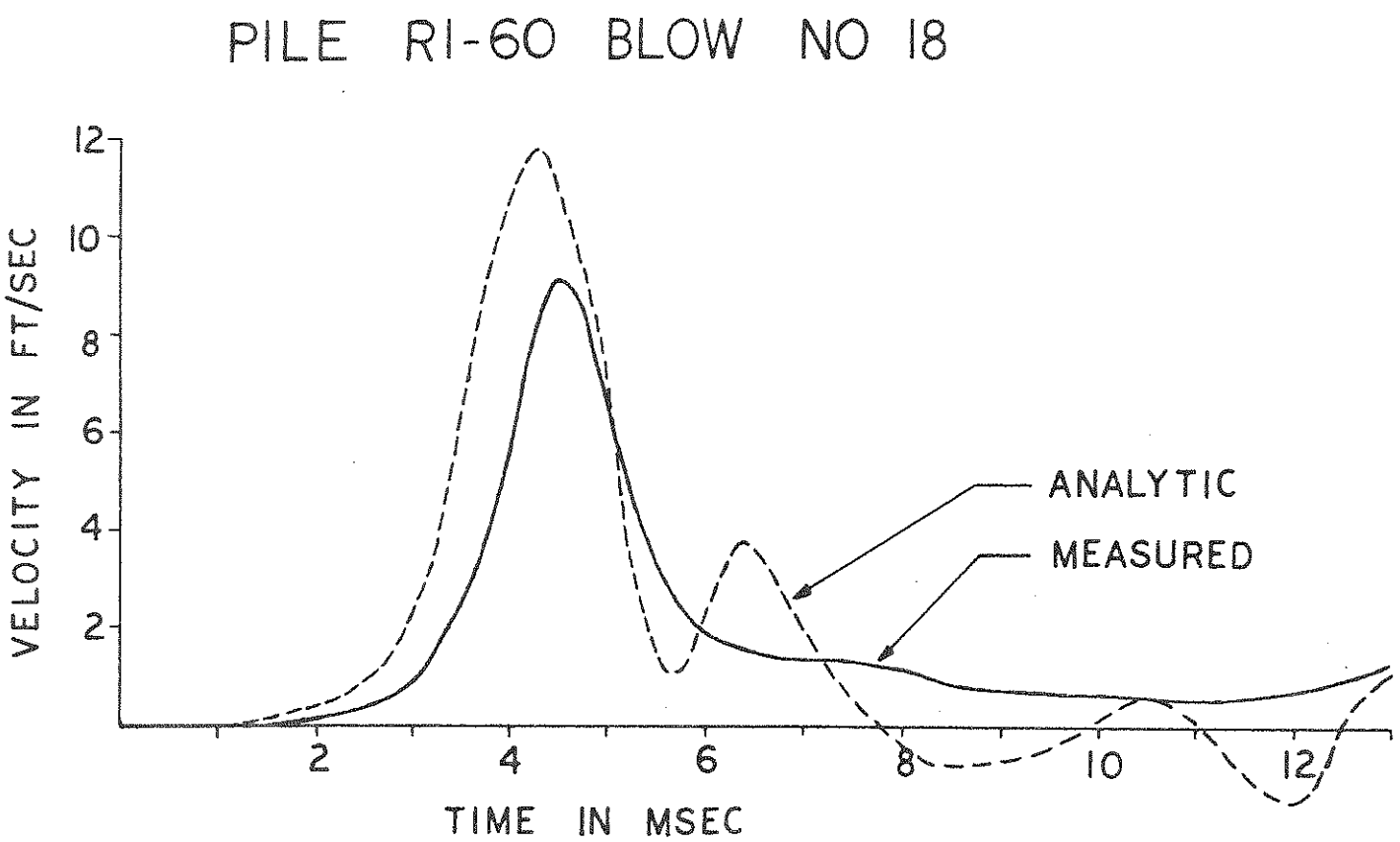

FIGURE 3.56: VELOCITY AT PILE TIP

COMPARISON BETWEEN MEASUREMENT AND ANALYSIS

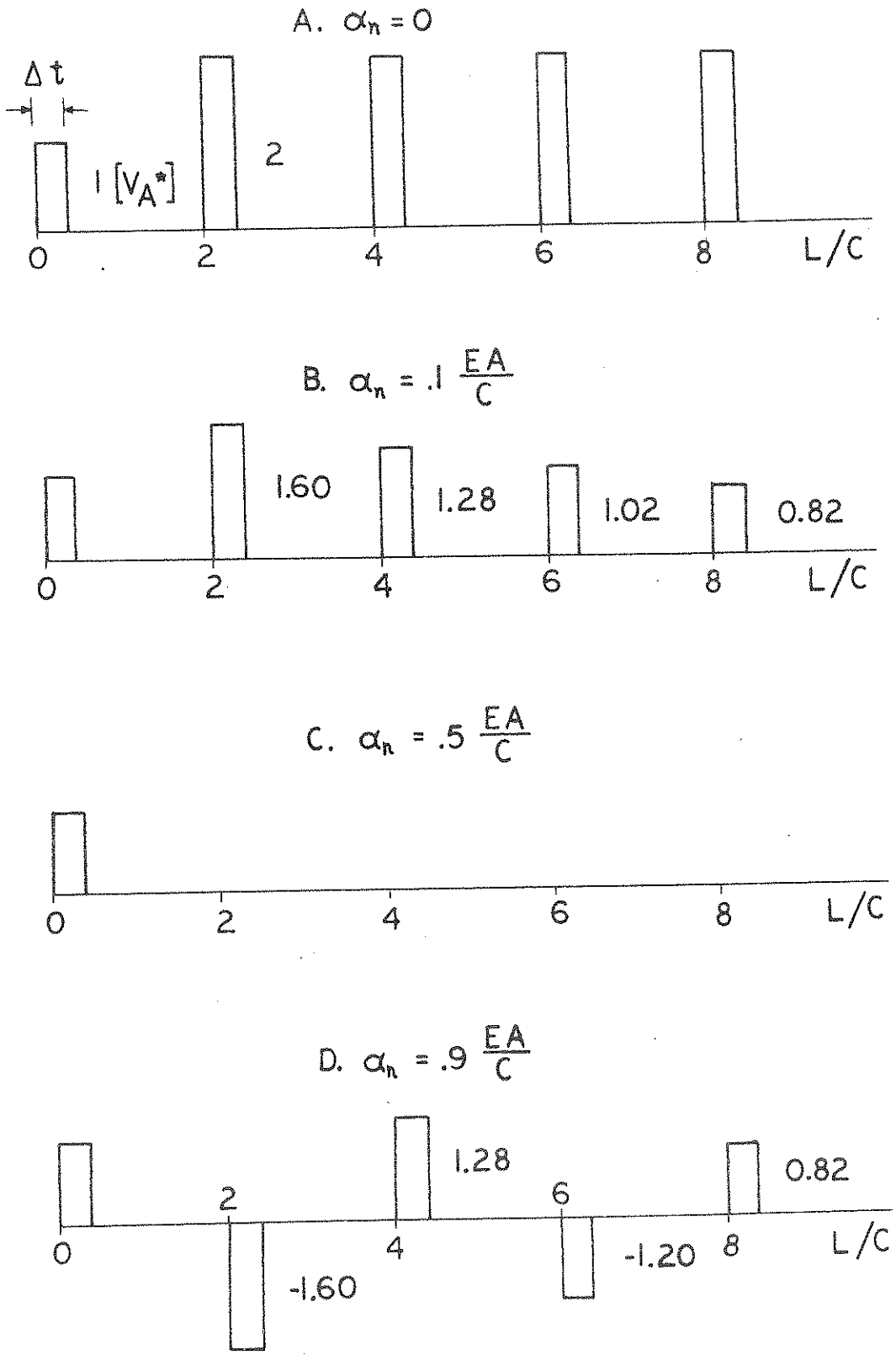

FIGURE 4.1: PILE TOP VELOCITY DUE TO A INPUT AT TIME t = 0 AND A DAMPER AT THE PILE BOTTOM

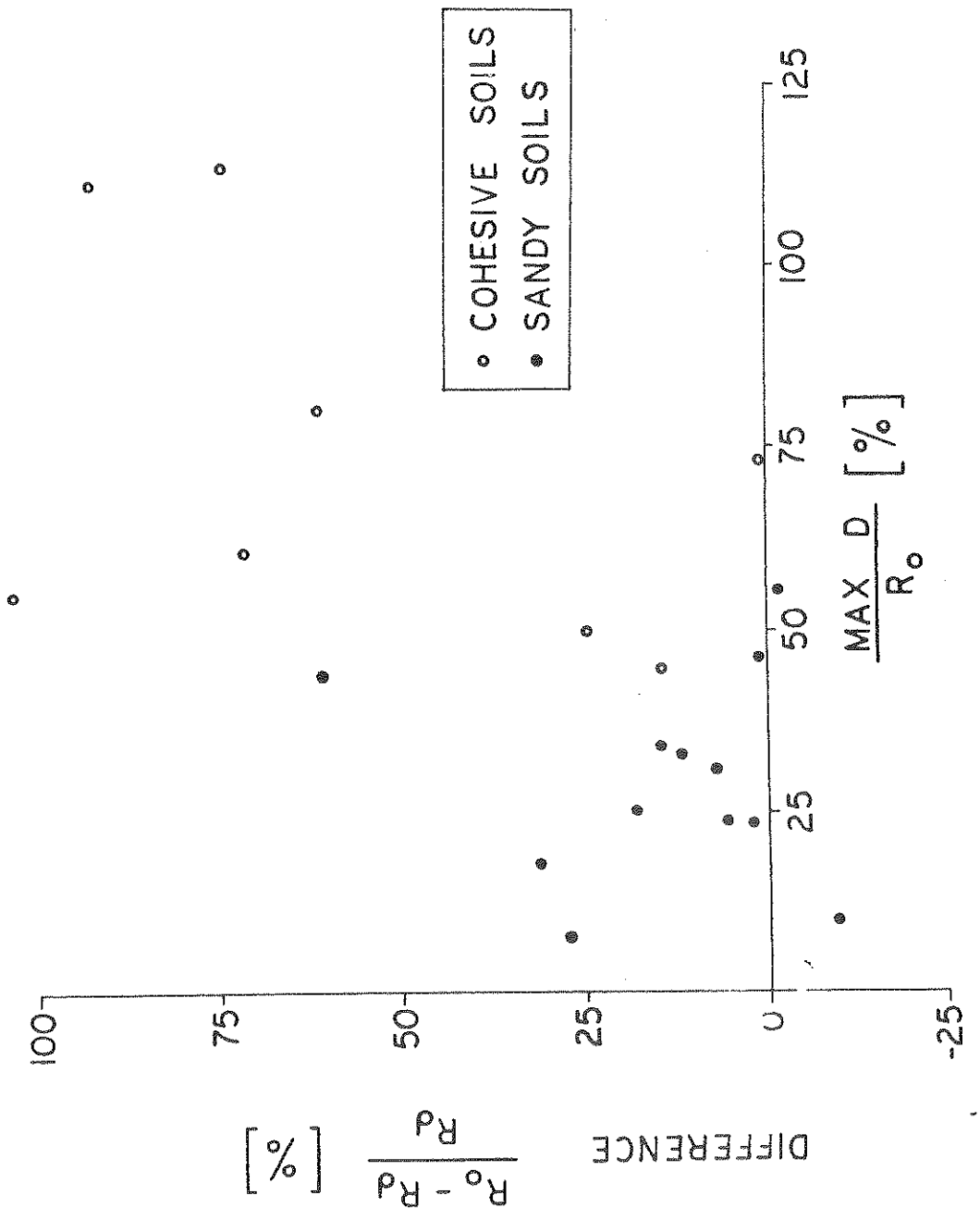

FIGURE 4.2: RELATIVE DIFFERENCES BETWEEN PHASE III PREDICTION AND STATIC LOAD TEST RESULT AS A FUNCTION OF RELATIVE MAGNITUDE OF DAMPING